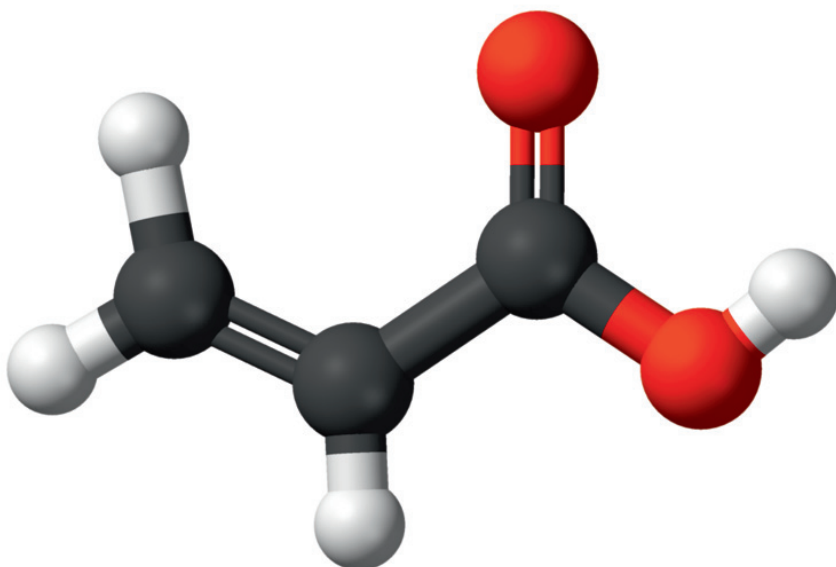


A NEW APPROACH TO INDUSTRIAL MELT CRYSTALLIZATION OF ACRYLIC ACID



Axel Hengstermann

Propositions accompanying the thesis of Axel Hengstermann

A NEW APPROACH TO INDUSTRIAL MELT CRYSTALLIZATION OF ACRYLIC ACID

1. Water influences the crystal growth of certain crystal faces of acrylic acid. Additionally, water induces the occurrence of a hollow cavity on face {002}. The higher the water content and the supercooling of the melt, the more needle-like the crystal shape becomes and the longer the occurring cavity (Chapter 2).
2. The operation of a melt crystallization and purification unit is limited by the filterability of the occurring crystals. The filterability of acrylic acid crystals is influenced by the water content and supercooling of the melt due to the occurring needle-like shape and the hollow cavity on face {002} of acrylic acid crystals (Chapter 3).
3. The comparison of different measurement techniques for crystal size distribution often leads to strong confusion or to the wrong conclusions (Chapter 3).
4. The measurement of the particle size distributions of different morphologies occurring in a homogenous suspension is technically not possible, but needs to be developed for the optimal design of eutectic (melt) crystallization processes (Chapter 4).
5. The attention to the precise prediction of solid liquid equilibria needs to be improved (Chapter 5).
6. The eutectic freeze crystallization (EFC) is a new technique to purify an organic compound from an aqueous melt at a higher yield and a higher specific throughput. (Chapter 6).
7. The internalization of a take home message of an auditorium is always a question of the moderator's presentation.
8. There is a big difference between correlation and causality – engineers can identify problems by correlations, but they should only trust in causalities.
9. One should snap at the offered chances – some will be unique in life, like the proposal for this PhD thesis.
10. The main difference between German and Dutch people is quite simple. For German people the distance between Berlin and Amsterdam is exactly 651 km. For Dutch people the distance is roughly 650 km.

These propositions are regarded as opposable and defendable, and have been approved as such by the supervisor, Prof. dr. ir. P.J. Jansens.

A NEW APPROACH TO INDUSTRIAL MELT CRYSTALLIZATION OF ACRYLIC ACID

1. Water beïnvloedt de kristalgroei van sommige kristalvlakken van acrylzuur. Bovendien heeft de aanwezigheid van water de vorming van holtes op de {002} kristalvlak tot gevolg. Hoe hoger het watergehalte en de onderkoeling in de smelt, des te sterker naaldvormig de kristallen en des te langer de gevormde holtes. (Hoofdstuk 2).
2. Het bedrijven van een smeltkristallisatie- en opzuiveringsproces wordt beperkt door de filtreerbaarheid van de gevormde kristallen. De filtreerbaarheid van acrylzuur kristallen wordt beïnvloed door het watergehalte en de onderkoeling van de smelt tengevolge van de vorming van naaldvormige acrylzuur kristallen met holtes op de {002} kristalvlakken (Hoofdstuk 3).
3. Het vergelijken van resultaten van verschillende meettechnieken voor de kristalgrootteverdeling leidt vaak tot verkeerde conclusies (Hoofdstuk 3).
4. Het meten van deeltjesgrootteverdelingen van deeltjes met een verschillende kristalvorm, aanwezig in een homogene suspensie is momenteel technische niet mogelijk maar zal moeten worden ontwikkeld voor een optimaal ontwerp van eutectische smeltkristallisatie (Hoofdstuk 4).
5. De wetenschap zou meer aandacht moeten besteden aan de nauwkeurige voorspelling van thermodynamische eigenschappen van vast-vloeistof evenwichten. (Hoofdstuk 5).
6. Eutectische vrieskristallisatie is een nieuwe technologie om een organische stof te zuiveren uit een waterige smelt met een hogere opbrengst en een hogere specifieke capaciteit. (Hoofdstuk 6).
7. Het zich eigen maken van een “mee naar huis” boodschap voor een gehoorzaal is altijd een vraag uit de presentatie van de moderator.
8. Er is een groot verschil tussen correlatie en causaliteit – ingenieurs kunnen problemen identificeren met behulp van correlaties, maar zij zouden alleen vertrouwen moeten hebben in causaliteiten.
9. Men moet in het leven gebruik moeten maken van de aangeboden kansen – sommige zullen uniek blijken te zijn, zoals bijvoorbeeld het voorstel om dit proefschrift te schrijven.
10. Het belangrijkste verschil tussen Duitsers en Nederlanders is heel eenvoudig uit te leggen. Voor Duitsers is de afstand tussen Berlijn en Amsterdam 651 km. Voor Nederlanders is deze afstand ruwweg 650 km.

Deze stellingen worden oponeerbaar en verdedigbaar geacht en zijn als zodanig goedgekeurd door de promotor, Prof. dr. ir. P.J. Jansens.

**A NEW APPROACH TO
INDUSTRIAL MELT CRYSTALLIZATION
OF ACRYLIC ACID**

AXEL HENGSTERMANN

Bibliographic information published by the Deutsche Nationalbibliothek

The Deutsche Nationalbibliothek lists this publication in the Deutsche Nationalbibliografie; detailed bibliographic data are available in the Internet at <http://dnb.d-nb.de>.

Zugl.: Delft University of Technology, Diss., 2010

Copyright Shaker Verlag 2010

All rights reserved. No part of this publication may be reproduced, stored in a retrieval system, or transmitted, in any form or by any means, electronic, mechanical, photocopying, recording or otherwise, without the prior permission of the publishers.

Printed in Germany.

ISBN 978-3-8322-9501-1

ISSN 0945-1021

Shaker Verlag GmbH • P.O. BOX 101818 • D-52018 Aachen

Phone: 0049/2407/9596-0 • Telefax: 0049/2407/9596-9

Internet: www.shaker.de • e-mail: info@shaker.de

A NEW APPROACH TO INDUSTRIAL MELT CRYSTALLIZATION OF ACRYLIC ACID

Proefschrift

ter verkrijging van de graad van doctor
aan de Technische Universiteit Delft,
op gezag van de Rector Magnificus Prof. ir. K. C. A. M. Luyben,
voorzitter van het College voor Promoties,
in het openbaar te verdedigen op maandag 22 november 2010 om 10:00 uur

door

Axel HENGSTERMANN

Diplom-Ingenieur (FH) of Chemical Engineering;
University of Applied Science, Muenster, Germany
geboren te Muenster / Germany

Dit proefschrift is goedgekeurd door de promotor:

Prof. dr. ir. P. J. Jansens

Samenstelling promotiecommissie:

Rector Magnificus

Prof. dr. ir. P. J. Jansens

Dr. ir. H. J. M. Kramer

Prof. dr. ir. A. Stankiewicz

Prof. Dr.-Ing. Dr. h. c. Joachim Ulrich

Dr. ir. Dirk Verdoes

Dr. H. L. M. Meekes

Prof. dr. R. F. Mudde

Prof. dr. ir. B. J. Boersma

Voorzitter

Technische Universiteit Delft, promotor

Technische Universiteit Delft,

Technische Universiteit Delft

Martin-Luther-Universität Halle-Wittenberg

TNO Science & Industry

Radboud Universiteit Nijmegen

Technische Universiteit Delft

Technische Universiteit Delft, reservelid

**To Claudia
and my parents**

TABLE OF CONTENTS

CHAPTER 1

INTRODUCTION

1.1	INDUSTRIAL NEEDS AND ADVANTAGES OF MELT CRYSTALLIZATION.....	1
1.2	MELT CRYSTALLIZATION	2
1.2.1	Solid-liquid equilibrium	3
1.2.2	Industrial crystallization techniques	4
1.2.3	Driving force for melt crystallization	7
1.3	CRYSTAL GROWTH	8
1.3.1	Growth mechanisms in suspension	8
1.3.2	Growth rates	10
1.4	SOLID-LIQUID SEPARATION AND CRYSTAL PURIFICATION IN SUSPENSION CRYSTALLIZATION.....	11
1.4.1	Wash columns	13
1.5	THE SYSTEM ACRYLIC ACID	14
1.5.1	Physical properties	15
1.5.2	Solid-liquid phase diagram acrylic acid and water	16
1.6	OBJECTIVES.....	17
1.7	OUTLINE OF THE THESIS.....	19
	NOMENCLATURE.....	21
	REFERENCES	23

CHAPTER 2

INFLUENCE OF SUPERCOOLING AND WATER CONTENT ON CRYSTAL MORPHOLOGY OF ACRYLIC ACID

	ABSTRACT.....	27
2.1	INTRODUCTION	28
2.2	STATE OF KNOWLEDGE	28
2.2.1	Acrylic acid crystal structure.....	28
2.2.2	Chemical composition of the faces	29
2.2.3	Morphology development in presence of water	31
2.2.4	Extension of the theory for surface integration processes	32
2.2.5	Prediction of crystal face growth rates	37
2.3	EXPERIMENTAL	38
2.3.1	Equipment and setup.....	38

TABLE OF CONTENTS

2.3.2 Experimental procedure.....	39
2.3.3 Experimental results	40
2.3.4 Discussion of evaluated results.....	43
2.4 CRYSTAL MORPHOLOGY DEVELOPMENT – A QUALITATIVE APPROACH.....	44
2.4.1 Growth rate analysis and modeling	45
2.4.2 Cavity angle analysis	47
2.5 CONCLUSION	48
NOMENCLATURE	49
REFERENCES.....	51

CHAPTER 3

THE INFLUENCE OF WATER AND SUPERCOOLING ON PERMEABILITY AND COMPRESSIBILITY OF ACRYLIC ACID CRYSTAL BEDS

ABSTRACT	55
3.1 INTRODUCTION.....	56
3.2 STATE OF KNOWLEDGE.....	56
3.2.1 Permeability model for spherical particles	57
3.2.2 Extended input to the permeability calculations for nonspherical particles	60
3.3 PERMEABILITY MODEL FOR NONSPHERICAL PARTICLES.....	61
3.4 EXPERIMENTAL	63
3.4.1 Apparatus and setup.....	63
3.4.2 Crystal property measurements	65
3.4.3 Experimental procedure.....	67
3.5 RESULTS	67
3.5.1 Supercooling.....	67
3.5.2 CLD measurement.....	68
3.5.3 Filtration results	70
3.5.4 Compressibility	71
3.6 MODELING RESULTS.....	72
3.6.1 Growth rates.....	73
3.6.2 Porosity	74
3.6.3 Specific surface	74
3.6.4 Permeability.....	75
3.7 DISCUSSION.....	76
3.8 CONCLUSIONS AND OUTLOOK	77
NOMENCLATURE.....	78
REFERENCES	81

CHAPTER 4**COMPRESSIBILITY IMPROVEMENT OF AN ACRYLIC ACID CRYSTAL BED BY THE IN-SITU FORMATION OF ICE CRYSTALS**

ABSTRACT	85
4.1 INTRODUCTION.....	86
4.2 STATE OF KNOWLEDGE ABOUT EUTECTIC FREEZING	86
4.3 APPROACH TO FILTRATION IMPROVEMENT	89
4.3.1 Qualitative approach to porosity improvement with an in-situ formed filter aid	89
4.3.2 Data estimation of an acrylic acid crystal bed near eutectic composition	90
4.3.3 Theoretical estimation of the porosity of nonspherical particles mixtures	94
4.4 EXPERIMENTAL	99
4.4.1 Objectives.....	99
4.4.2 Experimental setup and procedure	99
4.4.3 Experiments.....	101
4.4.4 Results	102
4.5 DISCUSSION AND OUTLOOK	107
4.6 CONCLUSION	108
NOMENCLATURE.....	110
REFERENCES	112

CHAPTER 5**SOLVENT SCREENING AND MEASUREMENT OF PHASE DIAGRAMS FOR THE YIELD MAXIMIZATION OF AN ACRYLIC ACID CRYSTALLIZATION**

ABSTRACT	115
5.1 INTRODUCTION.....	116
5.2 SOLID-LIQUID EQUILIBRIUM	116
5.2.1 Theoretical prediction of a solid-liquid phase equilibrium	116
5.2.2 Thermal analysis methods for determination of thermodynamical properties	120
5.2.3 Determination of the binary eutectic point and equilibrium diagram	121
5.2.4 Approach to determine the ternary eutectic point and solid-liquid equilibrium ...	123
5.3 APPROACH TO A FAST SOLVENT SCREENING METHOD	125
5.3.1 Approach to a data base request for fast solvent screening.....	125
5.3.2 State of the art	127
5.3.3 Screening results.....	128
5.4 EXPERIMENTAL	129
5.4.1 Objectives.....	129

TABLE OF CONTENTS

5.4.2 Experimental setup and procedure	130
5.4.3 Results	130
5.5 DISCUSSION.....	136
5.6 CONCLUSION AND OUTLOOK.....	137
NOMENCLATURE.....	139
REFERENCES	141
APPENDIX	143

CHAPTER 6

BENCH MARK STUDY FOR A NOVEL ACRYLIC ACID RECOVERY

ABSTRACT	147
6.1 INTRODUCTION.....	148
6.2 STATE OF KNOWLEDGE.....	148
6.2.1 Reaction – acrylic acid from propene	148
6.2.2 Recovery of acrylic acid	150
6.3 SIMULATION	152
6.3.1 Simulation tool	152
6.3.2 Simulation of crystallization units	152
6.3.3 Specification of utilities.....	153
6.3.4 Simulation margin and feed composition	153
6.3.5 Conventional acrylic acid recovery process	154
6.3.6 Novel acrylic aid recovery process using eutectic crystallization	157
6.4 RESULTS	159
6.4.1 Heat balance	162
6.4.2 Dimension of main process units	166
6.4.3 Result summary.....	170
6.5 DISCUSSION.....	171
6.6 CONCLUSION AND OUTLOOK.....	172
NOMENCLATURE.....	174
REFERENCES	176

APPENDIX

ENGLISH SUMMARY	181
NEDERLANDSE SAMENVATTING.....	187
GERMAN SUMMARY	193
ACKNOWLEDGEMENTS.....	199
CURRICULUM VITAE.....	203
PATENT APPLICATION - WO2009130085A1	207

CHAPTER 1

INTRODUCTION

1.1 Industrial needs and advantages of melt crystallization

In the recent past the economical and ecological requirement standards for the production of all kind of chemical products have become tighter. Furthermore, the customer's demand for high purity products gets stronger. An example is acrylic acid as a pre-product for the production of diapers and other hygiene products. The installed acrylic acid production processes are often energy intensive and the common purification steps are not able to fulfill the above-listed requirements. Therefore, the acrylic acid producers are anxious to develop new innovative acrylic acid production processes to reduce the specific energy demand and to improve the product quality.

As one of the oldest separation techniques, melt crystallization can still contribute to these requirements. In comparison to distillation and extraction, crystallization demonstrates a much higher selectivity per separation step, consumes less energy, and operates at lower temperatures. The low operating temperatures offer the opportunity to carry out a separation without thermal degradation, too.

Regarding the increasing demand for high purity acrylic acid melt crystallization is a promising separation technique to reach these purity levels. Additionally, the cold separation step leads to a higher achievable yield of acrylic acid due to the reduced propensity to polymerize. Therefore, the scope of this thesis is to strengthen the innovative installation of melt crystallization for the purification of acrylic acid on an industrial scale.

Currently, the most favored industrial technology for melt crystallization of acrylic acid is the layer crystallization process. Layer crystallization requires liquid handling only but, unfortunately, due to a low surface area for crystal growth it comes along with poor distribution coefficients of the secondary components per stage. Therefore, it often leads to a multi-stage process in order to reach high product qualities.

On the other hand suspension crystallization is an interesting technique for the separation and purification of acrylic acid on industrial scale. Due to low crystal growth rates, the technique offers the possibility of a single-step purification process. However, the process potential and the resulting purity are always limited by the performance and the efficiency of

the downstream solid-liquid separation technology. Therefore, the scope of this introduction chapter is to elucidate the basic principle, the state-of-the-art of suspension melt crystallization, and the required downstream separation technologies.

Table 1-1 gives a small overview of substances mainly purified by melt crystallization because of a low temperature level, thermal instability or a required high purification level. These products are predominantly purified by layer crystallization. The world production scales [1] emphasize the potential for the installation of new innovative suspension crystallization units.

Table 1-1 World production scale of several chemicals [1].

product	world production scale / [mio t/a]	basis
acrylic acid	3.2	2006
phenol	8.3	2004
p-xylene	3.2	2006
caprolactam	3.9	2005

1.2 Melt crystallization

Crystallization is generally defined as the formation of a solid state from a supersaturated liquid. Supersaturation is present, if the thermodynamic solid-liquid equilibrium is exceeded by evaporation of the solvent, cooling of the complete system, by a combination of both, or by the addition of an anti-solvent. In case of melt crystallization supersaturation is generated by cooling, therefore it is common to use the term supercooling instead of supersaturation.

Ulrich et al. [2] suggested a scientific definition to precisely differentiate the occurring crystallization mechanisms:

- If mass transfer dominates the liquid-solid phase change, it is defined as "solution crystallization".
- If heat transfer dominates the liquid-solid phase change, it is defined as "melt crystallization".

1.2.1 Solid-liquid equilibrium

The knowledge of the solid-liquid equilibrium is essential in order to design melt crystallization as a product purification and separation step. Additionally, the solid-liquid phase diagram provides insight in crystal phase and thus the purity of the product that is formed under the process conditions and in the general separation potential of a component. The eutectic point in a phase diagram represents a special equilibrium state of the system. Cooling below the eutectic point of a binary systems leads to the formation of two crystal phases. This makes a further separation and purification of one component impossible, but offers the possibility to form a second crystal phase which can be separated similarly from the melt. Phase diagrams of many common binary systems are available in literature.

Matsuoka [3] published a stochastic analysis of a large number of binary organic solid-liquid systems in 1977. According to the analysis, 86% of all investigated binary systems exhibit a eutectic or peritectic behavior, and hence allow the separation of pure crystals. Obviously, this depends on the feed composition and on the location of the eutectic and peritectic points, respectively. The remaining systems (14%) form solid solutions and are not attractive for separation by crystallization as they need multi-stage operation.

The eutectic point (EP) and its corresponding concentration x_{EP} , respectively, limit the yield of a crystallization step. Crossing the eutectic point is followed by the crystallization of more than one component. The maximum recovery of a component from any eutectic system can be calculated easily by the relating concentrations as shown in eq. 1-1.

$$R = \frac{x_F - x_{EP}}{x_F(1 - x_{EP})} \quad \text{eq. 1-1}$$

The industrial separation of a pure component from a melt is often an operation in a multi component system. The graphical representation of multi-component systems with more than three substances is not possible. However with a computer program it is still possible to describe the system or it can usually be reduced to a ternary system consisting of the substance to be crystallized, a major secondary component, and a set of side products which can be summarized by one pseudo component. This approach is feasible because the concentration distribution of the side products is often constant.

The graphical presentation of a solid-liquid equilibrium phase diagram of a ternary system is quite complicated. The general concentration of a ternary mixture can be presented in a triangular diagram. Figure 1-1 shows a typical graphical presentation of the ternary solid-liquid equilibrium of acrylic acid, water, and acetic acid. The color graduation represents the different levels of the equilibrium temperatures.

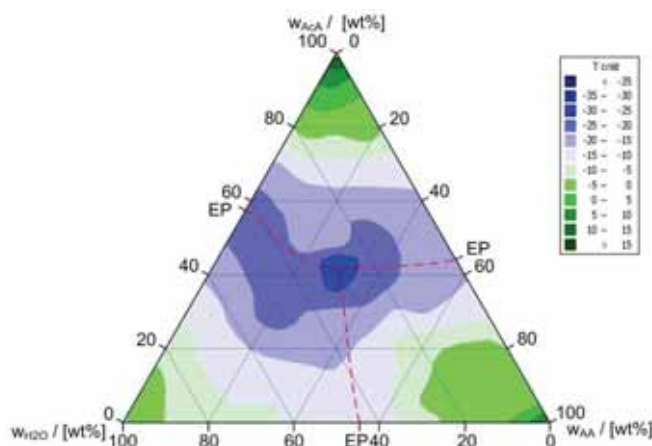


Figure 1-1 Ternary phase diagram of the system acrylic acid, water, and acetic acid.

1.2.2 Industrial crystallization techniques

The industrial product separation and purification by melt crystallization can be carried out in a suspension or a layer mode. Layer crystallization is a well known technology and is quite comfortable to operate as it requires handling of liquid phases only. In contrast, the suspension crystallization always deals with the transportation and filtration of solid particles which often leads to complex operations. However, it is advantageous as it also leads to formation of highly pure crystals in a single step operation in contrast to layer crystallization with low crystal purities. Therefore, the layer crystallization often requires a multi-stage operation. The major differences in the crystal purities can be explained, if the interactions between the heat and mass transfer at the solid surface boundary layer in a supercooled state are considered.

In the layer growth, the supercooling is generated through a cooled wall. The growth of crystals takes place directly on a cooled wall. The schematic temperature and concentration profiles are shown in figure 1-2. The heat of crystallization is removed through the crystal layer, whereas the impurities are transported into the bulk which is not supercooled. The formation of a pure crystal layer is possible, if the solid phase is in equilibrium with the liquid phase at the crystal surface and the growth rate is small. However, these conditions result in extremely low growth rates and large apparatus scales which would make this technology uneconomical.

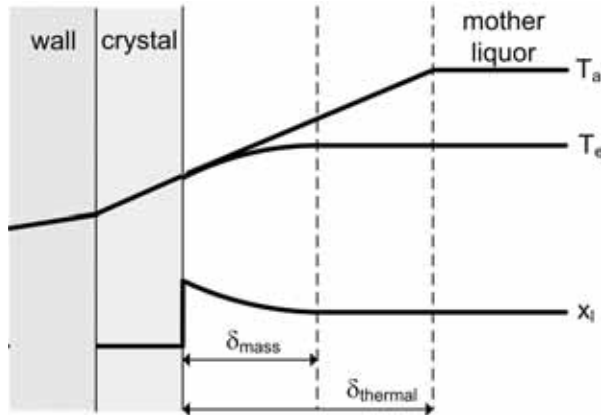


Figure 1-2 Profiles for layer growth under stable conditions.

On the other hand, it is possible to have equipment sizes and production capacities which allow economically feasible operations if high growth rates from 10^{-6} to 10^{-5} m/s are established. The occurring temperature and concentration profiles of the boundary layer are shown in figure 1-3. High growth rates in layer crystallization lead to increased supercooling from the crystal layer towards the bulk. Furthermore, an occurring impurity gradient in the crystal boundary layer lowers the equilibrium temperature T_e and hence the supercooling. This combination favors intrinsically unstable growth. Unstable growth occurs, if the supercooling in the melt is higher than that at the crystal interface. This results in a random protrusion on the flat crystal layer. The growing protrusion enters the region of higher supercooling in the melt and minimizes the supercooling by a rough growth of the surface or by a fast dendrite outgrowth. Due to fast growth impurities of the mother liquor are incorporated in the crystal layer. This condition on the crystal layer is referred as constitutional supercooling [4] and its occurrence on industrial scale is responsible for low purity in a single crystallization step. Therefore, layer crystallization often requires a multi-stage process.

In suspension growth, the crystals grow always from a supercooled bulk. In that case, the maximum supercooling is localized in the bulk and decreases towards the crystal surface. Additionally, a gradient of impurities occurs which decreases the equilibrium temperature. These two conditions result in some degree of constitutional supercooling. Therefore, a suspension growth is also intrinsically unstable. Figure 1-4 shows characteristic temperature and concentration profiles at the solid surface boundary layer.

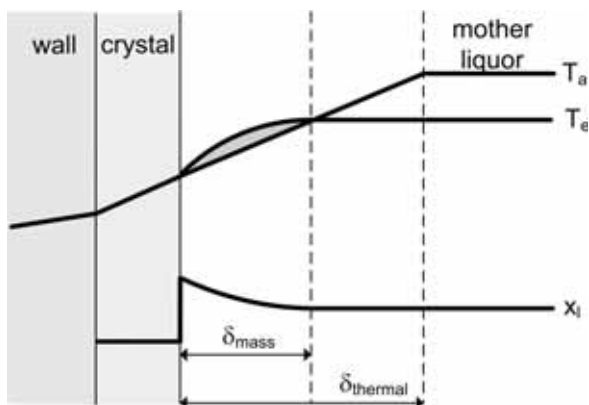


Figure 1-3 Profiles for layer growth under unstable conditions.

In suspension crystallization, the growth rates can be kept low between 10^{-8} - 10^{-7} m/s due to a high available crystal surface for growth and good mixing conditions. If these conditions are maintained, the degree of constitutional supercooling is rather small. Additionally, the system is striving for minimization of its surface tension and consequently a reduction of its surface stabilizes the system. This effect becomes stronger with a stronger curvature of the crystal surface and compensates the unstable growth conditions due to constitutional supercooling. In spite of the conditions leading to intrinsically unstable growth, suspension crystallization offers a high selectivity at high specific production capacities because of low growth rates, high available crystal surfaces, and good mixing conditions.

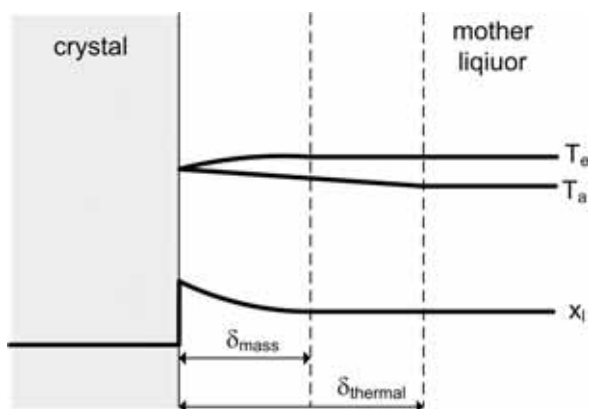


Figure 1-4 Profiles under constitutional supercooling in suspension growth.

1.2.3 Driving force for melt crystallization

Generally, a system at equilibrium has a minimum free energy ΔG . If a deviation from the equilibrium state exists, the free energy would be above the minimum and the system would have a tendency to reduce its free energy. In the crystalline state, the free energy is lower than in the liquid state. The difference between these states can be regarded as the driving force for melt crystallization. Crystallization is possible as long as a suitable deviation from this thermodynamic equilibrium is established.

The driving force can be expressed by the difference between the chemical potentials of the crystallizing component in the liquid state and in the equilibrium state:

$$\Delta\mu = R \cdot T \cdot \ln \left[\frac{a(p, T, x)}{a_e(p, T, x_e)} \right] \quad \text{eq. 1-2}$$

In the case of an ideal mixture or constant activity coefficients in the concentration range between x and x_e eq. 1-2 reduces to:

$$\Delta\mu = R \cdot T \cdot \ln \left(\frac{x}{x_e} \right) \quad \text{eq. 1-3}$$

When the relative supercooling term x/x_e is relatively small, the logarithmic term can be expanded in a Taylor series, resulting in the following term for the relative supercooling β :

$$\beta = \frac{\Delta\mu}{R \cdot T} \cong \frac{x - x_e}{x_e} \quad \text{eq. 1-4}$$

Differentiating eq. 1-4 allows an expression in terms of supercooling β :

$$\Delta\beta = \frac{-d \ln x_e}{dT} \Delta T \quad \text{eq. 1-5}$$

As the supercooling is zero in case of equilibrium, ΔT may be omitted. When the van 't Hoff equation is applied, the following expression of supercooling β , can be derived:

$$\beta = \frac{-\Delta H_m}{RT_e^2} \Delta T \quad \text{eq. 1-6}$$

Where:

ΔH_m = latent heat of fusion

ΔT = temperature difference between the melting point and the temperature of mother liquor

R = universal gas constant

T_e = equilibrium temperature

1.3 Crystal growth

Crystal growth takes place in a supercooled melt on existing surfaces. Different nucleation mechanisms which explain the formation of new surfaces are known but they will not be explained here as they fall out of the scope of this thesis.

The growth process on a crystal surface in a suspension can be divided into three steps:

- Mass transfer of the crystal growth units from the bulk through the solid-liquid boundary layer to the crystal surface.
- Diffusion of the crystal units on the crystal surface and integration into the lattice with the most favorable energy state.
- Transfer of the latent heat of fusion from the crystal surface into the bulk.

The addition of new crystal units will always take place at the most energetically favorable positions that offer a high number of faces and attachment possibilities to minimize the surface tension of the two-phase system. At low values of supercooling, the integration at a kink site is more probable than on a step site which in turn is more probable than on a flat site. Thus, the integration of new crystal units and hence the occurring growth mechanism depends on the supercooling.

Due to the focus of this thesis on suspension crystallization operating at low values of supercooling the following section will deal qualitatively with the growth mechanisms occurring at moderate supercooling. Growth mechanisms occurring at high supercoolings like crystal roughening and dendrite growth will not be part of the section.

1.3.1 Growth mechanisms in suspension

The addition of new crystal units on a crystal surface is always preferred at the most energetic favorable position. Burton et al. [5] proposed that crystal growth is an energetically cheap process, if it follows a “screw dislocation” mechanism. This mechanism avoids the generation of new surfaces and enables a nearly endless kink and the stepwise integration of the new crystal units. To maintain this ideal growth mechanism, a low supercooling and stable conditions have to be ensured. Figure 1-5 shows a schematic drawing of a crystal growth by “screw dislocation” mechanism.

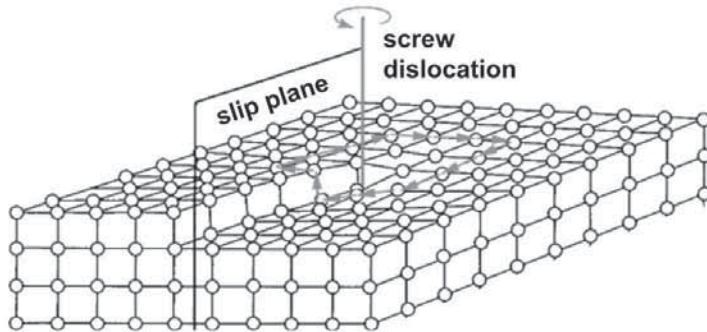


Figure 1-5 Mechanism of screw dislocation.

An increase of supercooling leads to the integration of new crystal units at less energetic favorable positions. Therefore, the formation of a new crystal layer takes place by the integration of new crystal units on a flat surface. Bennema and Gilmer [6] named this mechanism as the “birth and spread” model. This mechanism generates a higher specific crystal surface which is needed for a higher heat transport in the direction of the bulk. Figure 1-6 shows schematically the layer-by-layer “birth and spread” mechanism at a low growth rate.

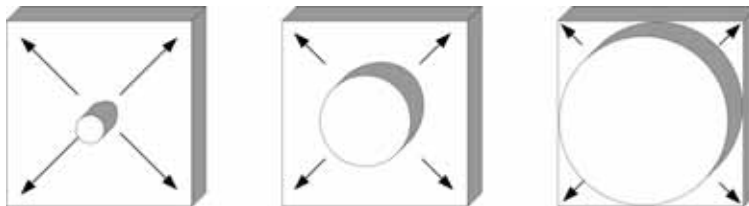


Figure 1-6 Birth and spread mechanism – layer by layer.

If the supercooling increases further, the formation of two-dimensional nucleus increases and it approximates the size of the growth units. This may lead to the effect that the formation of a new layer is as probable as the outgrowth of an already existing one. This fast formation of a new two-dimensional nucleus can change the defined crystal shape. The layer-by-layer mechanism changes into a surface roughening one. This effect is called “kinetic roughening” [5]. Figure 1-7 shows the “outgrowing” effect of a “birth and spread” mechanism at a high growth rate.

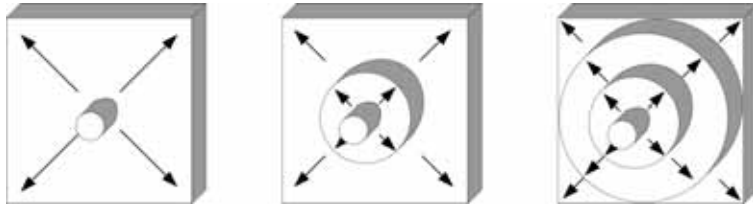


Figure 1-7 Birth and spread mechanism - outgrowing crystal shape.

1.3.2 Growth rates

The velocity of crystal growth is defined as crystal growth rate. The simplest theory of crystal growth bases on a spherical geometry without any preferred direction. However, crystals growing at moderate supercooling will mostly provide a shape with regular defined flat faces so that a differentiated look is necessary. The geometry of the crystal lattice as smallest crystal unit defines the macro shape of the crystals. Additionally, the composition of the melt and the occurring supercooling influence the growth of the different crystal faces. Therefore, it is necessary to define specific crystal growth rates.

1.3.2.1 Linear growth rate G :

The linear growth rate G is related to the growth of a characteristic dimension L per time. Most calculations of industrial crystallizers are based on the linear growth rate. Calculations with the linear growth rate G have to be used with care, because of different measurement methods for the characteristic length L and its definition. The characteristic length L can be a particle diameter from a laser diffraction measurement or e.g. a length-based mean chord from a Focus Beam Reflected Measurement (FBRM). The characteristic lengths of both measurements are correct, but represent completely different particle dimensions.

There are different approaches existing to determine the linear growth rate. The mostly used method is the MSMPR concept developed by Randolph and Larsen [7]. The method uses the crystal size distribution after the steady state is reached following eq. 1-7.

$$n = n_0 \cdot \exp\left(-\frac{L}{G \cdot \tau}\right) \quad \text{eq. 1-7}$$

The linear growth rate by a characteristic length L is defined by the following equation:

$$G = \frac{dL}{dt} \quad \text{eq. 1-8}$$

1.3.2.2 Face growth rate

The face growth rate s' is the growth velocity of one specific face described by the Miller Indices (hkl-crystal planes). Face growth rates s' can be measured by simple lab experiments with a single crystal. The knowledge of the different face growth rates s' of a crystal is useful to characterize the crystal shape grown from realistic melts. The face growth rate s' is clearly defined by the Miller Indices and only valid for this crystal face.

$$s' = \frac{ds}{dt} \quad \text{eq. 1-9}$$

1.3.2.3 Overall mass growth rate

The overall mass growth rate R_G is defined as the increase of the crystal mass m_s of crystal units from the melt onto the overall crystal surface A_c by time.

$$R_G = \frac{1}{A_c} \cdot \frac{dm_s}{dt} \quad \text{eq. 1-10}$$

With the knowledge of the volume area shape factor k_v , the surface shape factor k_s , the solid density ρ_s , and the linear growth rate G eq. 1-10 can be transformed to:

$$R_G = \frac{1}{L^2 \cdot k_s} \cdot \frac{d(k_v \cdot \rho_s \cdot L^3)}{dt} = \frac{3 \cdot k_v \cdot \rho_s}{k_s} \cdot \frac{dL}{dt} \quad \text{eq. 1-11}$$

$$R_G = \frac{3 \cdot k_v \cdot \rho_s}{k_s} \cdot G$$

1.4 Solid-liquid separation and crystal purification in suspension crystallization

The product purity of a single crystallization step depends on the crystal growth rate which in turn depends on the supercooling and the applied crystallization technique as presented in section 1.2.2. Suspension crystallization offers the opportunity to form pure crystals in a single step.

However, the generation of pure crystals does not necessarily mean a pure product. To ensure this, crystals have to be separated from the mother liquid by a solid-liquid separation and an additional washing device. In case of melt crystallization, the product melt is used partially as the washing liquid to remove the adhering impure mother liquid. To ensure a high overall yield of the crystallization unit, the wash liquid which is loaded with the side components has to be recycled to the crystallizer. An accumulation of side components can be avoided by a defined purge stream of mother liquid out of the crystallization unit. The

required wash liquid which is recycled back to the crystallizer unit and is crystallized again. This increases the energy consumption of the crystallization unit. Figure 1-8 demonstrates all typical steps of a common melt crystallization process.

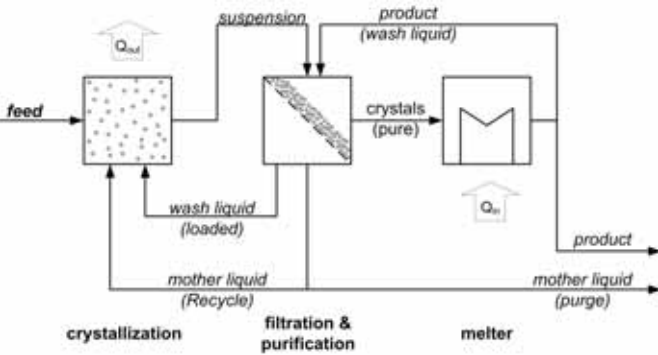


Figure 1-8 Melt crystallization process [8].

On industrial scale, different techniques are available for filtration and washing of the crystals. The differences are in the operation technology. The technology selection depends on the required product purity. Figure 1-9 taken from Ulrich et al. [2] shows a benchmark of different separation technologies and the reachable product qualities as a function of the impurity concentration in the crystallizer. An ideal case is given, if the separation of crystals, the washing step and the melting of the crystals are combined in one device.

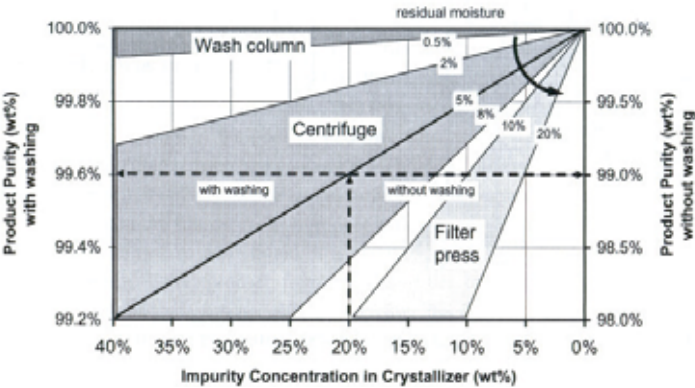


Figure 1-9 Dependence of the product purity on the separation and washing technology [2].

1.4.1 Wash columns

Wash columns offer the opportunity to combine solid-liquid separation, washing, and melting of the crystals in one apparatus. All types of wash columns are designed as cylinders. At least one filter unit inside the cylinder separates the mother liquid from the crystals in such a way that a crystal bed is formed. The crystal bed is transported through the cylindrical column. The type of the crystal bed transport depends on the type of the wash column. In all cases the crystal bed is disintegrated at the end of the column and the disperse crystals are molten in the melt circuit. By closing the product outlet, pure melt is pushed backwards to the crystal bed for a counter current washing. Due to the two occurring equilibrium states of the crystals with the impure mother liquid and the pure melt, respectively, a sharp temperature change occurs. This temperature change is called “wash front” and can be used to control the efficiency of the counter current washing.

Three types of wash columns can be distinguished based on the transport mechanism of the crystal bed. This transport can be under gravity, via mechanical force using a piston or a screw, or hydraulic pressure. Figure 1-10, taken from Ulrich et al. [2], shows the three different types of wash columns classified by their transport principles.

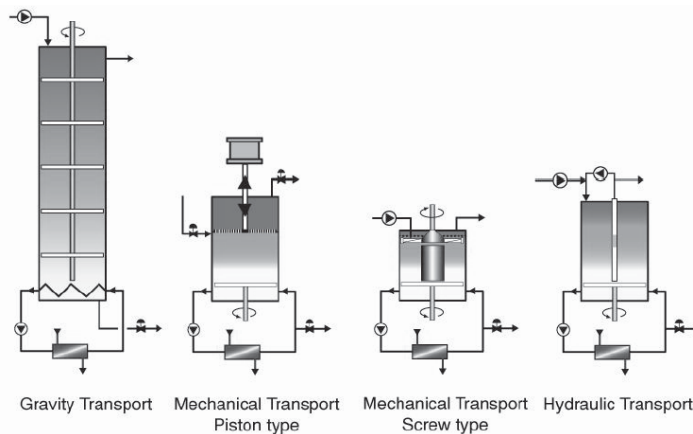


Figure 1-10 Different wash columns classified by their transport principles [2].

The product capacities of all types of wash columns are limited by the crystal bed properties. The properties can be expressed in terms of porosity, permeability, and compressibility. These properties are largely influenced by the occurring crystal morphology and the crystal size distribution. With the help of Darcy's law the liquid velocity v through a porous crystal bed with height h_{Bed} , a liquid pressure p , and a viscosity of the liquid η via the occurring permeability B is given by:

$$v = B \cdot \frac{p}{\eta \cdot h_{Bed}} \quad \text{eq. 1-12}$$

In terms of a changing bed height, eq. 1-12 is reformulated to calculate the occurring pressure drop.

$$\frac{dp}{dh_{Bed}} = \frac{v \cdot \eta}{B} \quad \text{eq. 1-13}$$

Regarding eq. 1-12, it is obvious that the liquid flow through a porous bed at constant parameters in terms of bed height and viscosity is a function of the permeability and the pressure drop. If the permeability decreases by one order of magnitude at a constant pressure drop, the liquid flow decreases by a factor of ten or the cross sectional area has to increase by a factor of 10. It is also possible to compensate this with a higher pressure drop dp . But in case of a compressible crystal bed this may lead to a further permeability and porosity loss following the correlation of Tiller et al. [9]. Eq. 1-14 uses the compressibility coefficient λ for the description of the porosity change and σ for the description of the permeability change:

$$1 + \frac{p}{p_0} = \left(\frac{\varepsilon}{\varepsilon_0} \right)^{\frac{-1}{\lambda}} = \left(\frac{B}{B_0} \right)^{\frac{-1}{\sigma}} \quad \text{eq. 1-14}$$

The interrelations between the permeability, porosity, compressibility, the crystal morphology, and the crystal size distribution will be the main objective of chapter 3 of this thesis. A detailed explanation will be given in that chapter.

1.5 The system acrylic acid

The crystallization of acrylic acid from an aqueous melt is the scope of this thesis. Acrylic acid is the smallest unsaturated carboxylic acid with the chemical formula $C_3H_4O_2$. The official IUPAC declaration is propenoic acid. The chemical structure consists of a vinyl group directly connected to the carboxylic acid group. The molecular structure of acrylic acid is shown in figure 1-11.

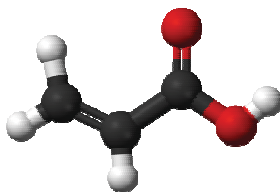


Figure 1-11 Molecular structure of acrylic acid.

The world production scale of acrylic acid in 2006 was around 3.2 mio t/a [1]. Acrylic acid is generally produced by a two-step oxidation of propylene with oxygen via acrolein as an intermediate [10]. Acrylic acid is mainly used for the production of esters as copolymer and for the production of superabsorbent polymers. Due to their application in diapers and sanitary products, the production of superabsorbent polymers requires an ultra high purity. In the recent years, the required purity level has increased consecutively so that it is not economically possible to reach this level by a common distillation step. Therefore, melt crystallization of acrylic acid has achieved great significance to satisfy the market requirements.

1.5.1 Physical properties

Acrylic acid is a clear, colorless liquid. The boiling point at atmospheric pressure is 141.0°C and the melting point is 13.5°C. Acrylic acid forms rectangular crystals in the solid state [11]. Other important physical properties of acrylic acid are listed in table 1-2:

Table 1-2 Physical properties of acrylic acid.

molar mass	72.06 kg/kmol
refractive index n^{20}	1.422
density of the liquid (15°C)	1.056 kg/m ³
viscosity (25°C)	1.149 mPas
heat of vaporization (1013 mbar)	45600 kJ/kmol 632.8 kJ/kg
heat of melting (13°C)	11100 kJ/kmol 154.0 kJ/kg

1.5.2 Solid-liquid phase diagram acrylic acid and water

Chubarov [12] determined the solid-liquid equilibrium of acrylic acid and water, shown in figure 1-12. The eutectic point is at 62 wt% acrylic acid and -11°C .

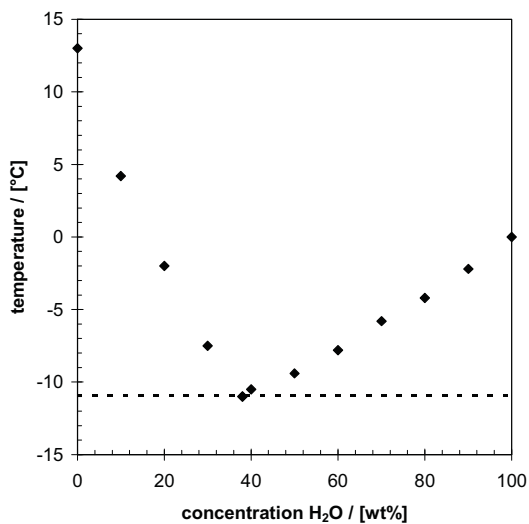


Figure 1-12 Solid-liquid equilibrium [12].

1.6 Objectives

The purification of acrylic acid by melt crystallization offers several advantages in contrast to other separation techniques. Melt crystallization allows a separation at reduced thermal stress coming along with less polymerization and a higher purity level.

In comparison to the currently installed layer crystallization processes the suspension crystallization has several advantages for the separation and purification of acrylic acid on industrial scale. Due to low crystal growth rates, this technique often offers the possibility of a single-step purification. However, the process potential and the resulting purity are always limited by the performance and the efficiency of the downstream solid-liquid separation technology as reported in section 1.4. Wash columns represent an excellent technology to combine the solid-liquid separation with a countercurrent washing device in one single unit. The general feasibility as an end-of-pipe purification technology is reported in different textbooks [8], papers, and company brochures [13].

However, the major parameters influencing the performance and also the resulting scale of a crystallizer and a solid-liquid separation unit are often not reported in literature. Therefore, it is essential to get knowledge of possible occurring problems. For instance the crystal shape can be negatively influenced by different face growth rates of the crystal which are influenced by the containing secondary components and the resulting equilibrium temperature. Different face growth rates could lead in undesirable shapes like needles or plates. Furthermore, the properties of a crystal bed, like permeability and compressibility are influenced by the shape and especially by the occurring particle size distribution. A crystal bed with a low permeability and a high compressibility reduces the capacity of a solid liquid separation and raises the apparatus scale.

Therefore, the main task of the thesis was to investigate the technical feasibility of the acrylic acid separation by suspension melt crystallization at an early stage of the production process from an aqueous melt. This investigation requires the basic knowledge of the crystal morphology and the slurry properties at various conditions. Therefore, the sub objectives of this thesis are:

1. Analysis of the acrylic acid morphology and its dependency on various process parameters, like water content and supercooling of the melt.

2. Investigation of the solid-liquid separation performance at different process conditions, like water content of the melt, supercooling, and pressure difference over the filter cake.
3. Elaboration of possible improvements on the crystallization process to extend the operation window and to increase the yield of the crystallization step.
4. Benchmark analysis of the process improvement with one of the common industrial process.

1.7 Outline of the thesis

The thesis starts in chapter 2 with the morphology measurements of acrylic acid crystals in a single crystal growth cell. The influence of water as a solute and of different supersaturation in terms of supercooling on the morphology was investigated. Additionally, a possible face growth mechanism explaining the cavity appearance on a certain face is postulated.

In chapter 3, the influence of the occurring morphology of acrylic acid crystals on the filtration behavior of a crystal bed was examined. Continuous MSMPR experiments under different conditions were carried out to generate required suspensions. The characterization of the suspensions in relation to the morphologies and the crystal size distributions accompanied the MSMPR experiments. The permeability and the compressibility behavior of the generated suspension were determined by filtration experiments. Additionally, a model was developed to predict the filtration behavior of an industrial solid-liquid separation step using simple process variables.

Chapter 4 deals with the improvement of the filtration behavior due to the limited operation range shown in chapter 3. Ice crystals, generated at the eutectic point, were identified to act as permeability and compressibility enhancers. The influence of different fractions of ice crystals on the permeability and compressibility was investigated systematically by simple filtration tests.

The screening of a solvent to establish a novel eutectic crystallization step at a maximum yield is the purpose of chapter 5. Therefore, a structured solvent screening method was developed for a rapid identification of possible candidates to increase the yield of a eutectic crystallization. For a fast validation, an experimental stage gate process was developed to come up with the required information of each stage at a minimum work load. The experimental stage gate bases completely on a thermal analysis using Differential Scanning Calorimetry. Three different organic solvents were identified for this purpose. The ternary solid-liquid phase diagrams of acrylic acid, water and each of the three solvents were determined and a first qualitative and quantitative validation of the solvents' applicability use was carried out.

In chapter 6, the novel eutectic crystallization process is compared with a conventional industrial downstream. Acetic acid was used as a solvent to increase the yield, because it is a secondary product of the reaction anyway [14]. The technology benchmark considers variables like the specific energy demand, the quantitative apparatus sizes, and the qualitative evaluation regarding reduction of the possible polymerization due to thermal load.

Nomenclature**Notation**

A_c	crystal surface	[m ²]
B	permeability	[m ²]
G	linear crystal growth rate	[m/s]
ΔG	free enthalpy change	[J/mol]
ΔH_m	heat of fusion	[J/mol]
h_{Bed}	bed height	[m]
k_S	surface shape factor	[-]
k_V	volume area shape factor	[-]
L	characteristic length	[m]
m_s	crystal mass	[kg]
p	pressure	[Pa]
R	gas constant	[J/(mol·K)]
R_G	overall mass growth rate	[kg/(m ² ·s)]
s'	face growth rate	[m/s]
s	characteristic length of a specific face	[m]
t	time	[s]
T	temperature	[K]
v	velocity of a liquid	[m/s]
x	mass fraction	[wt%]

Greek symbols

β	supercooling	[-]
δ	boundary layer	[m]
ε	porosity	[%]
η	viscosity	[Pa·s]
λ	compressibility coefficient for porosity	[-]
τ	residence time	[s]
μ	chemical potential	[J/mol]
ρ	density	[kg/m ³]
σ	compressibility coefficient for permeability	[-]

Subscripts & Superscripts

a	actual
EP	eutectic point
e	equilibrium state
F	feed
l	liquid phase
mass	mass
s	solid phase
thermal	thermal
0	initial state

References

- [1] PERP Product Reports, Nexant, Inc., San Francisco, California, USA, 2006.
- [2] Ulrich J.; Glade H.; Melt Crystallization – Fundamentals, Equipment, and Application, Shaker-Verlag, Aachen, 2003.
- [3] Matsuoka, M.; Solid-liquid Equilibria of Binary Organic Mixtures, Bunri Gijutsu; Separation Process Engineering, 1977, pp245-249.
- [4] Tiller, W. A.; Rutter, J. W.; Jackson, K. A.; Chalmers, B.; The redistribution of solute atoms during the solidification of metals, Acta Met. Vol. 1, 1953, pp428-437.
- [5] Burton, W. K.; Cabrera, A.; Frank, F. C.; The Growth of Crystals and the Equilibrium Structure of their Surfaces, Phil. Trans. Roy. Soc., 1951, Vol. 243, p299-358.
- [6] Bennema, P; Gilmer, G. H.; Kinetics of Crystal Growth, Crystal Growth: An Introduction, P. Hartmann ed., Amsterdam, North Holland, 1973, pp263-357.
- [7] Randolph, A.; Larson, M.; Theory of Particulate Processes, San Diego, Academic Press Inc., 1988.
- [8] Arkenbout, G. F.: Melt Crystallization Technology, Technomic Publishing Company, Inc., Lancaster, 1995.
- [9] Tiller, F.; Yeh, C. S.; The Role of Porosity in Filtration, AIChE J., 1999, Vol. 3 (8), p1241.
- [10] Ullmann's Encyclopedia of Industrial Chemistry, Acrylic Acid and Derivatives, Wiley-VCH Verlag, Weinheim, Germany, 2010, 7th Edition, pp1-19.

- [11] Boese, R.; Blaser D.; Steller I.; Latz R.; Baumen A.; *Acta Crystallogr., Sect. C: Cryst. Struct. Commun.*, 1995, Vol. 55, 9900006.
- [12] Chubarov, G. A.; Danov, S. M.; *Liquid-Solid Equilibrium in the Systems Acrylic Acid - Water, Acrylic Acid - Acetic Acid, and Methacrylic Acid – Water*, *J. Appl. Chem., USSR*, 1978, Vol. 51 (8), pp1796-1798.
- [13] TNO Environment, Energy and Process Innovation, company brochure, 2006.
- [14] Machhammer, O.; Dams, A.; Eck, B.; Proll, T.; *Verfahren zur Reinigung von Acrylsaeure und Methacrylsaeure*, BASF Aktiengesellschaft, 1996, German Patent DE 19606877A1.

CHAPTER 2

INFLUENCE OF SUPERCOOLING AND WATER CONTENT ON CRYSTAL MORPHOLOGY OF ACRYLIC ACID

Abstract

The morphology of single acrylic acid crystals in a growth cell is studied as function of the water content and of the supercooling β in the melt. The intention is to measure absolute growth rates of the different crystal faces and the resulting aspect ratio of the crystals at different process conditions to provide a basis for the design of suspension crystallization process.

The presence of water in the melt of acrylic acid induces the formation of hollow cavities at the crystal extremities and increases the propensity to form a needle-like crystal habit. Further, the higher the supercooling, the higher the tendency to form needle-like crystals and larger cavities.

The measured growth rates of the developed faces are simulated by using the birth and spread model [6]. A model of the occurring growth mechanism which also involves the formation of a hollow cavity at the crystal extremities is developed.

Based on the measured data, a general prediction of the filtration behavior is possible and a pre-selection of rough process parameters can be made.

Published in Crystal Growth & Design, 2009, Vol. 9 (4), pp. 2000–2007.

2.1 Introduction

For the industrial acrylic acid production melt crystallization is an important separation technique to reach required high-end purity levels. It suffices industry's demands like high selectivity, low energy demand, eco friendliness, etc. This highly selective process often results in pure crystals which should be separated from their mother liquid. Adhered mother liquid on the crystal surface requires an additional downstream washing step.

For design and scale-up of all known solid-liquid separation processes, the knowledge of filtration parameters is necessary. They depend on crystal size distribution and crystal shape. This work provides an insight of how the shape of acrylic acid crystals evolves at different conditions and makes possible general prediction of filtration behavior.

2.2 State of knowledge

2.2.1 Acrylic acid crystal structure

The crystal structure of acrylic acid was resolved by Boese et al. [2] at a temperature of 125 K and is published in the Cambridge crystal structure database. Acrylic acid crystallizes in a centered orthorhombic Bravais system, space group "Ibam" ($z=8$). The crystallographic parameters are $a=9.952$ Å, $b=11.767$ Å and $c=6.206$ Å. The complete theoretical structure resolved by Boese et al. [2] is shown in figure 2-1. The morphology of the crystal is dominated by the main faces $\{110\}$, $\{002\}$, and $\{121\}$ as shown in figure 2-2.

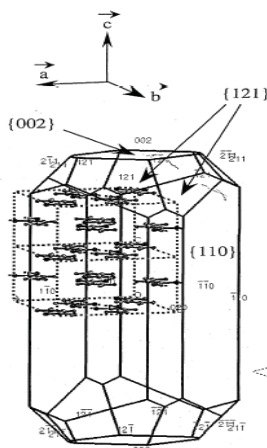


Figure 2-1 3D view of an acrylic acid crystal [2].

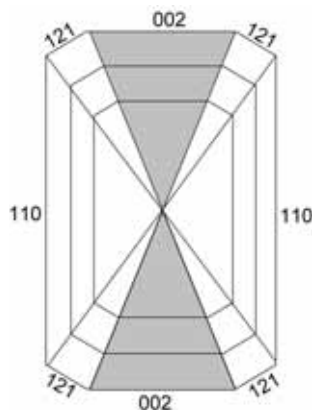


Figure 2-2 2D view of an acrylic acid crystal [2].

The BDFH-method describes the correlation between importance of a crystal face and its interplanar distance. Prywer [3] stated that the larger the interplanar distance, the more morphologically important is the corresponding crystal face. Therefore, a crystal growing under realistic conditions possesses a limited number of faces which are the ones growing most slowly. Hence, only the faces that are morphologically important and do not disappear fast, as faces $\{110\}$, $\{121\}$, and $\{002\}$, will be considered. Face $\{121\}$ is the fastest growing one of the mentioned three faces. Based on its outgrowing character, it disappears quickly and is observed only in the beginning of growth processes. The other faces resolved by Boese et al. [2] were not found during growth experiments.

Sections 2.2.2 and 2.2.3 summarize the morphology of acrylic acid in presence of water as an impurity based on work of Nordhoff et al. [1]. First, chemical composition of various faces using Cerius² Software is explained. Then the effect of water as an impurity on the morphology is scrutinized.

2.2.2 Chemical composition of the faces

The influence of polar secondary components on crystal growth of predominant faces and on the resulting morphology development can be understood, if the chemical composition of these faces is analyzed. The chemical composition of the developed faces of acrylic acid is described by Nordhoff et al. [1] based on the structure resolved by Boese et al. [2].

2.2.2.1 Face {110}:

The face {110} has polar moieties on whole of the surface [1]. Hydroxyl groups are oriented perpendicular to the surface and therefore it is considered as a polar face. The growth rate of this face can be affected by the presence of polar substances in the surrounding.

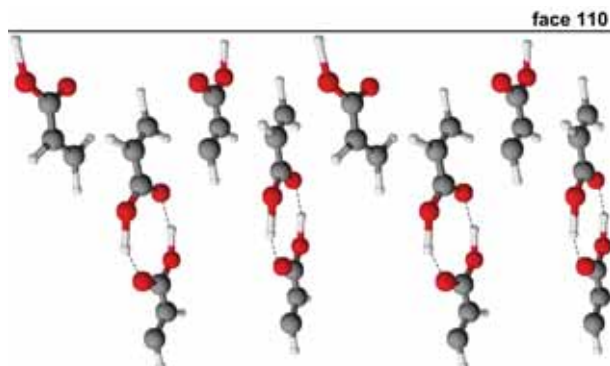


Figure 2-3 Polar moieties on face {110} surface.

2.2.2.2 Face {002}:

Face {002} consists of acrylic acid molecules associated in the form of dimers which are held together by hydrogen bonds as shown in figure 2-4 [1]. They are aligned in planes parallel to the face as shown in figure 2-4.

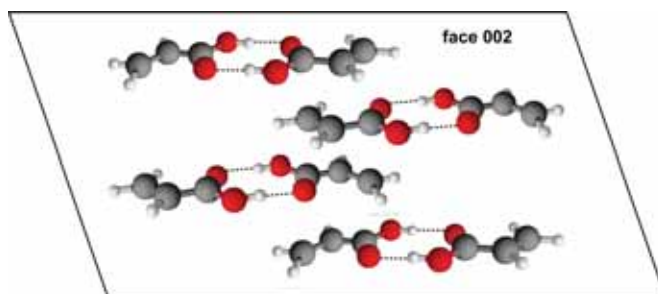


Figure 2-4 Acrylic acid dimers on face {002}.

The dimers, stacking layer by layer on the surface, are held together by Van der Waals forces and are spread over the surface. In this case, carboxylic groups as well as hydroxyl groups are implicated in dimer association. The hydroxyl groups are less available than on the face {110}. Nevertheless, polar parts of the surface are easily accessible and polar substances can be easily adsorbed onto the surface. This face can be seen as a semi polar surface constituted by polar and nonpolar regions. The main structural feature of an acrylic

acid crystal is the presence of planes parallel to face $\{002\}$ and constituted by coplanar dimer motifs. These two acrylic acid molecules connected together by two hydrogen bonds correspond to the motif of the mesh. Each motif is joined to its neighbors by Van der Waals contacts and molecular planes are also held together by means of Van der Waals forces.

2.2.2.3 Face $\{121\}$:

Face $\{121\}$ is a nonpolar surface constituted mainly of the ethylene part of acrylic acid. Polar substances are strongly repulsed by these nonpolar moieties and hence there should be only very little influence on this face. Caused by highest face index and a high lattice density plane, it grows very fast and disappears quickly as mentioned in section 2.2.1. This fact was verified during the experiments and is described in this paper. The qualitative illustration of this face is quite difficult and therefore not presented within this chapter.

2.2.3 Morphology development in presence of water

Nordhoff et al. [1] discovered that the crystal shape and habit of acrylic acid crystals in the presence of water differed substantially from crystal shape and habit published by Boese et al. [2]. A crystal shape with a cavity appearing on face $\{002\}$ was observed. The authors came up with calculations of face bounding energies between water and acrylic acid to explain competitive interactions between the surface integration of new crystal units during growth and a water blockage of the crystal faces, respectively.

Figure 2-5 shows a representative drawing and a picture of an acrylic acid crystal with cavities, grown from a melt with 5 wt% water.

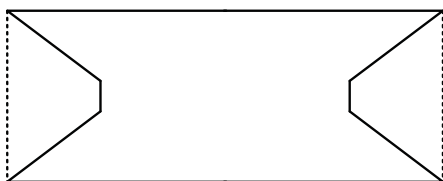


Figure 2-5 Acrylic acid crystal with cavities grown from a melt with 5 wt% water.

2.2.3.1 Influence of face bounding energies on surface integration processes

As already mentioned in section 2.2.2.3, face $\{121\}$ is nonpolar in nature. Therefore, it is assumed that water does not have any impact on it.

From chemical composition of the other faces, it appears obvious that face $\{110\}$ is preferred for adsorption of water molecules caused by its perpendicular orientated hydroxyl groups.

Bonding of water molecules via hydrogen bonds with hydroxyl groups should be stronger than the one with a semi polar face. In addition, calculated docking energies of one water molecule on different faces confirm this theory. Nordhoff et al. [1] calculated a docking energy of 14.65 kJ/mol and 41.05 kJ/mol for face {002} and {110} respectively.

In contrast the stronger hydrophilic character of the {110} face, it was stated by Nordhoff et al. [1] that on face {002} water molecules create a network strongly bounded to the surface by several hydrogen bonds. This water molecule network would pose additional resistance for acrylic acid molecules to stack on face {002}. Due to this, the mass growth rate of this face would be reduced drastically. Considering the surface binding energies only, face {110} should be more affected by the presence of water than face {002}. An analysis of the surface area which is blocked by one hydrogen bonded water molecule reveals that blockage is nine times higher in the case of face {002} than in the case of face {110} [1]. This fact leads to the conclusion that water has a stronger influence on face {002} than on face {001} as expected from the calculated docking energies of the different faces.

2.2.4 Extension of the theory for surface integration processes

In section 2.2.3 the theoretical approach of Nordhoff et al. [1] is described. It bases on bonding energy relations between water and acrylic acid. The authors give an idea, why crystal shape looks different from that one proposed by Bose et al. [2], but they were not able to come up with any growth mechanism to explain the cavity development. If a strong water network on face {002} should be the only reason for a cavity formation, a monomolecular layer induced by a very low impurity concentration would be sufficient to influence growth behavior, but the opposite is the case. The higher the water concentration, the bigger are the changes in crystal morphology. Therefore, there must be at least one additional effect induced by the presence and particularly the concentration of water molecules in the melt.

Nordhoff et al. [1] disregarded a second possible cut through the crystal which seems to be more probable. Using the Cerius² Software it is possible to establish another face {110}. This cut parallel to the previous one changes its chemical composition and makes it quite interesting for the prediction of the surface integration process of water on this face.

An additional influence on crystal growth and growth rates of different faces could be caused by changing chemical and physical properties of the liquid phase in presence of water.

The following sections describe a hypothetical prediction of another composition of face {110}, the changes of the liquid phase composition and a theoretical view of physical properties of the melt which should have a major influence on crystal growth.

2.2.4.1 Different chemical composition of face {110}

Nordhoff et al. [1] stated that face {110} has polar moieties all over. If face {110} is investigated using Cerious², it becomes obvious that it is also possible to cut the crystal on a different plane parallel to the one described by Nordhoff. Hence a completely different chemical composition and polarity of face {110} is given. The flat surface character changes into a wavier one which exist of dimers established perpendicularly to the surface. This wavy structure can be explained from the front end of the parallel planar dimer layers of face {002} as already shown in figure 2-4. If face {110}, seen as the front side of face {002}, is analyzed in detail, it is clear that it consists of the terminal nonpolar ethylene groups at the wave peaks and of polar hydroxyl groups of the dimer bonding down in the wave trough.

If the chemical composition predicted by Nordhoff et al. [1] is compared with that one predicted in this section, it is obvious that a planar cut through the crystal along hydroxyl groups being part of dimer bonding as stated by Nordhoff et al. [1] is more energy extensive than a wavy cut as described above in this section. If this fact is taken into account, an adsorption of water molecules on the flat face {002} with polar and nonpolar regions is easier than on a wavy one like {110}. If a polar water molecule should adsorb on this wavy face {110}, a water molecule would have to pass peaks of nonpolar regions before docking on a polar dimer bonding with complete nonpolar ethylene neighbor groups. An approach of the possible wavy structure of face {110} is shown in figure 2-6.

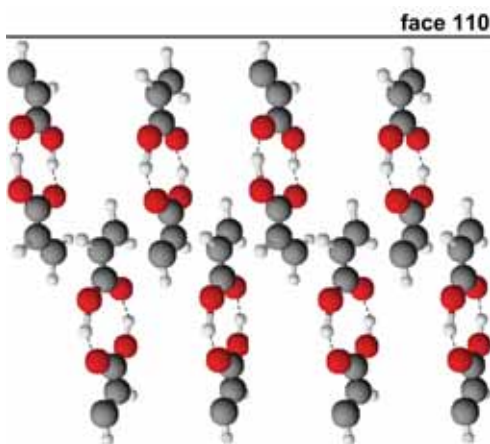


Figure 2-6 Alternative chemical composition of face {110}.

Considering the more nonpolar chemical composition of face {110} the higher affinity of water to adsorb on face {002} can be clearly understood. Therefore, it is possible to dispose a new series of face polarities shown below, incipient at the lowest polarity as well as according to the affinity of water to it.

$$\{121\} < \{110\} < \{002\}$$

2.2.4.2 Potential influence of the liquid phase composition on crystal growth of acrylic acid

Boese et al. [2] figured out that face $\{002\}$ is a semi polar face and consists out of acrylic acid molecules associated in forms of dimers which are oriented in planes parallel to it. This fact leads to the assumption that growth of face $\{002\}$ is only possible, if dimers are already formed in the liquid phase. Therefore, it is important to have a look at possible chemical composition of the liquid phase and possible intra molecular interactions under influence of water.

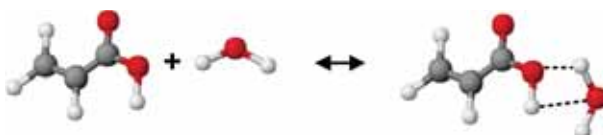


Figure 2-7 Hydrate formation out of acrylic acid and water.

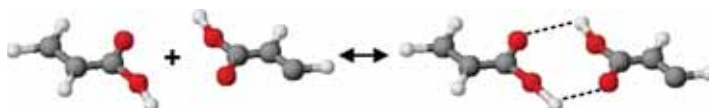


Figure 2-8 Dimer formation out of two acrylic acid molecules.

As shown in figure 2-7 and figure 2-8, there are competitive interactions in presence of water between forming associated dimers and hydrates from monomers and water molecules. Depending on the specific equilibrium constants of mentioned molecular interactions, it should be obvious that the concentration of needed dimers to implement on face $\{002\}$ decreases with an increasing water content.

Therefore, it is necessary to extend the theory postulated by Nordhoff et al. [1]. Beside the fact that water molecules should form a strong network on face $\{002\}$ caused by its higher polarity than that of face $\{110\}$, a second fact has to be taken into account. If increasing water content generates a competitive formation of hydrates in the liquid phase and if this formation of hydrates is more favored than that one of dimers, the concentration of required dimers for growth face $\{002\}$ decreases.

2.2.4.3 Potential influence of physical properties on crystal growth rate of acrylic acid

For an estimation of the overall growth rate trends under influence of water, it is necessary to consider physical data which are responsible for heat and mass transfer at the resulting solid-liquid equilibrium temperature. The estimation will give a rough indicator, if overall growth rates of the faces will be accelerated or slowed down by the effect of water due to decreasing equilibrium temperatures. The calculations will not be used to estimate crystal morphology, e.g. development of aspect ratio.

The required estimation will base on equations for heat and mass transfer coefficients of a liquid flow along a flat solid surface using the dimensionless numbers of Nusselt and Sherwood, respectively.

Both descriptions of transport phenomena are functions of the occurring viscosity of the liquid phase. Viscosity of pure acrylic acid is approximately three times higher than of pure water. Therefore, viscosity decreases with increasing water content. It should be noted that the increase in viscosity due to decreasing equilibrium temperature is compensated by presence of water in the system.

Calculations of the occurring heat transfer coefficient α are carried out by using the equation for the Nusselt number [eq. 2-1] suggested by Pohlhausen [10] und Krouzhiline [11]. The equation is valid for a laminar liquid flow induced by thermal convection along a flat solid surface. The required characteristic length L is set to a nominal crystal size of 500 μm . The characteristic velocity v is set approximately to 0.001 m/s representing a thermal convective liquid flow along the crystal surface. The velocity v is roughly calculated based on the occurring temperature differences [10]. However, it will not be presented in this chapter.

$$Nu = 0.663 \cdot Re^{\frac{1}{2}} \cdot Pr^{\frac{1}{3}} \quad \text{eq. 2-1}$$

The used dimensionless numbers are defined as follows:

$$Nu = \frac{\alpha \cdot L}{\eta} \quad \text{eq. 2-2}$$

$$Re = \frac{v \cdot L \cdot \rho}{\eta} \quad \text{eq. 2-3}$$

$$Pr = \frac{\eta \cdot c_p}{\lambda} \quad \text{eq. 2-4}$$

If eq. 2-2 up to eq. 2-4 are set into eq. 2-1, it is possible to convert it into an expression for the required heat transfer coefficient α .

$$\alpha = \frac{0.664 \cdot \lambda}{L} \cdot \left(\frac{v \cdot L \cdot \rho}{\eta} \right)^{\frac{1}{2}} \cdot \left(\frac{\eta \cdot c_p}{\lambda} \right)^{\frac{1}{3}} \quad \text{eq. 2-5}$$

The conclusion of analogy approves it to adopt the criteria equation for the Nusselt number for approximate calculations of the mass transfer coefficient ω . The characteristic length and velocity are equal.

$$Sh = 0.664 \cdot Re^{0.5} \cdot Sc^{\frac{1}{3}} \quad \text{eq. 2-6}$$

The used dimensionless numbers are defined as follows:

$$Sh = \frac{\omega \cdot L}{D_{(AA \ H_2O)}} \quad \text{eq. 2-7}$$

$$Re = \frac{v \cdot L \cdot \rho}{\eta} \quad \text{eq. 2-8}$$

$$Sc = \frac{\eta}{\rho \cdot D_{(AA \ H_2O)}} \quad \text{eq. 2-9}$$

If eq. 2-7 up to eq. 2-9 are set into eq. 2-6, it is possible to convert it into an expression for required mass transfer coefficient ω .

$$\omega = \frac{0.664 \cdot D_{(AA \ H_2O)}}{L} \cdot \left(\frac{v \cdot L \cdot \rho}{\eta} \right)^{\frac{1}{2}} \cdot \left(\frac{\eta}{\rho \cdot D_{(AA \ H_2O)}} \right)^{\frac{1}{3}} \quad \text{eq. 2-10}$$

The diffusivity coefficient of the system is calculated according to the equation suggested by Wilke [9].

$$D_{AA \ H_2O} = 7.4 \times 10^{-8} \left(\frac{(\varphi_{H_2O} M_{H_2O})^{1/2} T}{\eta V_{AA}^{0.6}} \right) \quad \text{eq. 2-11}$$

The association parameter φ in eq. 2-11 is set to 2.6.

With the converted eq. 2-10 and eq. 2-5, it is possible to calculate approximate values for heat and mass transfer coefficients as a function of the water content. The physical data used for these equations are taken at the equilibrium temperature belonging to the composition of the melt. A plot of the changing coefficients is shown in figure 2-9.

Mass and heat transfer coefficients increase with increasing water content in spite of a decreasing solid-liquid equilibrium temperature. The values of the heat transfer coefficient increase linearly. The values for mass transfer increase strongly at low water contents and converge to a limit afterwards.

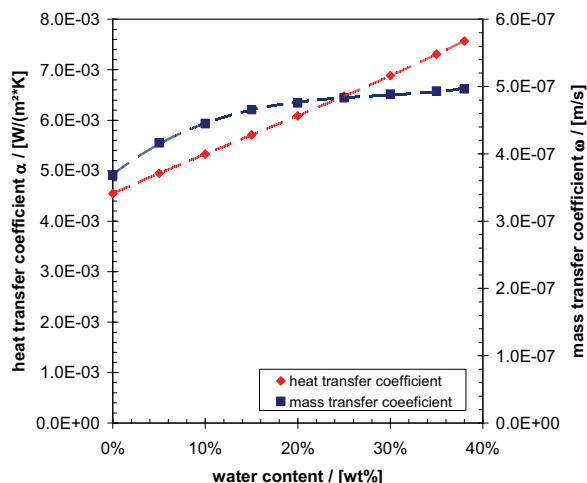


Figure 2-9 Heat and mass transfer coefficients at equilibrium conditions.

2.2.5 Prediction of crystal face growth rates

For a prediction of crystal shape and crystal growth rate trends under influence of water and supercooling, it is necessary to summarize all facts of section 2.2.

1. Nordhoff et al. [1] stated a stronger water network on face {002} than on {110} based on surface area calculations. Additionally, a second and more favorable possibility to cut the crystal along face {110} was proposed in this chapter. The formation of a water network on face {002} is more favored than on face {110} because of its polarity differences. If the monomolecular water network is formed on face {002} it is less energy attractive to integrate new acrylic acid units on the surface.
2. In this chapter it is postulated that there is a competitive formation of hydrates to the formation of dimers which are needed as crystal units for integration on face {002}, too.

Considering these two arguments, growth of face {002} should be reduced completely in the presence of water so that major growth takes place on faces {121} and {110}. Face {121} is nonpolar as mentioned in section 2.2.2.3 and therefore its growth rate should increase with

the increase in the polarity of the melt. If this theory holds, the growth rates should be in the following sequence:

$$G_{121} > G_{110} > G_{002}$$

A reliable qualitative prediction of the growth rates can be done, if the approximations of heat and mass transfer are regarded. Heat and mass transfer coefficients seem to improve with an increasing water concentration. This leads to the conclusion that growth rates of faces which are not blocked by water, increase. It has to be mentioned that mass transfer coefficients converge to a certain value, whereas the heat transfer coefficient improves further on, because of improving values for heat capacity and conductivity.

If predictions of crystal shape and growth rate trends are combined, it is possible to make a rough qualitative estimation of the growth rate experiments at different water contents as shown in table 2-1.

Table 2-1 Qualitative expected face growth rate trends.

	water content / [wt%]			
face	0	5	10	15
002	++	-	-	-
110	+	+	++	++
121	+	++	+++	++++

2.3 Experimental

2.3.1 Equipment and setup

The apparatus consisted of single crystal growth cell, thermostat, microscope, camera, computer, thermocouple, and a source of plane polarized light. All growth experiments were carried out in a single crystal growth cell. The cell had a cavity in the centre between two glass windows.

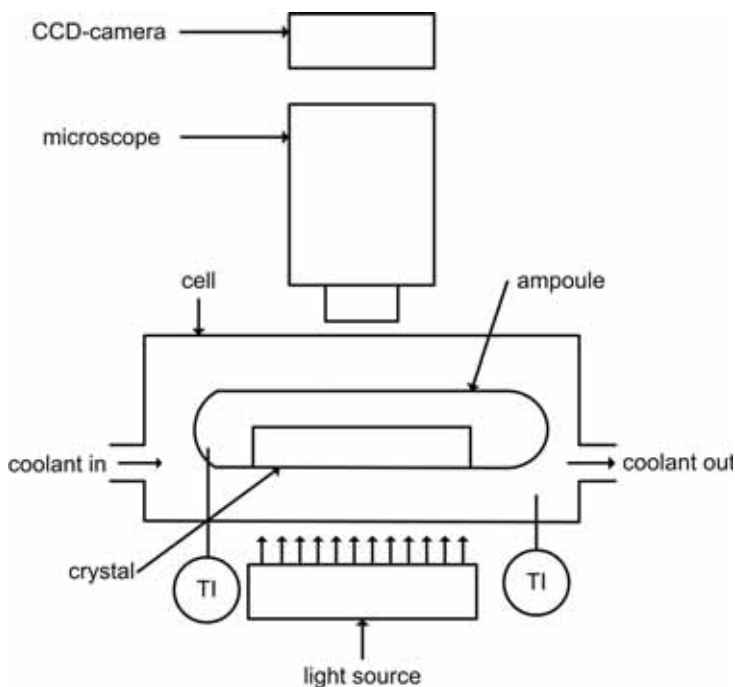


Figure 2-10 Schematic draft of used experimental single crystal growth cell setup.

The ampoule is 1 cm in width, approximately 0.5 cm in height and 3 cm in length with a volume of around 15 ml. Experiments were carried out in batch mode. The cooling of the cell was arranged by a thermostat circuit around the cavity.

The temperature in the cavity and around was monitored by two thermocouples with a diameter of 1.3 mm. The cell was illuminated with the help of a lamp, emitting plane polarized light, placed below the growth cell. Online monitoring of crystal growth was carried out via a CCD-camera connected to a computer working with AxioVisio LE 4.5 for online picture analysis.

2.3.2 Experimental procedure

The single crystal growth cell was fed with the mixture of acrylic acid and water in desired proportion. For start up, the complete melt inside the cell was thoroughly crystallized. Then the temperature of the cell was increased again until a single crystal was obtained. This single crystal was allowed to stay at the melting point for approximately 20 minutes and then the cell was cooled again to a desired temperature. The working procedure is analogue to that one described by Jansens [5]. This temperature was fixed based on the solid-liquid equilibrium diagram to maintain a desired driving force.

The driving force is expressed in terms of the dimensionless supercooling β . Calculations for supercooling were made by applying eq. 2-12 which is usually used in melt crystallization. This equation is obtained by simplifying definition of driving force based on chemical potentials. The derivation of this equation is explained in chapter 1.

$$\beta = \frac{\Delta H_m}{R \cdot T_m^2} \cdot \Delta T \quad \text{eq. 2-12}$$

Growing crystals were photographed at fixed time intervals. Images were transferred online to the computer. With the help of AxioVisio LE 4.5 crystal lengths and widths of the crystal were measured. Differences in length of each observed face were related to time. Herewith, it was possible to measure optical growth rates of two faces at water contents of 0 wt%, 5 wt%, 10 wt%, and 15 wt%.

2.3.3 Experimental results

2.3.3.1 Growth rate measurements

One of the major factors influencing morphology of acrylic acid crystals is the presence of water as an impurity in the system. Water alters and reduces the growth rate of face {002} which leads to the formation of cavities. Nevertheless, within all experiments fastest growth took place at the outer edge of face {002}. The images suggest that crystals growth takes place on face {002}.

However, a closer inspection learns that visible growth perpendicular to face {002} is due to growth of faces {121} at the outer edges surrounding face {002}. Therefore, the measured values of growth rates at the outer edges of face {002} were used as growth rates of faces {121}.

Figure 2-11 and figure 2-12 show the measured growth rates for face {110} and face {121}, respectively, as function of supercooling β and water concentration.

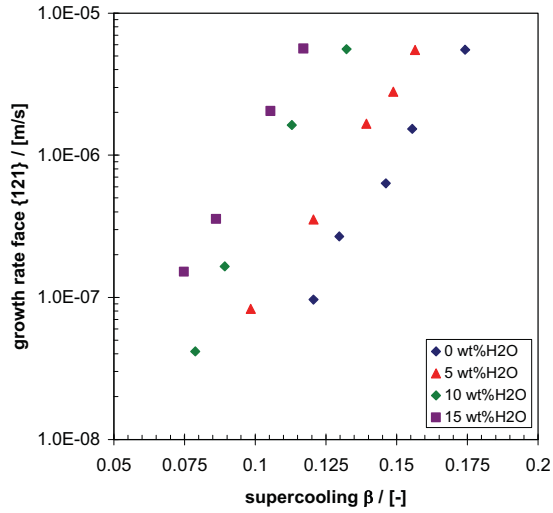


Figure 2-11 Optical growth rates of face {121}.

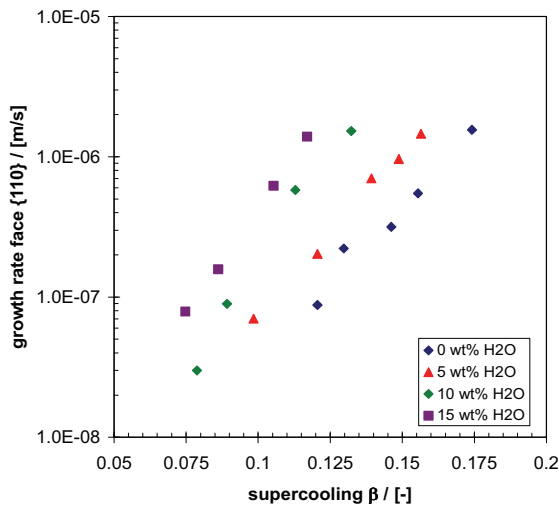


Figure 2-12 Optical growth rates of face {110}.

It is obvious that for all acrylic acid concentrations the growth rate of face {110} is lower than that of face {121}. The growth rates show a strong exponentially dependency on supercooling β .

A direct relation between growth rates of both faces could provide useful information with regards to overall crystal morphology. Figure 2-13 shows measured growth relations as a function of water and supercooling β . Relative growth rates increase exponentially with increasing supercooling. This indicates that the linear growth rate of face {121} is much higher than that of face {110}. The higher the linear growth rate of face {121} compared to {110} the more elongated are the crystals. This shape evolution of the crystals may have a strong influence on the performance of a downstream solid-liquid separation.

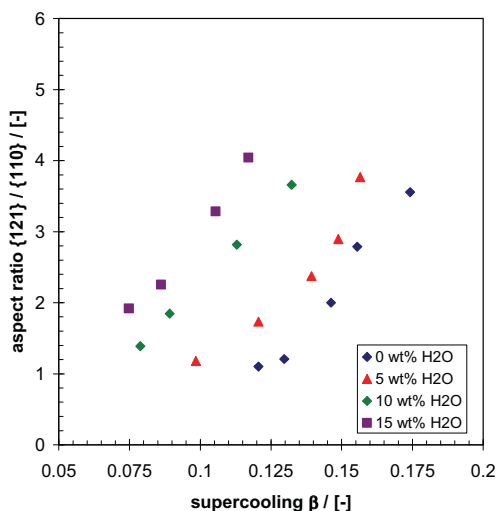


Figure 2-13 Aspect ratio as a function of supercooling and water content.

2.3.3.2 Cavity angle measurements

As described in section 2.3.3.1, if water content and supercooling β increases, a cavity starts appearing at the crystal extremities. It was observed that the cavity angle showed variations with supercooling β and water content. For a typically observed acrylic acid crystal with a cavity, the cavity angle γ was defined as shown in figure 2-14.

The values of γ were taken from all pictures and plotted against supercooling β at different water contents as shown in figure 2-15.

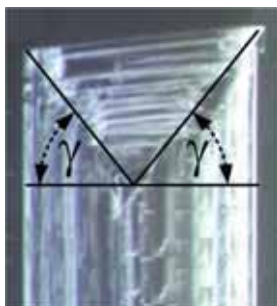


Figure 2-14 Definition of the cavity angle γ .

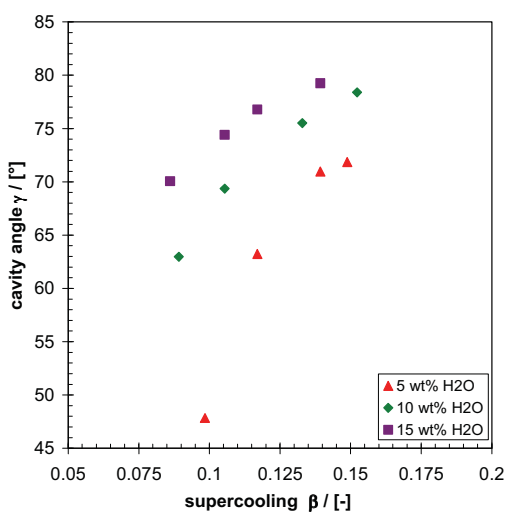


Figure 2-15 Cavity angle γ as a function of water content and supercooling.

As can be seen from figure 2-15, cavity angle γ increases with increasing supercooling and water content. At same values of supercooling β , the cavity angle increases with increase in the water content.

2.3.4 Discussion of evaluated results

Comparing the predictions of growth rate trends and crystal shape discussed in paragraph 2.2.5 with the experimental ones, it is obvious that they are in line. Growth rate trends follow qualitatively the predicted ones noted in table 2-1.

Apparently, the optical views on the growing crystals from an aqueous melt suggest that growth of face {002} takes place. If a strong water network is formed on this face, an immediate formation of a monomolecular layer of water should be sufficient to alter and

inhibit growth of face $\{002\}$. Therefore, the water network on these faces initiates the forming of a different crystal habit compared to the one proposed by Boese et al. [2]. However, this immediate blockage by water cannot be responsible for the outcome of an elongate crystal habit. For this purpose, growths of the other faces are probably responsible. The increased polarity of the melt and the improved heat and mass transfer conditions support this mechanism which was unknown until now.

2.4 Crystal morphology development – a qualitative approach

Based on the theory postulated in section 2.3.4, growth in the direction perpendicular to the blocked face $\{002\}$ is caused by growth of face $\{121\}$ at the outer edge of the crystal. A mechanism governing it can be described as follows. It will be explained based on a quarter section of a crystal shown figure 2-16. It has to be kept in mind that the growth mechanism takes place on a molecular scale, but to demonstrate the mechanism, the explanation is enhanced.

1. Growth starts up from a basic crystal shown in (1). This crystal reveals an initial shape with all developed faces. Faces $\{002\}$ are completely blocked with water.
 2. When supercooling is induced, growth of non-blocked faces starts and fastest growing faces $\{121\}$ disappear in a taper form as shown in (2). Any newly formed faces $\{002\}$ will be blocked again immediately by a strong water network.
 3. Growth of faces $\{110\}$ is proceeding step by step and new faces $\{121\}$ are generated continuously as shown in (3).
 4. New generated faces $\{121\}$ further disappear in a taper form as shown in position (4).
- The postulated mechanism is valid, if growth of faces $\{121\}$ takes place perpendicular to it and is limited by another growing face like face $\{110\}$.

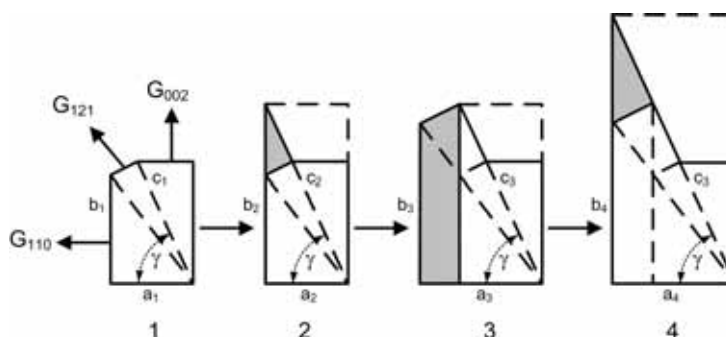


Figure 2-16 Schematic drawing of crystal morphology development.

It was demonstrated in section 2.3.3.2 that the angle of the cavity γ is a function of supercooling. Therefore, it should also be a function of face growth rates. If figure 2-13 is considered, angle γ must be a tangent function of growth rates of pseudo face {121} and {110}. To verify this growth mechanism with the help of the mentioned angle correlation, it is necessary to analyze and model growth rates of each face. With the help of modeled face growth rates, the cavity angle should be calculated and compared with angle values received from experiments.

2.4.1 Growth rate analysis and modeling

Considering the theory of paragraph 2.4, it should be helpful to investigate which growth mechanisms appear on these faces. A fit of the measured growth rates to well-known equations for different mechanisms show that growth of both faces seems to follow a birth and spread mechanism. Therefore, growth can be modeled via the equation proposed by Bennema and Gilmer [6]. Herein, growth rate depends on supercooling at the interface with two constant parameters A and B.

$$G = A \cdot \beta^{\left(\frac{5}{6}\right)} \cdot \exp\left(\frac{-B}{\beta}\right) \quad \text{eq. 2-13}$$

Table 2-2 summarizes the results of a parameter analysis for the faces following the birth and spread mechanism.

Table 2-2 Results of parameter analysis for faces {110} and {121}.

parameter			A		B	
x_{AA}	equilibrium temperature T_m		121	110	121	110
[wt%]	[°C]	[K]				
100	12.8	285.95	0.055	0.0009	1.39	0.90
95	8.5	281.65	0.013	0.0006	1.03	0.72
90	4.6	277.75	0.011	0.0006	0.87	0.69
85	1	274.15	0.009	0.0006	0.68	0.52

In contrary to the proposed theory of Bennema and Gilmer [6] an analysis of both parameters shows that the parameters A and B are not constant. It seems that water influences both faces, $\{110\}$ and $\{121\}$. This is demonstrated by a value jump of parameter A from pure acrylic acid to a diluted mixture. Therefore, it should be useful to extend eq. 2-13 for melt crystallization of acrylic acid as follows:

$$G(\beta, x_{AA}) = A(x_{AA}) \cdot \beta^{\left(\frac{5}{6}\right)} \cdot \exp\left(\frac{-B(x_{AA})}{\beta}\right) \quad \text{eq. 2-14}$$

The mentioned jump of A is probably caused by the influence of the water network formation on both faces as described in section 2.2.3. It has to be mentioned that it was not possible to distinguish the growth of face $\{121\}$ from that of face $\{002\}$ in an anhydrous melt. Therefore, it is probably that parameter A of face $\{121\}$ represents that one of face $\{002\}$ grown from pure acrylic acid. Furthermore, parameters A and B verify that the influence of water caused by its polarity is higher on face $\{121\}$ than on face $\{110\}$.

Parameter B decreases rapidly for both faces with an increasing water content, whereas parameter A is quasi constant for face $\{110\}$ and slightly increasing for face $\{121\}$. This could lead to the following allocation, if eq. 2-14 is compared with an equation describing a classic adsorption process:

- Parameter A should characterize the attachment frequency of new 2D nucleus on the growth face. Therefore, the attachment frequency of new 2D nucleus on face $\{110\}$ seems to be quite low and constant. This is obvious, if the loosen blocking monomolecular water network will be formed as calculated by Nordhoff et al. [1]. For face $\{121\}$ values of A decrease constantly. This could indicate that attachment frequency of new 2D nucleus on face $\{121\}$ is slightly decreasing with decreasing acrylic acid content.
- Parameter B should be related to the probability of a new 2D nucleus to attach finally on the crystal face. Therefore, it should include the temperature of the crystal and the Boltzmann constant.

Parameter A and B show a linear function of the acrylic acid content with exception of pure acrylic acid. With a linear fit of A and B to the acrylic acid concentration, eq. 2-14 can be adapted to the growth rate of each face.

$$G_{110}(x_{AA}; \beta) = (2 \cdot 10^{-5} \cdot x_{AA} - 6 \cdot 10^{-4}) \cdot \beta^{\left(\frac{5}{6}\right)} \cdot \exp\left(\frac{-2.03 \cdot x_{AA} + 1.18}{\beta}\right) \quad \text{eq. 2-15}$$

$$G_{121}(x_{AA}; \beta) = (0.041 \cdot x_{AA} - 0.025) \cdot \beta^{\left(\frac{5}{6}\right)} \cdot \exp\left(\frac{-3.42 \cdot x_{AA} + 2.22}{\beta}\right) \quad \text{eq. 2-16}$$

2.4.2 Cavity angle analysis

Using the postulated model of morphology development of section 2.4, it is obvious to check if the angle γ correlates directly with the growth rates of both faces. The definition of the cavity angle γ is already given in section 2.3.3.2. If the postulated model is correct, then the occurring cavity angle γ should be calculated via a tangent equation as follows. It is valid for aqueous diluted acrylic acid mixtures only.

$$\tan(\gamma) = \frac{G_{121}(x_{AA})}{G_{110}(x_{AA})} = \frac{(0.041 \cdot x_{AA} - 0.025) \cdot \beta^{\left(\frac{5}{6}\right)} \cdot \exp\left(\frac{-3.42 \cdot x_{AA} + 2.22}{\beta}\right)}{(2 \cdot 10^{-5} \cdot x_{AA} - 6 \cdot 10^{-4}) \cdot \beta^{\left(\frac{5}{6}\right)} \cdot \exp\left(\frac{-2.03 \cdot x_{AA} + 1.18}{\beta}\right)} \quad \text{eq. 2-17}$$

The measured angle values of γ from figure 2-15 and modeled ones from eq. 2-17 are plotted against each other in figure 2-17.

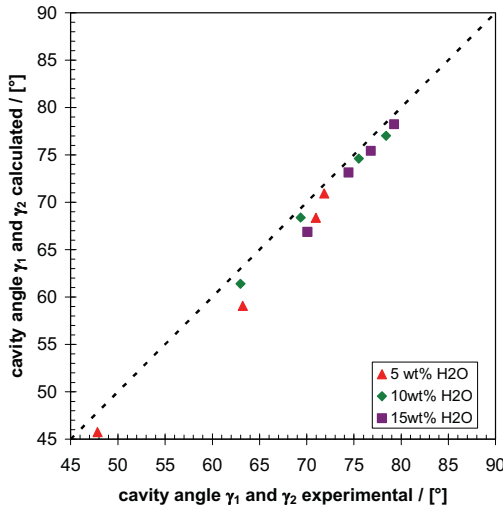


Figure 2-17 Comparison of measured and calculated cavity angles.

The deviation trend between measured and modeled cavity angles is obvious. All measured cavity angles show higher values than the calculated ones. The drift becomes smaller with increasing water content and higher supercooling. A significant explanation is currently not possible.

It has to be mentioned that growth rates and cavity forming were measured on a single crystal positioned inside the cell. Additionally, the calculation of cavity angles is very sensitive, so that small differences in modeled growth rates vary the angles a lot.

2.5 Conclusion

The main scope of this work was to investigate the effect of water and supercooling on crystal morphology of acrylic acid. In absence of water, growth rates of pure acrylic acid crystals follow a clear trend. It was observed that crystal morphology changes with increasing water content and supercooling from cubic to more and more to needle-like crystals. Aspect ratios of the crystals are important values to prove this behavior. A parameter fit of the growth rate equation of Bennema and Gilmer [6] to the measured values suggested that crystal growth of faces $\{110\}$ and probably faces $\{121\}$ follow a “birth and spread” mechanism. Extending this equation, it was possible to directly predict growth rates at given values of water content and supercooling.

One of the interesting facts noted, was the appearance of a cavity at the crystal extremity in presence of water as it has already been published by Nordhoff et al. [1]. However, it was not noted before that cavity geometry is a function of water content and supercooling. Within this chapter, the authors postulate that apparent growth of face $\{002\}$ in the presence of a cavity has to be declared as growth of face $\{121\}$. A possible growth model was evaluated.

Hence, this work will be helpful to identify favorable operating conditions for solid-liquid separation in terms of water content in the melt and the magnitude of driving force. Moreover, it provides the necessary insight into physical phenomena taking place at the solid-liquid interface which could assist further developments in this field. Further crystallization experiments should be performed in a suspension mode to use these obtained results. Experiments in suspension mode will help to outline, if the crystals can withstand the stresses in the solid-liquid separation. As crystals have cavities at their extremities they may crumble and choke filters. This could decrease the porosity and hence the permeability of filter cakes. Hence, after growing the crystals in suspension mode, crystal size distribution should be analyzed and tests according to permeability and filterability should be carried out.

Nomenclature**Notation**

a, b, c	crystallographic parameters	[Å]
A	first growth rate constant	[-]
B	second growth rate constant	[-]
c_p	heat capacity at constant pressure	[W/(kg·K)]
D_{AB}	diffusion coefficient	[cm ² /s]
G	linear crystal growth rate	[m/s]
ΔH_m	heat of fusion	[J/mol]
L	characteristic length	[m]
Nu	Nusselt number	[-]
Pr	Prandtl number	[-]
R	gas constant	[J/mol·K]
Re	Reynolds number	[-]
Sc	Schmidt number	[-]
Sh	Sherwood number	[-]
T	absolute temperature	[K]
T_m	melting point temperature	[K]
ΔT	temperature difference between melting point and inner cell temperature	[K]
V	molar volume	[cm ³ /mol]
V	characteristic velocity	[m/s]
x	mass fraction	[wt%]

Greek symbols

α	heat transfer coefficient	[W/(m ² ·K)]
β	supercooling	[-]
γ	cavity angle	[°]
λ	heat conductivity	[W/(m·K)]
η	viscosity of the melt	[cp]
ρ	density	[kg/m ³]
φ	association parameter	[-]
ω	mass transfer coefficient	[m/s]

Subscripts & Superscripts

AA	acrylic acid
A	component A
B	component B
e	equilibrium

References

- [1] Nordhoff, S.; Beilles, S.; Franke, R.; Influence of water as an impurity on acrylic acid melt crystallization, *Chemical Engineering Transaction*, 2002, Vol. 1, pp725-730.
- [2] Boese, R.; Blaser D.; Steller I.; Latz R.; Baumen A.; *Acta Crystallogr., Sect. C: Cryst. Struct. Commun.*, 1999, Vol. 55, 9900006.
- [3] Prywer, J; Correlation between growth of high-index faces, relative growth rates and crystallographic structure of crystal, *Eur. Phys. J. B*, 2002, Vol. 25, pp61-68.
- [4] Prywer, J.; Kinetic and geometric determination of the growth morphology of bulk crystals: Recent developments, Vol. 50, *Prog. Cryst. Growth Charact. Mater.*, 2005, pp1-38.
- [5] Jansens,P.J.; PhD Thesis, Fractional suspension crystallization of organic compounds, Delft, 1994 Chapter 4, pp74-75.
- [6] Bennema, P; Gilmer, G. H.; *Kinetics of Crystal Growth, Crystal Growth: An Introduction*, P. Hartmann ed., Amsterdam, North Holland, 1973, pp263 357.
- [7] de Goede, R.; van Roosmalen, G. M.; Modelling of crystal growth kinetics: a simple but illustrative approach, *J. Cryst. Growth*, 1990, Vol. 104, pp392-398.
- [8] Chubarov, G.A.; Danov, S.M.; *Liquid-Solid Equilibrium in the Systems Acrylic Acid - Water, Acrylic Acid - Acetic Acid, and Methacrylic Acid – Water*, *J. Appl. Chem., USSR*, 1978, Vol. 51 (8), pp1796-1798.
- [9] Bird, R.; Stewart, W.; Lightfoot, E.; *Transport phenomena*, John Wiley and Sons, Lewes, SU, United Kingdom, 1960.

- [10] Pohlhausen, E.; Der Wärmeaustausch zwischen festen Körpern und Flüssigkeiten mit kleiner Reibung und kleiner Wärmeleitung, Angew. Math. Mech., 1921, Vol. 2, p115.

- [11] Krouzhiline, G.; Investigation de la chouche - limite thermique, Techn. Phys., 1936, Vol. 3, p183 and p311.

CHAPTER 3

THE INFLUENCE OF WATER AND SUPERCOOLING ON PERMEABILITY AND COMPRESSIBILITY OF ACRYLIC ACID CRYSTAL BEDS

Abstract

The performance of a solid-liquid separation process is mainly determined by the size distribution and the morphology of the crystals. To predict the filtration behavior a robust and an applicable model based only on the crystallization process parameters is necessary.

Therefore, a model has been developed for the industrial system of aqueous acrylic acid melt to predict the compressibility and the permeability of a crystal bed. For this purpose, common equations derived for spherical particles have been adapted to nonspherical particles. The Chord Length Distribution (CLD) obtained from an inline FBRM probe and the crystal aspect ratio have been used in combination to determine the major input parameters for the model. The integration of a complex mathematical convolution of the CSD from CLD data by the use of complex models is avoided in this approach. Considering acceptable fault tolerances of the model, a simple approach is combined with a robust measurement technique. The adjustment of all required constants used in the permeability model was based on the simple filtration tests.

Published in Chemical Engineering Technology, 2010, Vol. 33 (3), pp.433-443

3.1 Introduction

Suspension crystallization is a highly efficient separation technology for industrial applications. In the recent past, several developments have been made to push this promising technology successfully to industrial scale. The overall efficiency of the process is largely determined by an effective solid-liquid separation. To obtain high product purities, the complete separation of the crystals and the mother liquor is required along with an efficient washing step.

In chapter 2 [1] it was demonstrated that the amount of the water in the melt and the driving force in terms of the supercooling are main influencing factors in the crystallization of acrylic acid. With increase in the water content and the supercooling, a cavity starts appearing at the crystal extremity of face {002} goes along with a needle-like shape development. This morphology trend is often an indicator of problems coming up in the downstream facilities like the solid-liquid separation and washing devices. Simple tests at lab scale confirm these issues and show challenging filtration conditions at higher water content and supercooling.

Therefore, the scope of this chapter is to investigate the influence of the water content and the supercooling in the melt on the performance of the downstream solid-liquid separation. The filterability of the different crystal suspensions was determined by simple filtration tests. In these tests different compressive stresses were applied on the crystal bed by means of different liquid pressure drops. Later on, the experimental results were used as input parameters for an extended model developed previously to calculate the permeability and the compressibility.

3.2 State of knowledge

The main scope of the required model is to describe the permeability performance of a crystal bed formed from the nonspherical acrylic acid crystals under the influence of the mechanical stress. In chapter 2 [1] the water content and supercooling in the melt were identified as the main parameters influencing the morphology of the acrylic acid crystals. The permeability model for nonspherical acrylic acid crystals was based on the extension of the well-known approaches for the spherical particles. Therefore, the approach for spherical particles will be derived starting from the demanded permeability in paragraph 3.2.1 and will then be extended to nonspherical particles by consideration of the aspect ratio α in 3.2.2. The resulting calculation flow scheme will be drawn top down starting with all input parameters in paragraph 3.3.

3.2.1 Permeability model for spherical particles

3.2.1.1 Permeability as a function of compressibility

The resulting permeability B hardly depends on the compressibility of the crystal bed. The compressibility of a crystal bed is defined as the change in the porosity or the permeability as a response to a pressure change. Tiller [2] investigated the general compressibility behavior of the particles. He found a correlation between the initial porosity ε_0 and the permeability B_0 , respectively, due to a certain pressure change. The correlation uses the specific compressibility coefficients λ for porosity and σ for permeability, respectively, as shown in eq. 3-1 from Tiller [2]:

$$\left(\frac{\varepsilon}{\varepsilon_0}\right)^{\frac{-1}{\lambda}} = \left(\frac{B}{B_0}\right)^{\frac{-1}{\sigma}} = 1 + \frac{p}{p_0} \quad \text{eq. 3-1}$$

In this study, the relation between the permeability and the compressive pressure is used to determine the compressibility coefficient σ . The permeability was chosen over porosity because the experimental measurement of permeability is much easier than measurement of porosity. The next upwards requirement for the model is the determination of the initial permeability B_0 .

3.2.1.2 Permeability without compression

For the calculation of the initial permeability B_0 at zero stress, as an input parameter for eq. 3-1, a number of relations are available. All relations base on the porosity. The most common one is the Kozeny-Carman equation, where K_{kc} is the Kozeny constant and S_0 is the specific surface area of the crystals. The Kozeny constant is 5 for spherical particles and has to be determined experimentally for nonspherical particles [3].

$$B_{KC} = \frac{1}{K_{KC}} \cdot \frac{\varepsilon^3}{(1-\varepsilon)^2} \cdot \frac{1}{S_0} \quad \text{eq. 3-2}$$

Based on the length mean size, a relation is suggested by MacDonald et al. [3] as written in eq. 3-3. K_{Mc} is the MacDonald constant and $L_{2,1}$ is the length-based mean size. The MacDonald constant is 44.4 for spherical particles.

$$B_{Mc} = \frac{1}{K_{Mc}} \cdot \frac{\varepsilon^3}{(1-\varepsilon)^2} \cdot (L_{2,1})^2 \quad \text{eq. 3-3}$$

3.2.1.3 Porosity model for spherical particles

To predict the initial porosity ε_0 as an input parameter for the permeability equations presented in paragraph 3.2.1.1, a model developed by Ouchiyama and Tanaka [4] can be used. This model is based on a simplified packing model and predicts the porosity from the particle size distribution and the initial porosity, ε_0 . The initial porosity is defined as the porosity of the uniformly sized particles and is usually equal to 0.40 for loose random packing or to 0.36 for dense random packing [5]. The particle size distribution is expressed as the number fraction $f(L)$.

Ouchiyama and Tanaka [4] developed the following equation for the calculation of the porosity:

$$\varepsilon = 1 - \frac{\int_0^{\infty} f(L) \cdot L^3 dL}{\int_0^{\infty} f(L) \cdot (L \approx \bar{L}_n)^3 dL + \frac{1}{n} \cdot \int_0^{\infty} f(L) \cdot \left[(L + \bar{L}_n)^3 - (L \approx \bar{L}_n)^3 \right] dL} \quad \text{eq. 3-4}$$

Where

\bar{L}_n = number based mean size

$$\begin{aligned} (L \approx \bar{L}_n) &= 0 & \text{for } L < \bar{L}_n \\ (L \approx \bar{L}_n) &= L - \bar{L}_n & \text{for } L > \bar{L}_n \end{aligned}$$

and parameter \bar{n} is defined as:

$$\bar{n} = 1 + \frac{4}{13} \cdot (7 - 8 \cdot \varepsilon_0) \cdot \bar{L}_n \cdot \frac{\int_0^{\infty} f(L) \cdot (L + \bar{L}_n)^2 \cdot \left(1 - \frac{3}{8} \cdot \frac{\bar{L}_n}{L + \bar{L}_n} \right) \cdot dL}{\int_0^{\infty} f(L) \cdot (\bar{L}^3 - (L \approx \bar{L}_n)) \cdot dL} \quad \text{eq. 3-5}$$

Strictly speaking, the model is only applicable to spherical particles packed under either loose or dense random packing conditions, where the particle size and the initial porosity are clearly defined. However, the crystals involved in industrial crystallization processes are usually not spherical and the particle shape has a strong influence on porosity. Applications to nonspherical particles has been successfully done by Ouchiyama & Tanaka in 1988 [4] but cannot generally be used.

3.2.1.4 Porosity from MSMPR kinetics

The model of Ouchiyaama and Tanaka [4] uses the particle size distribution expressed as the number fraction $f(L)$ as an input parameter.

It is also possible to calculate the required variable $f(L)$ via the well-known MSMPR-theory developed by Randolph and Larson in 1988 [6]. This theory is based on the population balance and accounts the size distribution of the crystals. The population density distribution is defined as the number density of the particles as function of the size of the particles in a certain volume. If the population balance is solved as suggested by Randolph and Larson [6], the population density distribution for an ideally mixed MSMPR crystallizer can be written as:

$$n = n_0 \cdot \exp\left(-\frac{L}{G \cdot \tau}\right) \quad \text{eq. 3-6}$$

Herein, L represents a characteristic length of a crystal, G its growth rate, n and n_0 the population density at size (L) and at size 0 respectively, and τ the residence time of the crystal under supercooling conditions. The required conditions within the experiment are explained in details in paragraph 3.4.1.1.

The population density from the MSMPR-theory can be transformed to a size distribution function for spherical particles as needed for the porosity model suggested by Ouchiyaama and Tanaka [4]:

$$f(L) = \frac{n(L)}{\int_0^\infty n(L) \cdot dL} = \frac{n_0 \cdot \exp\left(-\frac{L}{G \cdot \tau}\right)}{n_0 \cdot G \cdot \tau} = \frac{1}{G \cdot \tau} \cdot \exp\left(-\frac{L}{G \cdot \tau}\right) \quad \text{eq. 3-7}$$

The number based mean size can be written as a function of $G \cdot \tau$ and n_0 using the MSMPR-theory [6]. Inserting these values in the porosity model of Ouchiyaama and Tanaka [4], results in the following equation:

$$\varepsilon = 1 - \frac{6}{6 \cdot e^{-1} + \frac{1}{n} \cdot (16 - 6 \cdot e^{-1})} \quad \text{eq. 3-8}$$

Where

$$\bar{n} = 1 + \frac{17}{13} \cdot \frac{(7 - 8 \cdot \varepsilon_0)}{(6 - 6 \cdot e^{-1})} \quad \text{eq. 3-9}$$

Hence, the porosity of the crystals grown in an ideal MSMPR-crystallizer is not a function of crystallization kinetics but only of the porosity of uniform-sized particles, ε_0 . The porosity of the uniformly sized crystals is a function of the morphology of the crystals [8].

From Randolph and Larsson [6] it is known that the mean size of the particles in a MSMPR crystallizer is determined by the growth rate and the residence time:

$$\begin{aligned} L_{1,0} &= G \cdot \tau \\ L_{2,1} &= 2 \cdot G \cdot \tau \\ L_{3,2} &= 3 \cdot G \cdot \tau \end{aligned} \quad \text{eq. 3-10}$$

The values can be used in the Kozeny-Carman and MacDonald relations to determine the permeability. The permeability can now be calculated directly from the crystal size distribution data (CSD) or from the MSMPR-fit. The MSMPR-fit includes the growth rate G , the residence time τ , the nucleation rate B_0 , and the initial population density n_0 , respectively, from the semi-logarithmic plot of the population density vs. the crystal size data which has to be determined.

3.2.2 Extended input to the permeability calculations for nonspherical particles

The model of Ouchiya and Tanaka [4] demands the particle size distribution for both approaches presented in paragraphs 3.2.1.3 and 3.2.1.4. The characteristic length L and its distribution depend on the chosen particle size measurement. Therefore, the model of Ouchiya and Tanaka [4] and the model extended with the kinetics from MSMPR must be used with care, because they are only valid in combination with the same measurement principles and the corresponding data.

The prediction of the permeability depends on the specific variables. The Kozeny-Carman equation uses the specific surface of the crystals, whereas the MacDonald equation uses the length-based mean size. The specific surface is a strong function of the size and the shape. For needle-like crystals, the morphology can be described by an aspect ratio α which is the proportion of two characteristics, e.g. L_2/L_1 . For acrylic acid L_1 represents the distance between two faces {110}, whereas L_2 represents the distance between faces {002} [1]. The Kozeny-Carman and MacDonald equations, respectively, require the knowledge of the specific surface or a characteristic length L_1 . Table 3-1 gives an overview on the conversions of the characteristic length L_1 depending on different aspect ratios α into the required specific variables.

Table 3-1 Conversion of a characteristic length L_1 into specific variables for different aspect ratios.

shape	cube	rectangle	needle	general
aspect ratio α / [-]	$L_2/L_1=1$	$L_2/L_1=4$	$L_2/L_1=16$	α
projected area A [m ²]	L_1^2	$4 \cdot L_1^2$	$16 \cdot L_1^2$	$\alpha \cdot L_1^2$
volume V [m ³]	L_1^3	$4 \cdot L_1^3$	$16 \cdot L_1^3$	$\alpha \cdot L_1^3$
surface S [m ²]	$6 \cdot L_1^2$	$18 \cdot L_1^2$	$66 \cdot L_1^2$	$(2+4 \cdot \alpha) \cdot L_1^2$
specific surface S_0 [m ² /m ³]	$6/L_1$	$4,5/L_1$	$4,125/L_1$	$[(2+4 \cdot \alpha)/\alpha]/L_1$

3.3 Permeability model for nonspherical particles

The permeability prediction for a crystal bed of nonspherical particles as a function of occurring pressure drop is possible using the extended models for spheres presented in paragraphs 3.2.1 and 3.2.2. For an industrial application of the model, it is worthwhile to use the input data in form of simple process conditions as follows:

- Water content in the melt
- Supercooling
- Pressure drop over the crystal bed

Several system specific input parameters must be determined by pilot plant experiments as a function of water content and supercooling:

- The compressibility coefficient σ for the compressibility model of Tiller [2].
- The Kozeny-Carman constant, K_{KC} for the zero permeability model of Kozeny-Carman [3].
- The function for the aspect ratio $\alpha(x_{H_2O}, \beta)$ determined in chapter 2 [1].
- The initial porosity ε_0 of a bed of uniform-sized crystals for the model of Ouchiyaama and Tanaka [4].
- MSMR [6] calculation to determine the crystal growth rate G , the nucleation rate B_0 , and the aspect ratio α as the input parameters for the calculation of the specific surface.

The resulting workflow of the integrated final model is shown in the figure 3-1. The current process conditions are used as the input parameters on the right side. The model is

applicable for all different kinds of particle size measurements. Therefore, the PSD is used in the model flow scheme for all kinds of size distributions. It is important to assure that the determined model parameters are only valid for the used particle size measurements. The flowsheet of the model will be explained by means of the subsequent path:

1. From growth rate G the PSD is calculated with the MSMPR model as a function of water content x , supercooling β , and residence time τ .
2. The porosity for the uniform-sized particles ($\varepsilon_0 = 0.40$) is then calculated from the PSD by using the Ouchiyama and Tanaka model.
3. The calculation of the specific surface via the PSD is adjusted by the aspect ratio α as a function of water content x and supercooling β .
4. The calculated porosity ε and the specific surface S_0 are then input parameters for the Kozeny-Carman relation together with the Kozeny-Carman constant K_{KC} to calculate the zero-stress permeability B_0 .
5. Finally, the compressibility coefficient σ and the occurring pressure drop Δp over the crystal bed are taken into account to calculate the resulting permeability B .

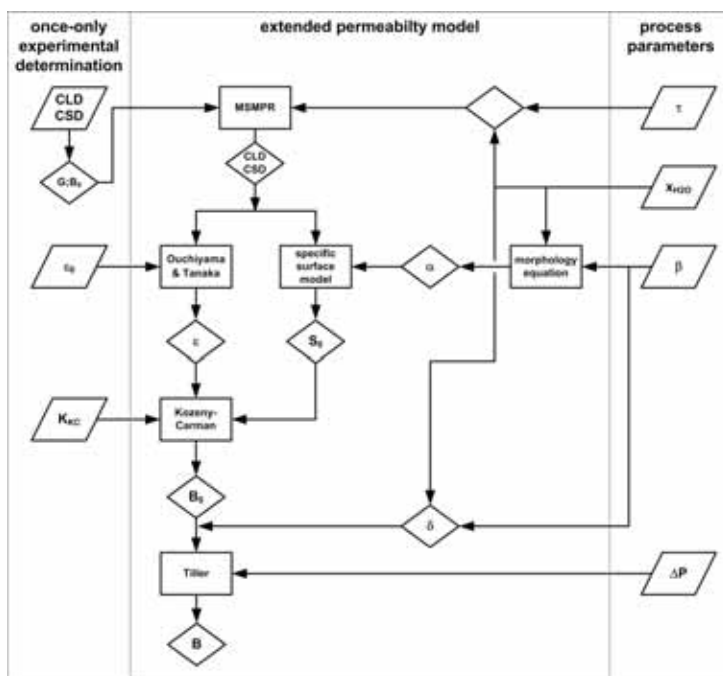


Figure 3-1 Model flow scheme of the extended permeability model using specific parameters and process conditions.

3.4 Experimental

3.4.1 Apparatus and setup

3.4.1.1 Continuous MSMPR crystallizer

To approach realistic process conditions as close as possible, a continuously operated crystallizer, fulfilling the requirements of the Mixed-Suspension-Mixed-Product-Removal (MSMPR) theory [6], must be applied. From a practical point of view, the fulfillment of the requirements can be checked by following facts:

- PSD is constant at the top and the bottom of the crystallizer.
- Temperature gradient from top to bottom is zero, so that the supercooling is homogeneous.
- Gentle mixing to avoid the crystal breakage.
- The process parameters and the particle size distribution are constant over time.

The flow sheet of the experimental setup is shown in figure 3-2. The crystallizer (CC) is a 17 litre double-walled stainless steel vessel with a two-bladed PTFE scraper inside rotating at a constant revolution rate of 15 rpm. The internals are equipped with vanes to improve mixing. Cooling is carried out through a cooling-jacket. The temperature is constantly monitored by thermocouples (T) in the crystallizer. The crystal slurry is withdrawn from the bottom of the crystallizer and is transported to two glass-tube heat exchangers (E). Here, the crystals are melted to provide a crystal-free feed again to the crystallizer as required for the MSMPR operation. The residence time in the crystallizer can be varied by changing the feed flow measured by a flow meter (F). The chord length distribution is measured by an inline Focused Beam Reflectance Measurement (FBRM).

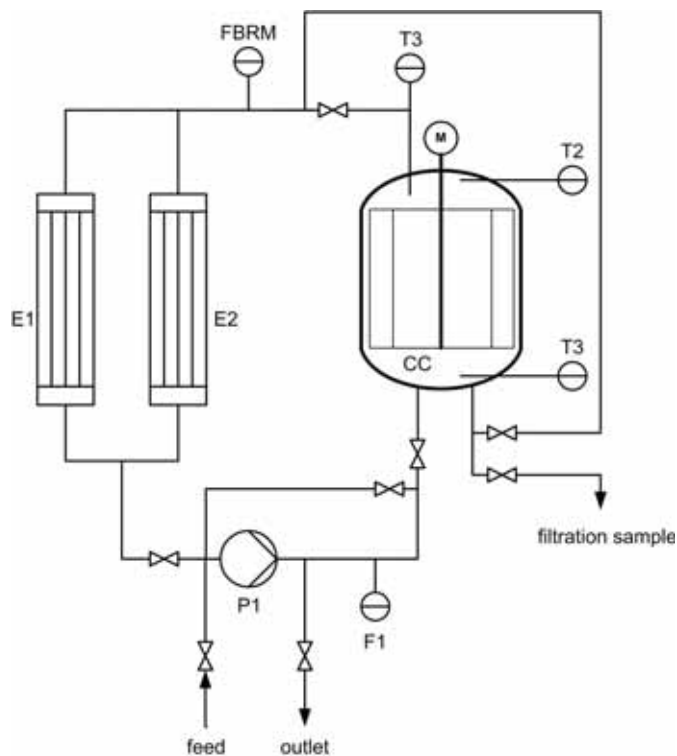


Figure 3-2 Flow sheet of the continuously operating crystallizer setup.

3.4.1.2 Operating conditions and supercooling

To identify the influence of the operating conditions on the crystal bed properties, the water content in the feed and the supercooling are varied during different experiments. The variation of the supercooling is realized by varying the residence time τ and is calculated by comparing the measured solid content with the calculated theoretical value corresponding to the solid-liquid equilibrium at the measured temperature. In this way, the supercooling is expressed as the difference between the equilibrium temperature at the measured mother liquor concentration from the measured solid content and the actual temperature of the mother liquor.

$$\beta = \frac{-\Delta H_m}{RT^2} \cdot \Delta T \quad \text{eq. 3-11}$$

3.4.1.3 Permeability experiments

The main objective of this study is to identify the permeability of a crystal bed formed out of acrylic acid crystals as a function of water content and supercooling and relate this to the crystal properties. The filtration behavior is determined in filtration tests with a constant pressure difference. The used setup is shown in figure 3-3. A glass tube with a filter in the bottom is filled with the slurry of mother liquor and crystals. The crystals sediment and a bed builds up to a final height h_b . As the bottom valve is opened to the vacuum flask, the mother liquor flows through the packed bed. The permeability can be calculated with eq. 3-12:

$$B = \frac{\eta \cdot h_b}{\rho_l \cdot g \cdot (t_2 - t_1)} \cdot \ln(H_2 / H_1) \quad \text{eq. 3-12}$$

In this way, the hydrostatic head is used as the driving force for the flow and the pressure difference over the bed is limited. To determine the permeability change as a response to the pressure, different vacuum values are applied over the crystal bed in the filtration setup. To calculate the permeability subsequently the pressure difference is translated into a liquid head and is used as an input for eq. 3-12. The measured permeability is in any case corrected for the resistance of the glass filter in the bottom which is determined in a filtration experiment with pure liquid acrylic acid.

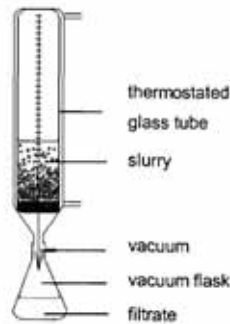


Figure 3-3 Filtration set-up for permeability measurements [7].

3.4.2 Crystal property measurements

3.4.2.1 Particle size distribution PSD

Two different measurements for particle size distribution were available for characterization: an offline Forward Laser Light Scattering (Malvern) method and an inline Focused Beam Reflectance Measurement (FBRM) technique.

The Forward Laser Light Scattering method uses an expanded laser light beam which passes through a slurry flow cell. The laser light beam is diffracted by the particles and the scattered light is focused by a Fourier transform lens on a detector. The laser light interactions with the crystals in the flow cell result in an integrated intensity pattern on the detector. The instrument software assumes that the particles are spherical. Therefore, the diffraction patterns are converted into the particle size distribution of the spheres with the equivalent projection area. The use of shape factors is possible to correct the deviation between the assumption of a sphere and the effective occurring morphology.

The FBRM technique consists of a focused laser beam rotating at a constant high velocity, propagating into the suspension. When the beam emitted by the laser hits a particle, it is reflected through the probe window. The corresponding chord length is calculated as the product of the duration of the backscattered signal and the beam velocity. The FBRM technique only provides the distribution of chord length and does not assume any particle morphology. Worlitschek [9] demonstrated the direct impact of the particle shape on the chord length distribution. The transformation of the CSD from CLD data with complex probability functions has been the subject of many publications [9;10;11].

Hence, the data of both measurement principles can be used carefully as input parameters for the porosity model of Ouchiya and Tanaka [4], if the measurement method, the morphology of the crystals, and the morphology development are considered.

Due to the sensitivity of the binary system of acrylic acid and water to temperature, the inline measurements of the particle size distributions provide an essential advantage. The inline measurement of the particle size is less defective than an offline measurement, especially if small fast-melting crystals are the focus of interest.

Therefore, experiments in this study have been carried out with the inline FBRM technique which provides the online and the in-situ information about the Chord Length Distribution (CLD) of a crystal population. With respect to the developed complex mathematical models for restoration of CSD from CLD data [9;10;11], a simple approach as an engineering industrial application is foreseen. If the measurement principle and the crystal morphology of the elongated acrylic acid crystals are taken into account, the following assumption can be made. The most detected chord length of an elongated crystal by FBRM is assumed to be the one perpendicular to the elongated direction L_2 . It is taken into account that this is not accurate and the results will be defective within a certain area. Therefore, the thus determined chord lengths will relate to the characteristic dimension L_1 . Taking the aspect ratio α and the conversions of table 3-1 into account all required specific variable, like volume, specific surface, etc. can be calculated from L_1 .

3.4.2.2 Used compounds and mixtures

It is known that water significantly influences the growth of acrylic acid crystals. Part of this study is to identify the influence of water content on the crystal properties in a suspension and the filtration behavior of the acrylic acid crystals. Fine Glacial Acrylic Acid (FGAA) is used to prepare mixtures with 5 wt%, 10 wt%, and 15 wt% water.

3.4.3 Experimental procedure

3.4.3.1 Crystallizer

The setup is filled with a defined acrylic acid water mixture. A defined temperature gradient program is used to cool down the crystallizer first in a batch mode to induce first nucleation. Thereafter, the feed pump is started to operate the crystallizer in a continuous mode. The absolute values of the present supercooling can be calculated by eq. 3-11. Based on the constant supercooling, the solid content and the chord length distribution measured from the FBRM, it was possible to detect the steady-state conditions.

3.4.3.2 Experiments

Once the steady state was achieved in the crystallizer and the related supercooling was measured, the filtration experiments were started. The time required to sediment the crystals was fixed to 2 minutes for all the experiments.

For all combinations of water content, supercooling, and pressure drop, experiments were carried out twice. Table 3-2 summarizes the experimental parameters.

Table 3-2 Overview on experiment parameters.

water content x / [wt%]	5 wt%	10 wt%	15 wt%	-
residence time τ / [min]	60	30	20	15
pressure drop Δp / [mbar] (2x)	0	250	500	750

3.5 Results

3.5.1 Supercooling

The supercooling at different conditions was measured via the method mentioned in section 3.4.1.2. Results of the supercooling vs. the residence time are shown in the figure 3-4. The supercooling increases with decreasing residence time. It is remarkable that the supercooling at low water contents is higher than at the higher ones. This goes along with the qualitative

mass transfer calculations demonstrated in chapter 2 [1]. They showed that the improvement of mass transfer by water is more relevant than the decline of viscosity effects by lower operating temperatures.

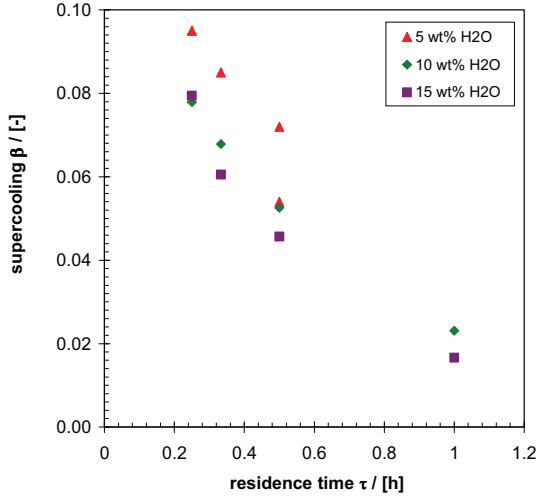


Figure 3-4 Plot of appearing supercooling β vs. adjusted residence time τ .

3.5.2 CLD measurement

The chord length distribution has been measured continuously during the experiments. All the data is averaged to give the results for each experiment and is expressed in terms of length-based mean chord $l_{2,1}$ and coefficient of variation $CV_{2,1}$. The data is plotted against supercooling for varying water contents in figure 3-5.

The length-based mean chord $l_{2,1}$ decreases for all water contents with increasing supercooling. In general, this trend was expected for all water contents assuming that $l_{2,1}$ represents the distance between two faces {110} as already explained in paragraph 3.4.2.1. At higher supercooling, more small particles are generated by a higher nucleation rate. Due to the crystallizer setup, high supercooling is induced by short residence times only. Therefore, expected higher growth rates cannot compensate the nucleation of the small particles.

However, the length-based mean chord $l_{2,1}$, assumed to represent primarily the distance between the faces {110}, does not increase significantly with higher water contents. This was also expected based on the results of chapter 2 [1]. Only a small increase of the face growth rate of {110} by increasing the water content was found.

The coefficients of variation ($CV_{2,1}$) characterizing the distribution of the chord length are plotted versus the supercooling in the figure 3-6. The $CV_{2,1}$ for all the experiments were

calculated from the squared CLD. The $CV_{2,1}$ show a clear increasing trend with increasing supercooling. Thus, with increasing supercooling the crystals become smaller and the distributions wider.

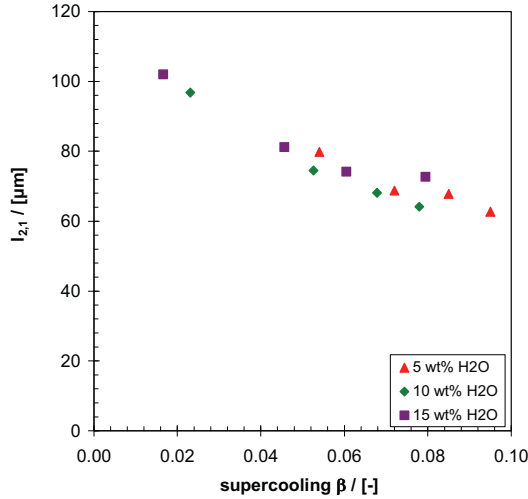


Figure 3-5 Plot of length-based mean chord $l_{2,1}$ vs. supercooling β .

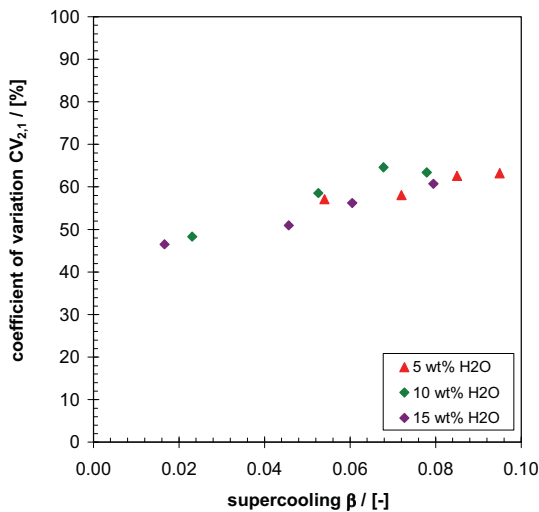


Figure 3-6 Coefficient of variation $CV_{2,1}$ vs. supercooling β .

3.5.3 Filtration results

Filtration experiments were carried out twice for various water contents and supercoolings. The calculated permeabilities are plotted as a function of the pressure drop over the crystal bed. Figure 3-7 shows a representative plot for a water content of 5 wt%. Permeability decreases significantly with increasing pressure drop. The trend lines indicate a power relation, as predicted by Tiller [2]. Apart from the pressure drop over the crystal bed, the permeability decreases with increasing water content as shown in figure 3-8 and figure 3-9. This trend is especially clear for higher residence times and thus lower supercoolings, where the influence of the water content on the crystal growth is dominant as predicted in chapter 2 [1].

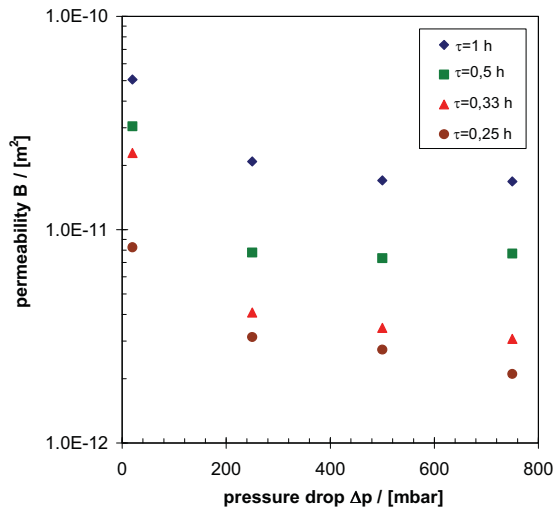


Figure 3-7 Permeability results for 5 wt% H₂O.

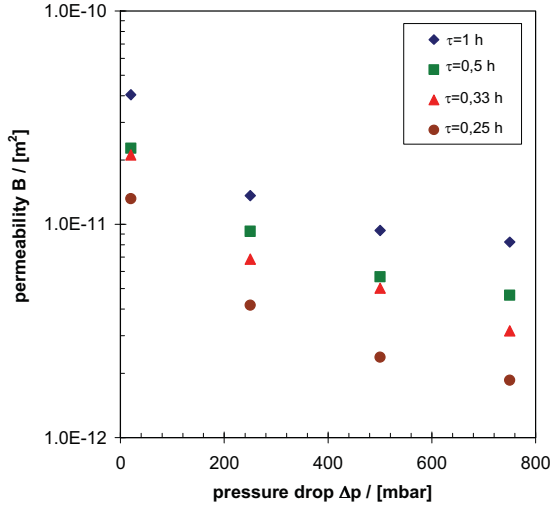


Figure 3-8 Permeability results for 10 wt% H₂O.

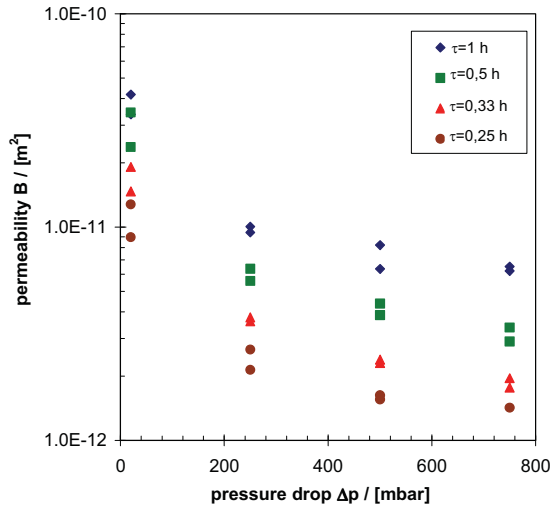


Figure 3-9 Permeability results for 15 wt% H₂O.

3.5.4 Compressibility

To determine the compressibility coefficient σ from the permeability as shown in eq. 3-1, the logarithm of the permeability is plotted against the logarithm of $(1+p/p_0)$. The slope of this plot reveals the compressibility coefficient. The pressure value p_0 is set to 25 mbar because this represents the pressure at the gravity force of a 25 cm liquid column. The resulting compressibility coefficients for different water contents are plotted against the supercooling in

figure 3-10. The compressibility coefficients increase with increasing water content and supercooling.

This was expected taking into account the results of chapter 2 [1]. Apparently, the morphology development influences the compressibility. The higher the water content and the supercooling, the more elongated the crystals become and the more distinct the cavities on faces {002} become. Cavities in general and higher cavity angles in particular make the crystal extremities physically weak. Hence, the compressive forces exerted on the crystals could easily break the crystals. Crystal breakage would imply a decrease of the crystal size. Besides, many small crystals fragments are created that negatively influence the permeability. To verify whether this phenomenon holds true in the filtration experiments, crystal properties should be analyzed after being subjected to compressive pressures.

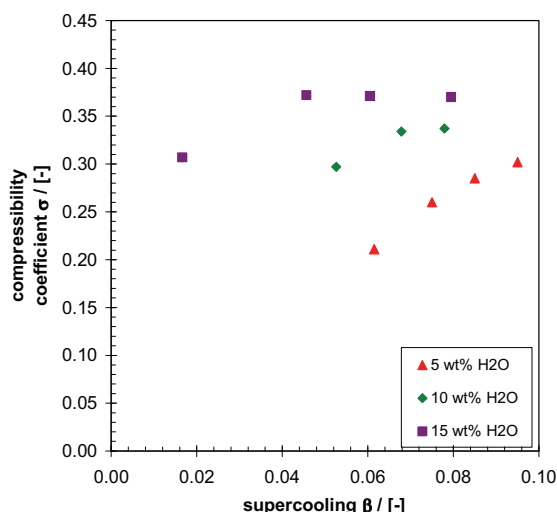


Figure 3-10 Compressibility coefficient σ vs. supercooling β .

3.6 Modeling results

The extended model is used to predict the permeability for varying water content, supercooling and pressure drop. The MSMR-fit is used to calculate the overall growth rates which are used as input data for the porosity model. Results are compared with the experiments from the previous paragraph and the parameters for the extended model are adjusted for optimal agreement.

3.6.1 Growth rates

The calculation of overall linear growth rates bases on the MSMPR-theory. The common MSMPR-theory has been developed to use the CSD data. The restoration of the CSD from CLD data has been the subject of several publications, for example of Ruf et al. [10] and Li et al. [11]. Kougoulos and Jones [12] have successfully used CLD data in combination with the morphology knowledge for MSMPR experiments. However, based on the assumptions made in paragraphs 3.2.2 and 3.5.2 the CLD data is used as input data to calculate overall growth rates. Calculated growth rates for all experiments are plotted against the occurred supercooling in figure 3-11.

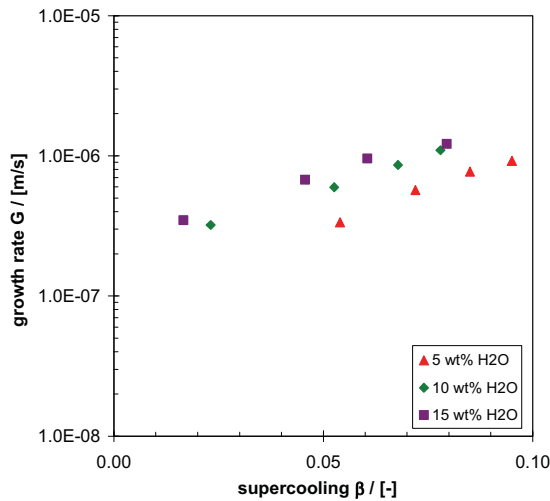


Figure 3-11 Growth rates G vs. supercooling β from MSMPR calculations.

The calculated values follow a clear trend as expected from the MSMPR experiments and the results of chapter 2 [1]:

- Growth rates increase with increasing supercooling.
- Growth rates increase with increasing water content. This was expected in spite of the decreasing temperature, because the viscosity of the mother liquor decreases with increasing water content.

The overall growth rates in the suspension are compared with the growth rates of face {110} from growth cell experiments [1]. They are in the same order of magnitude, although knowing that values of supercooling are much lower in suspension. This will be caused by the ideal mixing of the MSMPR crystallizer instead of a stagnant melt in growth cell experiments. Therefore, the overall growth rates are used for the model further on by considering the aspect ratio.

3.6.2 Porosity

The porosity is calculated by using the model of Ouchiyama and Tanaka. The porosity of a bed of uniform crystals, ε_0 , and the CLD data calculated from MSMPR are input parameters to the model. Typically, ε_0 has to be determined experimentally; but based on the experimental setup and the high temperature sensitivity of acrylic acid crystals, it was not possible to collect these data. Therefore, a standard value for ε_0 of 0.4 for densely packed particles is used [5].

However, the calculated porosities turn out to be more or less constant as shown in figure 3-12. This might be caused by applicability of the model of Ouchiyama and Tanaka [4] for uniform sized spherical particles only. The influence of the morphology change of acrylic acid to needle-like particles on porosity is disregarded in the calculation. The influence of a constant porosity to the further model results has to be regarded with care. The porosity calculation should be carried out again with a different PSD measurement principle accompanied by micrographs and should be verified with an experimental porosity determination.

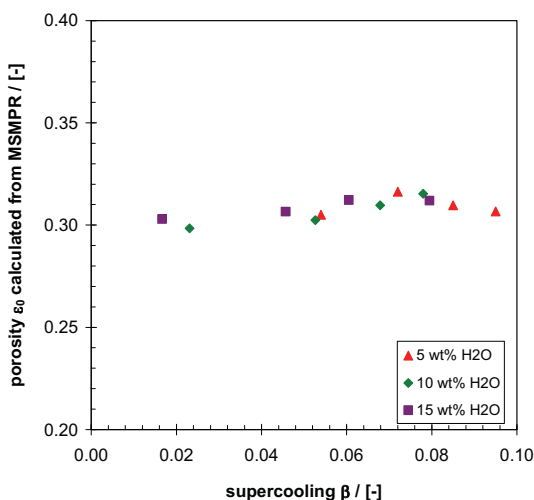


Figure 3-12 Calculated porosity ε_0 data from MSMPR data vs. supercooling β .

3.6.3 Specific surface

The specific surface is calculated via CLD data from the MSMPR model and the knowledge on morphology development from paragraph 3.2.2. The results are shown in figure 3-13. It is obvious that the specific surface increases with the increasing supercooling. Additionally, the

influence of water on morphology is stronger at low water content than at higher water content. This trend correlates with the development of the crystal shape. At higher water content and supercooling the crystal shape turns more and more to elongated needle-like crystals.

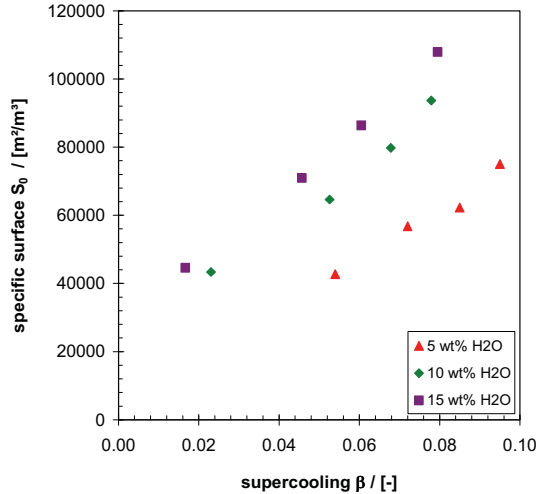


Figure 3-13 Calculated specific surface data S_0 from CLD plotted vs. supercooling β .

3.6.4 Permeability

Once the initial permeability B_0 is calculated, it is related to the porosity ε and specific surface S_0 by the equation developed by Kozeny-Carman. Additionally, it was necessary to fit the Kozeny constant for a better agreement with the absolute values of the experimental results. The constant found for the MSMPR fit is $K_{KC} = 6.25$. This value is constant in all experiments. Subsequently, the permeability is calculated under the influence of the mechanical stress in forms of the pressure drop. The permeability B is related to the initial permeability B_0 by the compressibility relation of Tiller [2] using the compressibility coefficient σ .

In the graph below all experimental results are compared with the results of the modified model extended to the morphology developments mentioned in chapter 2. In figure 3-14 the permeability calculated from the MSMPR-fit is plotted vs. the experimental values. The data points scatter around the line through the origin for equal calculated and measured permeability.

The quality of the model does not differ significantly from the experimentally determined permeabilities. The deviation is higher for higher water contents. This probably depends on increasing elongation of the crystals. The average deviation of the model results from the experimental results is 19.6%.

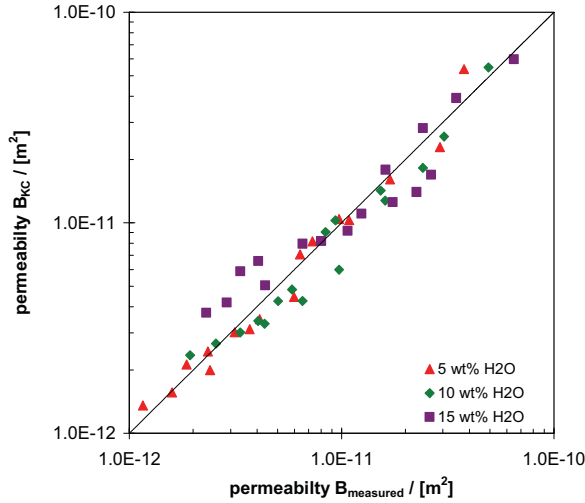


Figure 3-14 Comparison of experimental permeabilities and calculated permeabilities by Kozeny-Carman via MSMPR-fit.

3.7 Discussion

The extended permeability model shows a good agreement with experimental results. Especially, values at low water content and supercooling show a coherent behavior.

The more elongated the crystals at higher water content and supercooling, the bigger is the deviation between the modeling and the experimental results. This trend is mainly caused by the morphology changes of the particles. Crystal morphology changes with increased water content and supercooling from elongated cuboids to elongated needles with cavities at the extremities.

The changes in the initial porosity ε_0 over all experiments are low. This is based on the used porosity model for ideal spheres from Ouchiya and Tanaka [4]; it does not take into account the shape of the particles. Additionally, the used CLD data as input parameters for the porosity model are not sensitive enough to detect morphology changes of acrylic acid crystals either. This results in negligible changes of the initial porosity ε_0 . The porosity varies around a constant value of 0.3. Therefore, the impact of the porosity as one of the input parameters to the Kozeny-Carman equation for the calculation of the initial permeability B_0 is negligible.

Nevertheless, the CLD data from the FBRM provides important information if it is combined with the knowledge of morphology development described in chapter 2 [1]. Using this information, it is possible to calculate the required specific surface as another major input for

the Kozeny-Carman equation. The more elongated the crystals at higher water content and supercooling, the higher the specific surface and the lower the expected permeability. For all experiments the required Kozeny-Carman constant is equally set to 6.25. Subsequently, the prediction of the resulting permeability B as a function of the induced pressure drops is possible using the determined compressibility coefficient. In spite of all these deviations, the developed model is valid if the morphology change is taken into account and the determination of the required input parameters is carried out carefully.

3.8 Conclusions and outlook

The main objective of this chapter was to determine and understand the effect of water and supercooling on the permeability and compressibility of an acrylic acid crystal bed formed by crystals grown in a suspension crystallizer. The following conclusions regarding the crystallization and filtration processes can be drawn:

- The permeability of an acrylic acid crystal bed decreases with increasing supercooling and water content in the melt.
- The compressibility increases with increasing water content and supercooling as well.
- The permeability trends observed in the experiments agree with the morphology development to elongated crystals described earlier in chapter 2 [1].
- In conjunction with the morphology development of the particles, it is possible to use the CLD data from FBRM to calculate the specific surface as a major input parameter for the initial permeability by means of the Kozeny-Carman equation.
- The crystallization kinetics from the MSMPR experiments were obtained out with a common FBRM technique. Based on the obtained data it was possible to calculate overall growth rates. These data match with the growth rates of the particular crystal faces determined already by single crystal growth experiments.

Subsequently, a model to predict porosity and permeability for nonspherical particles was developed and applied with success. The model results show a strong dependency of the permeability on the specific surface of the particles. The complete disregard of the morphology change constitutes a major deficiency in the porosity calculation based on MSMPR data from CLD. Therefore, the model is less sensitive to porosity. It would be advantageous to determine experimentally the porosity as a function of the morphology and to extend the equation suggested by Ouchiyama and Tanaka [4].

The developed model can provide a basis for selecting the most favorable operating conditions to minimize the pressure drop over the crystal bed of a filtration unit.

Nomenclature**Symbols**

A	cross sectional area	$[\text{m}^2]$
B	permeability	$[\text{m}^2]$
B_0	nucleation rate	$[\text{m}^3/\text{s}^2]$
$f(L)$	density function	$[1/\text{m}^1]$
G	crystal growth rate	$[\text{m}/\text{s}]$
g	gravity constant	$[\text{m}/\text{s}^2]$
H	liquid level	$[\text{m}]$
h_B	crystal bed height	$[\text{m}]$
K_{kc}	Kozeny constant	$[-]$
K_{mc}	MacDonald constant	$[-]$
L	characteristic dimension of crystal	$[\text{m}]$
l	chord length	$[\text{m}]$
n	crystal population density	$[1/\text{m}^4]$
p	pressure	$[\text{Pa}]$
R	gas constant	$[\text{kJ}/(\text{mol}\cdot\text{K})]$
S	surface	$[\text{m}^2]$
S_0	specific surface	$[\text{m}^2/\text{m}^3]$
T	temperature	$[\text{K}]$
t	time	$[\text{s}]$
V	volume	$[\text{m}^3]$
x	water content	$[\text{wt}\%]$
ΔH_m	latent heat of fusion	$[\text{kJ}/\text{mol}]$

Greek Symbols

α	aspect ratio	[-]
β	supercooling	[-]
η	liquid viscosity	[Pas]
ε	porosity	[-]
ρ	density	[kg/m ³]
τ	residence time	[h]
σ	compressibility coefficient for permeability	[-]
λ	compressibility coefficient for porosity	[-]

Subscripts

1	characteristic index
2	characteristic index
1,0	number based
2,1	length based
3,2	surface based
0	zero stress
KC	Kozeny-Carman
Mc	MacDonald

Abbreviations

AA	acrylic acid
CLD	chord length distribution
CSD	crystal size distribution
CV	coefficient of variation
FBRM	Focused Beam Reflectance Measurement

FGAA	fine glacial acrylic acid
MSMPR	Mixed-Suspension-Mixed-Product-Removal
PSD	particle size distribution

References

- [1] Hengstermann, A.; Kadam, S.; Jansens, P.J.; Influence of water content and supercooling on crystal morphology of acrylic acid, *J. of Crystal Growth and Design*, 2009, Vol. 9 (4), pp2000–2007.
- [2] Tiller, F.; Role of Porosity in Filtration: Behavior of highly compactible cakes, *AIChE J.*, 1999, Vol. 44 (10), p2159.
- [3] MacDonald, M.; Chu, C.; Guillot, P.; A generalized Blake-Kozeny equation for Multisized Spherical Particles, *AIChE J.*, 1991, Vol. 37 (10), p1583.
- [4] Ouchiyaama, N.; Tanaka, T.; Porosity Estimation of Mixed Assemblages of Solid Particles with different Packing Characteristics. *J. Chem. Eng. Jpn.*, 1988, Vol. 21, pp157-163.
- [5] German, R.; Particle Packing Characteristics, Metal Powder Industries Federation, New Jersey, Princeton, USA, 1989.
- [6] Randolph, A.; Larson, M.; Theory of Particulate Processes, San Diego, Academic Press Inc., 1988.
- [7] Sluis, S. van der; A Clean Technology Phosphoric Acid Process, PhD Thesis, Delft University of Technology, Delft, The Netherlands, 1987.
- [8] Diepen, P.; Cooling Crystallization of Organic Compounds: Processes, Purity and Permeability, PhD Thesis, Delft University of Technology, Delft, The Netherlands, 1998.
- [9] Worlitschek, J.; Monitoring, Modeling and Optimization of Batch Cooling Crystallization. PhD Thesis, ETH Zurich, Zurich, Switzerland, 2003, Chapt. 3, pp27-35.
- [10] Ruf, A.; Worlitschek, J.; Mazzotti, M.; Modelling and Experimental Analysis of PSD Measurements through FBRM, *Part. Part. Syst. Char.*, 2000, Vol. 17, pp167-179.

- [11] Li, M.; Wilkonson, D.; Obtaining Particle Size Distribution from Chord Length Measurements, Part. Part. Syst. Charact., 2006, Vol. 23, pp170-174.

- [12] Kougoulos, A.; Jones, K.; Use of focused beam reflectance measurement (FBRM) and process video imaging (PVI) in a modified suspension mixed product removal (MSMPR) cooling crystallizer, J. Cryst. Growth, 2005, Vol. 273, pp529-534.

CHAPTER 4

COMPRESSIBILITY IMPROVEMENT OF AN ACRYLIC ACID CRYSTAL BED BY THE IN-SITU FORMATION OF ICE CRYSTALS

Abstract

The filtration performance of acrylic acid crystals is mainly influenced by the water content and the occurring supercooling in the melt. Both parameters may lead to low solid-liquid separation efficiencies and capacities by the reduction of the permeabilities and the increase of the compressibility. These problems can be effectively addressed by crystallizing acrylic acid and water at the eutectic point wherein the harder water crystals may act as an in-situ filter aid. Within this chapter the idea is verified with batch crystallization and filtration experiments.

The crystallization at the eutectic point of the binary system water and acrylic acid results in the formation of two different crystal habits. Acrylic acid crystallizes in a needle-like shape, whereas ice crystallizes with a spherical shape. The simultaneous formation of ice crystals as a filter aid improves the filterability behavior of a crystal bed formed from the acrylic acid crystals. The formation of ice crystals improves the initial permeability by a factor of 2. The major impact of ice crystals is the improvement of the compressibility behavior. The compressibility coefficients decrease from 0.25 for the acrylic acid crystals down to 0.15 with the ice crystals at the eutectic composition. To summarize, the crystallization of ice crystals at eutectic composition leads to a permeability improvement of 3-4 depending on the mechanical stress.

These promising results show that the filterability improvement of an acrylic acid crystal bed is possible by the in-situ formation of ice crystals. Additionally, the results reveal a possible increase of the yield by overcoming the eutectic limitation, if the generated aqueous product mixture can be used for any application.

Submitted for publication to AIChE on 02-11-2010

4.1 Introduction

The morphology of acrylic acid crystals is largely influenced by the water content and the supercooling in the melt as presented in chapter 2 [1]. It was found that the higher the water content and the supercooling, the more elongated are the acrylic acid crystals. This trend has a major influence on the compressibility of the crystal bed and hence on the downstream solid-liquid separation processes like the filtration as demonstrated in chapter 3 [2]. On the one hand, this can limit the capacity of a solid-liquid separation unit [3]. On the other hand, this can limit the feasible water content of a technical crystallization process unit. This second point requires an ambitious process synthesis.

Therefore, this chapter deals with the general idea for an improvement of the compressibility and the permeability of the acrylic acid crystal bed. This would allow the application of easy to operate process technologies as given by wash columns. The compressibility improvement is often possible by adding a filter aid directly to the crystal suspension. There are different requirements for a filter aid. In case of acrylic acid, the tendency to polymerize has to be considered and the chemical interaction regarding further application limits the use of any filter aids in general.

Therefore, the idea comes up to check the improvement of the compressibility by the formation of an in-situ filter aid like ice crystals. Water is one of the major secondary components of the technical production process. It is used in the further value chain of acrylic acid and is a product of the esterification.

The simultaneous crystallization of ice and acrylic acid is already published in the patent EP1492755A1 [4]. The formation of two separate crystal habits with different melting points is reported. This implies that an improvement of the crystal bed compressibility by another solid crystal phase e.g. ice crystals is possible. This has to be proven by simple bench mark tests.

The work starts with the state of knowledge on the common eutectic freeze crystallization process for salts and water. Subsequently, a theoretical model to calculate the porosity of the solid beds formed from two different morphologies is considered. This model helps to verify the idea of an in-situ formation of a filter aid. Thereafter, the crystallization and the filtration experiments are carried out with different solid fractions to determine the influence of ice on the permeability and the compressibility.

4.2 State of knowledge about eutectic freezing

Eutectic Freeze Crystallization (EFC) is a process to form two products simultaneously due to the eutectic property of a system. The crystallization at the eutectic point is only possible in a ternary or a multi-component system. If this is not the case, the system solidifies

completely. Often, a multi component system is reduced to a pseudo ternary system for the sake of simplicity. Figure 4-1 shows a typical ternary phase diagram. Generally, it exhibits three binary eutectic points and one ternary eutectic point (E).

Each arrowed line starts from the binary eutectic point of the corresponding two component system and ends in the ternary eutectic point. By cooling down a three component mixture of the composition F, the crystals of the component A start to form. Further cooling leads to more crystals of A and the liquid composition changes following the line F-L. On reaching the composition L, component C starts to crystallize as well. A further cooling changes the liquid composition along the line L-E. As soon as the ternary eutectic point E is reached, solid B starts to form in addition to A and C. The three components crystallize simultaneously and the system solidifies completely.

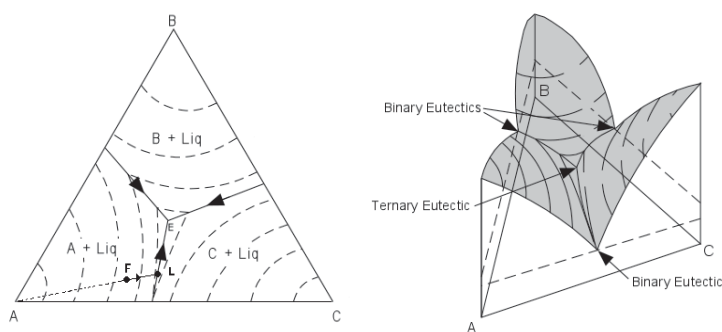


Figure 4-1 2D and 3D view of a ternary diagram.

A typical eutectic freeze crystallization process often starts from a pseudo binary system e.g. components A and B with only a small amount of the third component C. If the melt is cooled down below the eutectic equilibrium temperature of A and B, both solids of A and B are formed. If ice is produced within the process, the separation of the two different solids can easily occur due to the relative differences in the densities of the solids and the melt. Ice which has a density of app. 900 kg/m^3 , floats to the top, while salt possessing a typical density of 2000 kg/m^3 sinks to the bottom as shown in figure 4-2 [5].



Figure 4-2 Gravitational separation of ice and salt crystals [5].

The common eutectic freeze crystallization process for salt disposal and water recovery requires several unit operations as shown in the figure 4-3 [6]. The feed is cooled down in a suspension crystallizer below the eutectic temperature so that the salt and the water crystals are formed. The formation of ice crystals due to the primary nucleation is difficult. Therefore, the unit has to possess an additional crystallizer for the nucleation of ice followed by a ripening vessel for the growth of ice crystals. In 1972, Huige [7] demonstrated the occurrence of the so-called Ostwald ripening for ice crystals. Ostwald ripening means that the smaller crystals have a lower melting temperature than the larger ones. Therefore, it is possible to produce a suspension of large crystals, if the bulk temperature is established above the lower melting temperature of the small crystals and below the melting temperature of the larger ones. After the formation of the two different crystals, the suspension is fed to a solid-solid-liquid-separation unit (SSLS). The heavier salt crystals settle down, while the lighter ice crystals float to the top. Due to the high density difference between the ice and the salt crystals, the separation is very efficient. At the top of the SSLS unit a suspension of ice crystals can be collected and fed into a wash column for purification. The purified water leaves the wash column at the top. The salt suspension is taken from the bottom of the SSLS unit and is forwarded to a solid-liquid separation e.g. a belt filter sequence [5]. The arising mother liquor is recycled back and mixed with the crystallizer feed to increase the yield of the process. If a defined salt quality is required, a purge stream has to be realized.

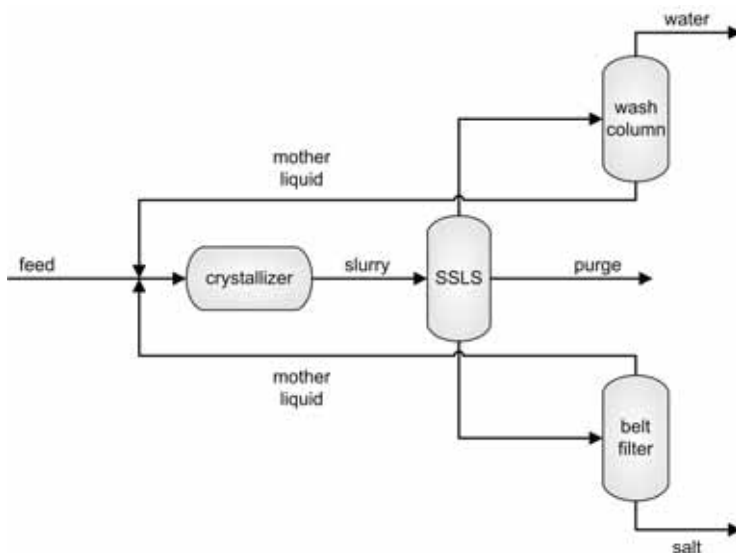


Figure 4-3 Scheme of the EFC process in analogy to Stepakoff et al. [6].

In the recent past, several developments have been made to improve the efficiency of a eutectic freeze crystallization process due to advances in apparatus design and process applicability. The presentation of the several developments is not a part of this chapter.

4.3 Approach to filtration improvement

4.3.1 Qualitative approach to porosity improvement with an in-situ formed filter aid

The improvement of the filtration characteristic of suspensions by the addition of another particulate solid material is one of the best measured [8]. In cases of compressible and low porous filter cakes, solid materials are added to the suspension to build up a porous, permeable, and low compressible structure for retaining the solid particles and allowing an easy pass-through of the liquid. Conventional filtration processes set several requirements to the selected filter aids as follows [8]:

- Low specific surface or a coarse size
- Narrow fractional size distribution by removing the finer size fractions
- Create a particle bridging by an uniform dispersion in the particle bed
- Chemical inert material to prevent medium cracking and clogging
- Solids should possess a certain hardness

Based on these requirements, an idea was developed to use ice crystals as a filter aid to improve the permeability and to decrease the compressibility of the crystal bed formed of

acrylic acid crystals. Due to the application areas of acrylic acid, it is possible to identify water as an optimal material which meets all required conditions of a filter aid:

- The solid hardness of ice at the eutectic crystallization temperature is high. This indicates a low breakage tendency with a low compressibility. Additionally, the hardness of ice increases with decreasing temperature [9].
- Water is an inert material in the major applications of acrylic acid.
- Water is part of the crystallization system so that it is possible to form ice crystals in-situ.
- It is possible to crystallize ice with a coarse distribution by the use of a ripening vessel to induce Ostwald-Ripening [7].

In 1988 Van Pelt [10] demonstrated the possibility to control the crystallization of water by adjusting the occurring supercooling so that large spherical ice crystals occur. Figure 4-4 shows spherical ice crystals with a diameter of 200 - 400 μm from a Sulzer ripening vessel (picture courtesy of Sulzer Chemtech) [11].

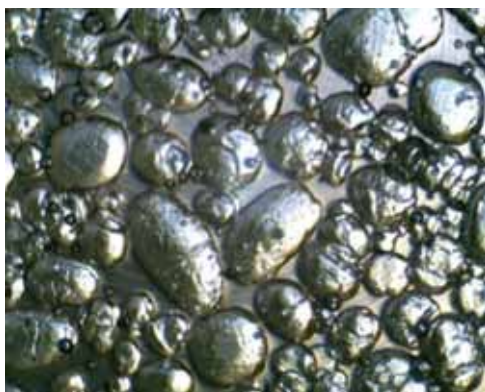


Figure 4-4 Ice crystals with a diameter of 200 - 400 μm in a ripening vessel by Sulzer [11].

4.3.2 Data estimation of an acrylic acid crystal bed near eutectic composition

The permeability and the compressibility of a crystal bed of acrylic acid crystals under the influence of supercooling and mechanical force in form of the liquid pressure drop was investigated in chapter 3 [2]. The experiments were carried out up to a water concentration of 15 wt%. Based on these experiments a model was developed to predict filterability under different conditions.

Before measuring the permeability and the compressibility of a crystal bed formed of acrylic acid and ice crystals at eutectic concentration, the performance of a crystal bed of acrylic

acid crystals has to be extrapolated. There are two ways to do this. First, the order of magnitude of the expected permeability can be estimated. Second, the quality of the extrapolation and therefore the validation of the developed model of chapter 3 [2] can be aligned by experimental data.

4.3.2.1 Initial permeability B_0 without compressive stress

The eutectic point of the binary solid-liquid equilibrium is about 38 wt% water. The approach of the extrapolation starts with the estimation of the initial permeability B_0 of the crystal bed at different supercooling conditions. Therefore, the initial permeabilities B_0 are plotted versus the water content of the melt at different supercooling β . The extrapolated graph is shown in figure 4-5.

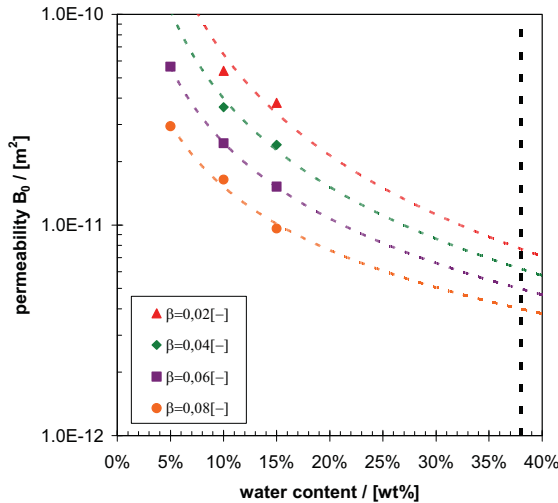


Figure 4-5 Initial permeability B_0 extrapolation to 38 wt% water.

The initial permeabilities decrease with increasing water content and increasing supercooling. At 38 wt% water the initial permeability of a crystal bed of acrylic acid crystals is between $3 \cdot 10^{-11} \text{ m}^2$ and $8 \cdot 10^{-12} \text{ m}^2$. If the logarithmic scale of the y-axis is taken into account, the differences in the permeability due to the different supercooling decrease.

4.3.2.2 Compressibility coefficient σ

The permeability of a crystal bed hardly depends on its compressibility. The compressibility is defined as the change in porosity or the permeability with the pressure change. Tiller [12] investigated the general compressibility behavior of particles. The change of the initial porosity ε_0 and the permeability B_0 at zero stress p_0 due to a certain pressure change was

found. It can be described by using the specific compressibility coefficients λ for porosity and σ for permeability, as shown in eq. 4-1 from Tiller [12]:

$$\left(\frac{\varepsilon}{\varepsilon_0}\right)^{\frac{-1}{\lambda}} = \left(\frac{B}{B_0}\right)^{\frac{-1}{\sigma}} = 1 + \frac{p}{p_0} \quad \text{eq. 4-1}$$

The knowledge of the compressibility coefficients σ is essential to calculate the resulting permeability due to the mechanical stress. The compressibility coefficients σ were calculated from the logarithmic permeability slopes for water contents up to 15 wt% and a liquid pressure drop up to 750 mbar.

If the compressibility coefficients σ are plotted against the supercooling for different water contents, straight lines occur. The extrapolation to water contents of 25 wt% and 38 wt% water is carried out by fits of the y-axis intercepts and the line slopes. The extrapolated behavior of the compressibility coefficients in dependence of supercooling is shown in figure 4-6.

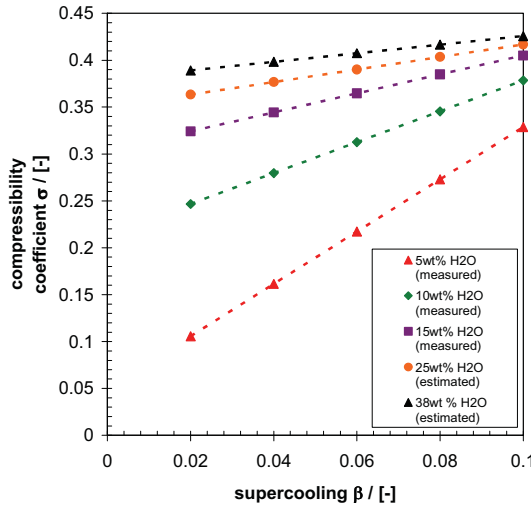


Figure 4-6 Extrapolation of the compressibility coefficients to water contents of 25 wt% and 38 wt%.

The extrapolation to water contents of 25 wt% and 38 wt% shows that the difference in compressibility due to the influence of water and supercooling gets smaller. This trend is plausible, if the findings on crystal growth of acrylic acid from an aqueous solution of chapter 2 [1] are considered.

A model was developed which considers the influence of water and supercooling on the crystal growth of acrylic acid in light of surface and bulk effects due to the coexisting water molecules. Water forms a monomolecular layer on face {002} inhibiting its growth. On the other hand, the consequences of bulk effect are two-fold. Firstly, for the growth of face {002}, dimers of acrylic acid are required as growth entities. In presence of water the competing formation of acrylic acid hydrates takes place and reduces the amount of acrylic acid dimers. Secondly, water improves the conditions of crystal growth by the improvement of heat and mass transfer conditions. This leads to a faster growth of the remaining faces {121} and {110} and finally to a needle-like crystal shape with a cavity on face {002}.

The needle-like shape and the appearing cavity consequently lead to breakable crystals and hence to a higher compressibility of the crystal bed. The changes in the compressibility are higher at lower water contents. This is plausible, if it is taken into account that the mentioned effects depend on the molar concentration of water. A water concentration of 5 wt% of water corresponds to a concentration of 17 mol%, whereas a concentration of 25 wt% corresponds to concentration of 57 mol%. Taking this fact into account, it is obvious that the changes in the compressibility at lower weight concentrations of water are higher and get negligible at higher weight concentrations of water.

4.3.2.3 Permeability performance near eutectic concentration

The transformation of Tiller's equation allows the calculation of the permeability under the influence of mechanical stress. The input parameters are the initial permeability B_0 and the compressibility coefficient σ . The transformation leads to eq. 4-2. The mechanical stress is involved in forms of a quotient of the occurring liquid pressure drop over the crystal bed and the pressure drop at zero stress.

$$B = \left(1 + \frac{p}{p_0} \right)^{-\sigma} \cdot B_0 \quad \text{eq. 4-2}$$

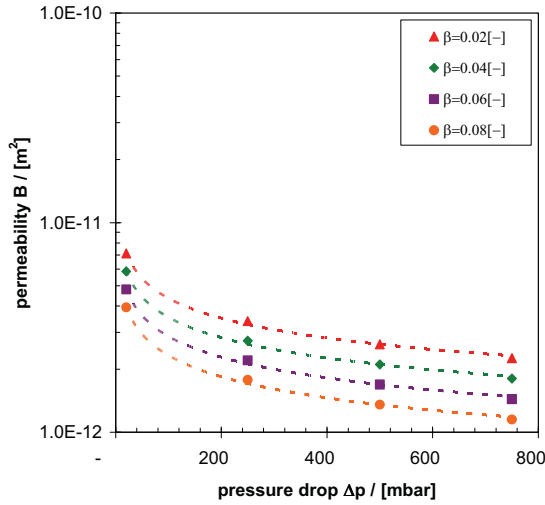


Figure 4-7 Permeability performance at 38 wt% water.

A comparison of the estimated values taken from figure 4-7 with the measured results at 15 wt% water shows a high difference at lower supercooling and less difference at higher supercooling. This is caused by the compressibility and the morphology development as a function of supercooling, respectively. Elongated crystals are observed already at a low water content and high supercooling. As the supercooling becomes higher, the influence of water on the development of elongated crystals becomes smaller.

4.3.3 Theoretical estimation of the porosity of nonspherical particles mixtures

An empirical correlation to predict the porosity ε of the binary mixtures of spherical particles was developed by Westman [13] based on the total bed volume V occupied by the specific volume of the solid material (eq. 4-3). The presented porosity correlation is only used theoretically to see the general trends by adding ice as a filter aid. The porosity trend is used as an indicator for the filterability only, knowing that the permeability is a function of porosity and compressibility.

$$V = \frac{1}{(1 - \varepsilon)} \quad \text{eq. 4-3}$$

Yu et al. [14] showed that the packing behavior of nonspherical particles is similar to the packing behavior of spherical particles. Based on this finding Yu et al. [15] modified the equation of Westman to apply it to both spherical and nonspherical particles. They added an

empirical constant G which is independent from the composition of the solid composition but depends on the aspect ratio of the particles.

$$\left(\frac{V - V_l X_l}{V_s}\right)^2 + 2G \left(\frac{V - V_l X_l}{V_s}\right) \cdot \left(\frac{V - X_l - V_s X_s}{V_l - 1}\right) + \left(\frac{V - X_l - V_s X_s}{V_l - 1}\right)^2 = 1 \quad \text{eq. 4-4}$$

Where

- V specific volume of the bed [m^3/kg]
- V_l initial specific volume of the large particles [m^3/kg]
- V_s initial specific volume of the small particles [m^3/kg]
- X_l volume fraction of the large particle [-]
- X_s volume fraction of the small particle [-]
- G empirical coefficient [-].

The general relation proposed by Yu et al. [15] for the coefficient G is shown in the equations below [15]. The empirical constant G depends on the ratio r_p of the diameter of the small particles d_s to the large particles d_l .

$$\frac{1}{G} = 1.335 \cdot r_p^{1.566} \quad (r_p \leq 0.824) \quad \text{eq. 4-5}$$

$$\frac{1}{G} = 1 \quad (r_p > 0.824) \quad \text{eq. 4-6}$$

$$r_p = \frac{d_s}{d_l} \quad \text{eq. 4-7}$$

Yu et al. [15] suggested to substitute the particle diameter by the packing equivalent diameter d_p for nonspherical particles from the volume equivalent particle diameter d_e and the Wadell's sphericity ψ .

$$d_e = (3.1781 - 3.6821 \cdot \frac{1}{\psi} + 1.5040 \cdot \frac{1}{\psi^2}) \cdot d_v \quad \text{eq. 4-8}$$

The Wadell's sphericity ψ is defined as the ratio of the surface area A_s of a sphere with the equivalent volume and the surface area of the actual particle A_a . The crystals are assumed to be regularly shaped. Therefore, the sphericity can be determined by eq. 4-9.

$$\psi = \frac{A_s}{A_a}$$

eq. 4-9

The practical application of the Westman equation to nonspherical particles as suggested by Yu et al. [15] by using the Wadell's sphericity ψ is disputable. The porosity calculations for the fraction limit values $X_s=1$ and $X_f=1$ always result in a porosity of $\varepsilon = 47.6$ vol% due to the geometry principles. For nonspherical uniformed single size particles, the porosity usually is equal to 0.40 for loose random packing or to 0.36 for the dense random packing [16].

However, the Westman equation extended to nonspherical particles is used to estimate the theoretical porosity of the mixtures formed of acrylic acid crystals and ice. Ice is assumed to have a spherical shape, whereas the rectangle acrylic acid crystals are included by the Wadell's sphericity ψ . For acrylic acid, the aspect ratio α as a function of water content in the melt was measured in chapter 2 [1]. For the eutectic concentration of 38 wt% acrylic acid and a maximum supercooling of 0.1 an aspect ratio for acrylic acid crystals of approximately 5.3 is expected. The calculations of the porosity are a function of the ratio of the diameters r_p of the small particles to the large particles only. The results for three different values of r_p are shown in the figure 4-8.

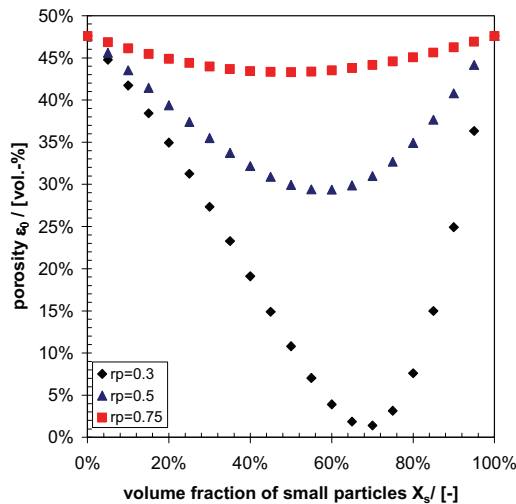


Figure 4-8 Porosity calculation via extended Westman equation.

The calculated porosity values strongly depend on the ratio of the diameters r_p . The porosity decreases significantly as the ratio r_p gets smaller. The drastic decrease in the porosity to values near zero depends on the critical size of the smaller spheres which can pass through

the openings formed by the larger monosized spheres. This results in a complete plug of the free volume between the large particles. This geometric explanation for two different sphere packings is shown in figure 4-9.

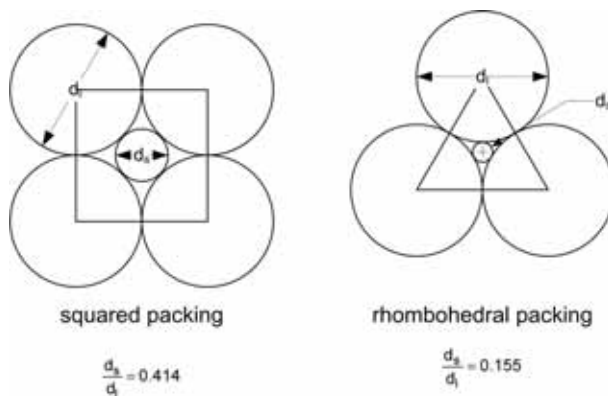


Figure 4-9 Critical ratio of entrance for different packings.

Based on the calculated porosities for different particle ratios resulting from the transformation of rectangle crystals to spheres, it is possible to calculate the theoretical permeability B_0 at zero stress by using the Kozeny-Carman eq. 4-10. The equation uses the porosity, the specific surface area S_0 , and the specific Kozeny constant K_{kc} . Based on the Westman equation which uses the area based sphericity defined by Wadell, the Kozeny constant for spherical particles can be used. The value for K_{kc} is 5 [17].

$$B_{KC} = \frac{1}{K_{KC}} \cdot \frac{\epsilon^3}{(1-\epsilon)^2} \cdot \frac{1}{S_0^2} \quad \text{eq. 4-10}$$

The aspect ratios r_p of the small particles (translated from rectangles) to the large ones has been differed from 0.33 to 0.75. The size of the small rectangle particles representing the acrylic acid crystals has been set to a length of 100 μm and 300 μm respectively. These particle diameters are in the order of magnitude of the real measured length of acrylic acid crystals. The permeabilities are plotted against the mass fractions of the small particles in figure 4-10. The plot represents the permeability translated to the monosized spherical particles only.

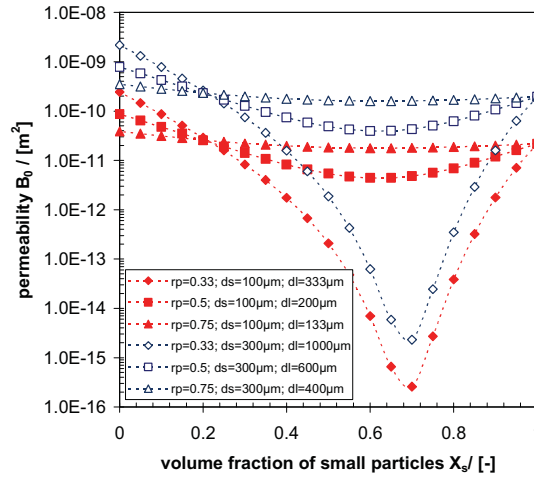


Figure 4-10 Theoretical permeability B_0 for monosized spheres and rectangles.

It is possible to draw the following conclusions for a rough transformation to a monosized system existing out of a binary particle mixture:

1. The larger the individual particle fraction, the higher is the initial permeability.
2. The lower the diameter ratio r_p , the lower is the permeability. The influence of the ratio r_p is significant.
3. The influence of the addition of a certain amount of large particles to the small particles is smaller than the contrary case.
4. For a random particle packing, the critical ratio of the entrance comparable with the diameter ratio is between 0.414 and 0.155. Below these values, it is possible that the small particles completely plug the porosity cavity of the large particles which leads to a dramatic permeability decrease.

The results could lead to the conclusion that addition of a filter aid is unfavorable due to an apparent decrease in the permeability. However, the results of the permeability calculations should be handled with care. In spite of the translation from rectangles to spheres, the model always bases on a random packing of spheres. Therefore, a mixture of different spheres will always result in a porosity and permeability minimum. A description of a random packing of two different morphologies is not available. Additionally, a prediction of a desired compressibility improvement based on the porosity and the permeability is not possible. Therefore, an experimental validation is necessary.

4.4 Experimental

4.4.1 Objectives

The main objectives were to carry out by batch crystallization experiments followed by permeability measurements to investigate the influence of ice crystals on the permeability and the compressibility of an acrylic acid crystal bed. Therefore, the initial permeabilities of crystal beds composed of pure ice and acrylic acid crystals, respectively, were determined first. These values are compared with values of a mixture of ice and acrylic acid crystals. The variation of the ratio is achieved by slightly differing the feed compositions from the eutectic one. The composition of the crystal bed is analyzed after filtration. Primarily, continuous crystallization experiments with a common scraped surface crystallizer were planned. However, several contrary problems occurred which were not solvable at this early feasibility stage.

4.4.2 Experimental setup and procedure

4.4.2.1 Batch crystallizer

All experiments were carried out with a batch crystallizer of 17 L hold-up. Figure 4-11 shows the setup schematically. The crystallizer is a common scraped surface crystallizer typically used for continuous experiments. It is equipped with an outer cooling jacket loaded with a coolant to remove the energy from the crystallizer. To avoid encrustation on the wall, two rotating spring-loaded PTFE scrapers oriented perpendicularly to the wall were installed. Additionally, the centered drive shaft was equipped with six mixing vanes to ensure ideal mixing. The crystallizer was fed batch-wise via the valve at the top. The crystallization process was temperature controlled via the installed temperature indicators at the top and the bottom. The two temperatures were used as the control parameter for the coolant temperature. The control loop and the cooling circuit are not shown in the figure.

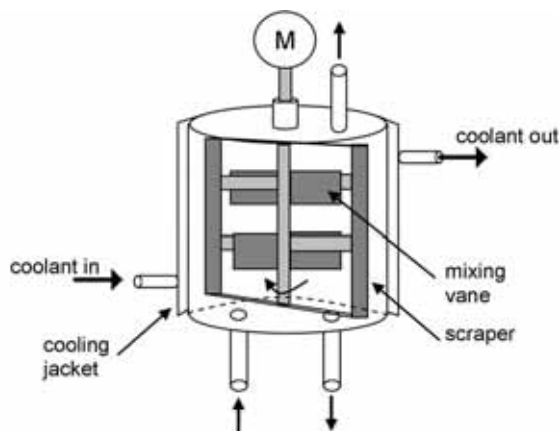


Figure 4-11 Batch crystallizer with a cooling jacket, a mixing device, and scrapers.

4.4.2.2 Procedure

After filling the crystallizer with the feedstock, the inlet temperature was set to the melting temperature of the mixture. When a constant crystallizer temperature was reached, a temperature gradient of -0.3 K/min was started. The cooling was stopped when the desired composition of the generated solids and the precalculated solid content was reached. The temperature was kept constant for 12 hours to provide similar ripening conditions throughout the experiments and to prevent the influence of the remaining supercooling. The slurry was used to carry out the required permeability tests described within the next paragraph.

4.4.2.3 Permeability experiments

The permeability is determined by a constant pressure filtration test using the setup shown in figure 4-12 [18]. Due to the floating crystals, the setup was enhanced by a small filter piston. With its help the separation of the different crystals was prevented. The downwards motion of the piston was done carefully to avoid any undefined compressing of the crystal bed. As a result a bed with a final height h_b was generated. Opening the bottom valve to the vacuum flask leads to a flow of the mother liquor through the packed bed. The permeability can be determined with eq. 4-11:

$$B = \frac{\eta \cdot h_b}{\rho \cdot g \cdot (t_2 - t_1)} \cdot \ln(H_1 - H_2) \quad \text{eq. 4-11}$$

In this way, the hydrostatic head is used as the driving force for flow and the pressure difference over the bed is limited. To determine the permeability change as a response to

pressure, different vacuum values are applied over the crystal bed in the filtration setup. To calculate the permeability, subsequently the pressure difference is translated into a liquid head and used as input for eq. 4-11. The measured permeability is in any case corrected for the resistance of the glass filter in the bottom which is determined in a filtration experiment with pure liquid acrylic acid.

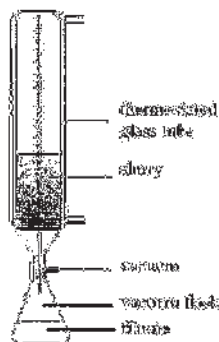


Figure 4-12 Filtration setup [18].

4.4.3 Experiments

The influence of water crystals as an in-situ filtration aid on the filterability of acrylic acid crystals was investigated for different water and acrylic acid fractions of the solids phase. All combinations of the various solid fractions are shown in table 4-1. Filtration experiments were carried out at four different pressure drops to determine additionally the compressibility behavior. The filtration experiments were carried out at least twice.

Table 4-1 Experiment overview.

solid fraction		pressure drop / [mbar]
X_{H_2O} / [wt%]	X_{AA} / [wt%]	
100 wt%	0 wt%	0 mbar
		250 mbar
		500 mbar
		750 mbar
70 wt%	30 wt%	0 mbar
		250 mbar
		500 mbar
		750 mbar
38 wt%	62 wt%	0 mbar
		250 mbar
		500 mbar
		750 mbar
20 wt%	80 wt%	0 mbar
		250 mbar
		500 mbar
		750mbar
0 wt%	100 wt%	0 mbar
		250 mbar
		500 mbar
		750 mbar

4.4.4 Results

4.4.4.1 Observations

The experiments confirmed the statement of patent EP1492755A1 [4]. Crystallization at the eutectic point results in two different crystal habits as shown in figure 4-13. As expected acrylic acid crystallizes in a rectangular morphology and ice crystallizes in a cubic or nearly spherical form. It was observed that the morphology of the ice crystals transforms from plate-like crystals within the ripening time to cubic or nearly spherical particles. The shape and the

size of the different crystals was roughly estimated with a microscope. The results of the visual characterization are shown in table 4-2.

Table 4-2 Visual particle characterization.

	shape	length	size	aspect ratio
ice crystals	cubes or spheres	diameter	app. 100 to 200 μm	app. 1
acrylic acid crystals	long rectangles	small distance	app. 50 to 100 μm	app. 4 to 5

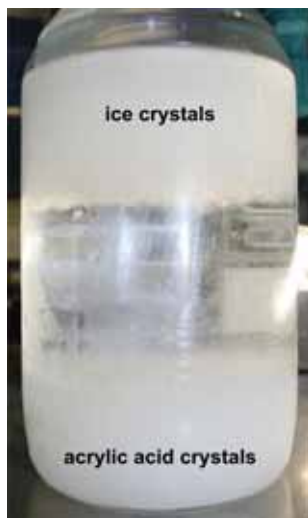


Figure 4-13 Separated ice and acrylic acid crystals.

4.4.4.2 Permeability

The permeabilities of all experiments follow a straight trend. The results are shown in figure 4-14 and figure 4-15. Figure 4-14 shows the initial permeability values B_0 plotted versus the solid phase composition. The initial permeability B_0 of a crystal bed formed of pure acrylic acid crystals is the lowest one. The crystal beds formed from ice crystals possess the highest permeability. The difference between permeabilities of the crystal beds formed of the pure components is a factor of 3.

- A straight increase of the measured initial permeability B_0 is observed with an increasing amount of ice crystals in the solid phase. Based on the theoretical

permeability calculations of paragraph 4.3.3 a minimum of the permeability was expected.

- The improvement of the permeability by the addition of 38 wt% ice crystals, representing the eutectic composition, is by a factor 2.
- With the help of the observed ranges of crystal sizes and aspect ratios of table 4-2, it a parameter fit was carried out to model the initial permeabilities B_0 using the presented Westman equation of section 4.3.3. The identified parameters for modeling the initial permeabilities B_0 are listed in table 4-3.

Table 4-3 Parameter fit for the Westman equation

Wadell's sphericity ψ / [-]	0.634
diameter ratio r_p / [-]	0.66
diameter of the large particles x_l [μm]	130
diameter of the small particles x_s [μm]	87

- The calculated values of the initial permeabilities B_0 are represented by the dashed lines in the figure 4-14. The calculated permeabilities show a good agreement with the experimental values. They show a straight increase with increasing ice crystal content.
- The calculation of the initial permeabilities is quite sensitive to changes of the diameter ratios. Already a diameter change of the small particles to 69 μm which goes along with the diameter ratio r_p of 0.5, leads to higher changes of the calculated initial permeability values as presented in figure 4-14 by the lower dashed line.

Figure 4-15 shows the permeability trend at different solid phase compositions as a function of the occurring pressure drop which is similar to mechanical stress to the crystal bed.

- For all solid mixtures the permeability decreases with an increasing pressure drop over the crystal bed.
- An increasing ice crystal fraction of the solid phase improves the permeability over the complete range of pressure drop
- The slopes of the permeabilities plots become flat with an increasing fraction of the ice crystals. This indicates an improvement of the compressibility by the addition of the ice crystals.

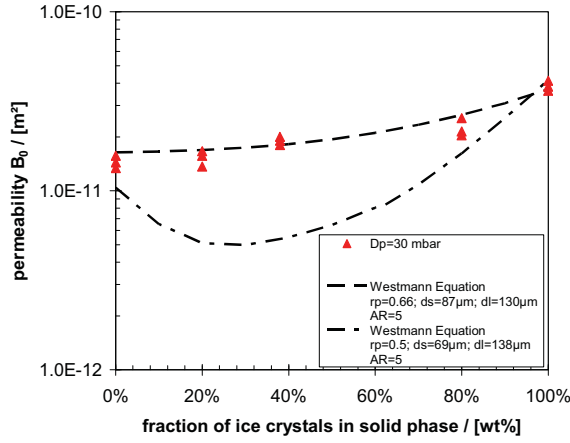


Figure 4-14 Initial permeabilities B_0 vs. solid phase compositions.

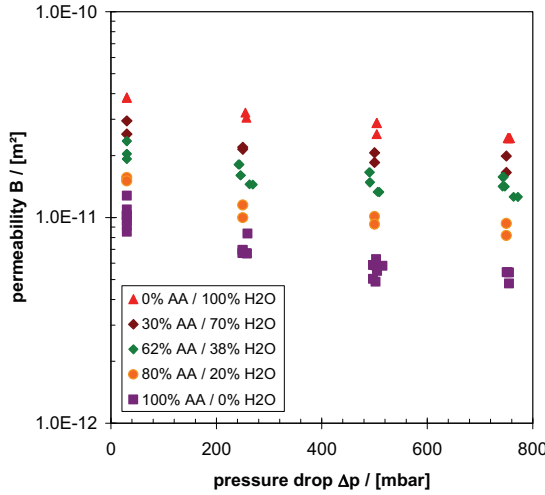


Figure 4-15 Permeabilities for different solid phase compositions vs. pressure drop.

4.4.4.3 Compressibility coefficients

The determination of the compressibility coefficients for all ratios of ice and acrylic acid crystals is carried out by the transformation of eq. 4-12 from Tiller [12].

$$\log\left(\frac{B}{B_0}\right) = \sigma \cdot \log\left(1 + \frac{p}{p_0}\right)$$

eq. 4-12

If the logarithm of the permeability quotients (B/B_0) are plotted vs. the logarithm of $(1+p/p_0)$, the compressibility coefficients are represented by the slopes of the straight lines. The pressure value p_0 is set to 25 mbar because this represents the pressure at gravity force of a 25 cm liquid column.

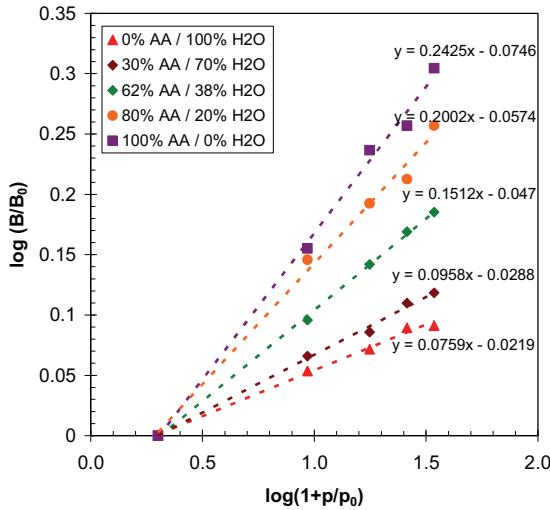


Figure 4-16 Compressibility coefficient determination.

The slopes of the lines decrease with an increasing fraction of ice crystals. The compressibility coefficients of all experiments are taken from the straight lines of figure 4-16 and are plotted vs. the ice crystal content of the solid phase as shown in figure 4-17.

The compressibility coefficients decrease with an increasing ice crystal fraction. The difference of compressibility coefficients of the crystal beds formed of the pure components is a factor of 3. The addition of ice up to a fraction value representing the eutectic composition of 38 wt% reduces the compressibility coefficient by 40%.

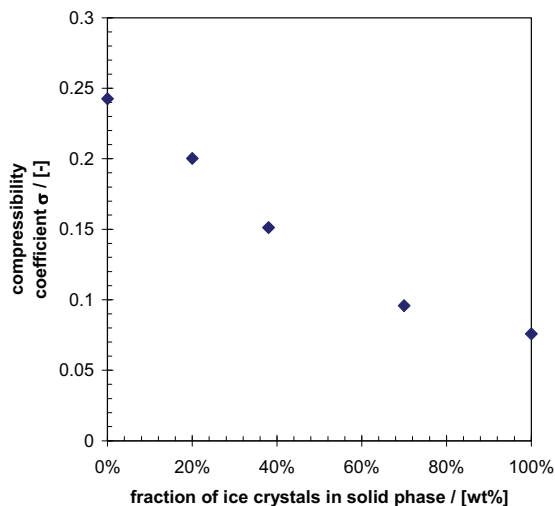


Figure 4-17 Compressibility coefficients vs. the AA concentration of the solid phase

4.5 Discussion and outlook

The experimental results provide an indication of the improvement in the filterability behavior of an acrylic acid crystal bed by the in-situ formation of ice crystals. A straight improvement of the permeability is possible by the addition of ice. The addition of 38 wt% ice crystals to an acrylic acid crystal bed improves the permeability by a factor of 2. Additionally, the formation of ice improves the compressibility of a crystal bed significantly. The compressibility coefficients decrease from 0.24 for acrylic acid crystals to 0.15 at an ice fraction of 38 wt%. This corresponds to an improvement of 40%. For ice fractions higher than 50 wt%, the change in compressibility coefficients gets smooth. This could be caused by the fraction ratios and sizes of the two crystal morphologies. To verify and explain this observation, it would be helpful to measure the crystal size distribution of ice and acrylic acid in the solid mixture. However, the measurements cannot be performed by available methods.

There is a difference between the measured and the estimated permeabilities and the compressibility coefficients for a pure acrylic acid crystal bed generated from a melt close to the eutectic composition. The estimated permeabilities of paragraph 4.3.2 are much lower, whereas the estimated compressibility coefficients are much higher than the experimental values presented in paragraph 4.4.4.3. The deviations are probably caused by the differences of the continuous and batchwise experimental procedures. In particular, the differences are in nucleation, nucleation temperature, conditions of supercooling, and crystal growth. However, the scope of this work was to check the general feasibility to use ice as a

permeability improver of an acrylic acid crystal bed. This has been demonstrated successfully.

The presented Westman equation [13] is used to calculate the initial porosities. Combined with the Kozeny-Carman equation a useful engineering model exists to carry out forecast calculations of the occurring initial permeabilities. Finally, it is possible to calculate the final permeability via the Tiller equation using the determined compressibility coefficients.

With the help of the complete model, a sensitivity analysis with different crystal sizes and aspect ratios for the acrylic acid crystals has been done. A parameter set of crystal size and shape was found to reproduce the experimental initial permeability values B_0 and finally the occurring permeability under the influence of mechanical stress. The identified parameters of crystal size and aspect ratio of acrylic acid crystals are within the range of values detected by the visual particle characterization of section 4.4.4.1. The calculated values of the initial permeabilities B_0 are in a good agreement with the experimental values.

However, it was also found that the calculation of the initial porosity via the enhanced Westman equation is quite sensitive and hence the absolute initial permeability values differ significantly. On the other hand, the trends of the curves are also quite sensitive to small changes in the diameter ratio r_p so that a minimum in porosity and permeability can occur.

The sensitivity and the resulting difference can be explained as follows:

- The consideration of the crystal morphology in the model is not sufficient. It uses the sphericity as an input parameter to adapt the model to nonspherical particles. This means, that all morphologies are transformed by their geometric ratios to spheres of different sizes. This must lead to a porosity minimum similar to that shown in that shown in figure 4-9. The model does not represent the influence of needle-like crystals accurately.
- The Westman equation [13] considers a monosized distribution only. An industrial suspension disposes a size distribution of particles which will have an enormous influence on the porosity and the permeability.

For the porosity modelling of the solid mixtures a random packing model considering different crystal morphologies is required. Additionally, the influence of the size distributions of the different morphologies has to be taken into account for a better prediction. However, this requires the measurement of the size distribution of each crystal fraction first.

4.6 Conclusion

The addition of ice to an acrylic acid crystal bed improves the performance of a solid-liquid separation process significantly. This trend offers the chance to develop a completely new generation of suspension crystallization process. The use of a common wash column for the

simultaneous purification of two solid phases crystallized under eutectic conditions is possible as already demonstrated in WO2009130085A1 [19].

Therefore, the following conclusions can be drawn with regard to a technical scale:

1. The formation of ice crystals as an in-situ filter aid improves the filterability of acrylic acid in general.
2. The improvement of the filterability generates permeability values which are comparable with the permeabilities of the crystal bed of acrylic acid crystals grown from a pure melt without the influence of water.
3. The ice crystals provide a major improvement of the compressibility behavior. The compressibility coefficients are reduced from around 0.25 down to 0.15. This represents a relative improvement of the absolute compressibility of 40%. The improvement of the compressibility is a major key parameter to increase the maximum capacity of wash columns [3].

Based on the improvement of the compressibility coefficients at a eutectic solid composition the process potential and the economic can roughly estimated. At a typical pressure drop of 2 - 4 bars an improvement of the compressibility coefficient of 40% results in an increase of the filtration capacity of approximately 50%. If the increase of the solid load caused by the amount of 38 wt% ice crystals is considered, the net capacity increase is approximately 12% at a constant filter cross-sectional area. On the other hand, the necessary cross-sectional area of a solid-liquid separation unit can be reduced by 12%.

The results of the feasibility tests have to be verified by experiments from a continuously operated crystallization process. Probably, a further improvement of the filterability is possible, if the crystal suspension is taken from a setup with a ripening vessel to generate bigger ice crystals.

The enhanced model of Westman enables the modeling of the porosities of two different solids with two different shapes using the Wadell's sphericity and finally the resulting initial permeabilities using the Kozeny-Carman and Tiller equations. This model can be used as an engineering tool to predict the resulting permeability of an industrial eutectic crystallization unit, if the shape, the size, and the compressibility coefficients are known.

Nomenclature**Symbols**

A	particle surface	$[m^2]$
B	permeability	$[m^2]$
d	diameter	$[m]$
G	empirical coefficient	$[m/s]$
g	gravity constant	$[m/s^2]$
h_b	height of crystal bed	$[m]$
H	liquid level	$[m]$
K_{kc}	Kozeny constant	$[-]$
K_{mc}	MacDonald constant	$[-]$
p	pressure	Pa
r_p	ratio of diameters	$[-]$
S_0	specific Surface	$[m^2/m^3]$
t	time	$[s]$
V	volume	$[m^3]$
X	solid fraction	$[-]$
x	mass fraction	$[wt\%]$

Greek Symbols

α	aspect ratio	$[-]$
β	supercooling	$[-]$
η	liquid viscosity	$[Pa*s]$
ε	porosity	$[-]$
ρ	density	$[kg*m^{-3}]$

σ	compressibility coefficient for permeability	[-]
λ	compressibility coefficient for porosity	[-]
ψ	sphericity	[-]

Subscripts

a	surface equivalent
e	equivalent
l	indication for large particles
s	indication for small particles
v	volume equivalent
0	initial state at zero stress
1	index number
2	index number
KC	Kozeny-Carman
Mc	MacDonald

References

- [1] Hengstermann, A.; Kadam, S.; Jansens, P. J.; Influence of water content and supercooling on crystal morphology of acrylic acid, *J. of Crystal Growth and Design*, 2009, Vol. 9 (4), pp2000–2007.
- [2] Hengstermann, A.; Harms, S.; Jansens, P. J.; The Influence of Water and Supercooling on Permeability and Compressibility of Crystal Beds formed out of Acrylic Acid Crystals, *Chemical Engineering Technology*, 2010, Vol. 33 (3), pp433-443.
- [3] Oord-Knol, L.; Hydraulic Wash Columns – Solid-liquid Separation in Melt Crystallization, PhD Thesis, Delft University of Technology, Delft, The Netherlands, 2000.
- [4] Nordhoff, S.; Balduf, T.; Bub, G.; Fornika, R.; Mosler, J.; Ratke, T.; Kobus, A.; Thong, D.; (Meth)Acrylsäurekristall und Verfahren zur Herstellung und Aufreinigung von wässriger (Meth)Acrylsäure, 2003; European Patent EP1492755A1.
- [5] Genceli, F. E.; Scaling-up Eutectic Freeze Crystallization, PhD Thesis, Delft University of Technology, Delft, The Netherlands, 2008.
- [6] Stepakoff, G. L.; Siegelmann, D.; Johnson, R.; Gibson W.; Development of a Eutectic Freezing Process for brine Disposal, *Desalination*, 1974, Vol. 14, pp235-238.
- [7] Huige, N. J. J.; Nucleation and Growth of Ice Crystals from Water and Sugar Solutions in Continuous Stirred Tank Crystallizers, Ph.D. thesis, Technical University Eindhoven, Eindhoven, The Netherlands, 1972.
- [8] Yang, W.-C.; Handbook of Fluidization and Fluid-Particle Systems, Amrcel Dekker, Inc. New York, USA, 2003.
- [9] Shumski, P. A.; Principles of a structural glaciology, Dover Publications, New York, 1964, pp39-40.

- [10] Van Pelt W. H. J. M.; Roodenrijs J. P.; Multi-stage countercurrent concentrating system and method and separator, US Patent 4430104, 1982.
- [11] Sulzer Chemtech, Personell Correspondence with Dr. Manfred Stepanski; Sulzer Chemtech Ltd; Sulzer-Allee 48, P.O.Box 65, CH-8404 Winterthur, Switzerland, 2009.
- [12] Tiller, F.; Role of Porosity in Filtration: Behavior of highly compactible cakes, AIChE Journal, 1998, Vol. 44 (10), p2159.
- [13] Westman, A.; The Packing of Particles: Empirical Equations for Intermediate Diameter Ratios, Journal of the American Ceramic Society, 1936, Vol. 19, pp127-129.
- [14] Yu, A. B.; Zou, R. P.; Standish, N.; The Packing of Ternary Mixtures of Nonspherical Particles. Journal of the American Ceramic Society, 1992, Vol. 75, pp2765-2772.
- [15] Yu, A. B.; Standish, N.; McLean, A.; Porosity Calculation of Binary Mixtures of Nonspherical Particles, Journal of the American Ceramic Society, 1993, Vol. 76, pp2813-2816.
- [16] German, R.; Particle Packing Characteristics, Metal Powder Industries Federation. New Jersey, Princeton, 1989.
- [17] Svarovsky, L.; Solid-Liquid Separation, Butterworths, London, 1989.
- [18] Sluis, S. van der; A Clean Technology Phosphoric Acid Process, PhD Thesis, Delft University of Technology, Delft, The Netherlands, 1987.
- [19] Hengstermann, A.; Kuppinger, F. F.; Leistner, J.; Mosler, J.; Jansens, P. J.; Method for Producing and Purifying Aqueous Phases, 2008, WO-Patent WO2009130085A1.

SOLVENT SCREENING AND MEASUREMENT OF PHASE DIAGRAMS FOR THE YIELD MAXIMIZATION OF AN ACRYLIC ACID CRYSTALLIZATION

Abstract

The yield of crystallization processes is mostly limited by the eutectic points as thermodynamic limits and the economically acceptable temperature level. In some cases it is possible to increase the yield and to improve the crystallization performance by the addition of a dedicated third component.

Therefore, a structured solvent screening method is developed to rapidly identify possible solvents to increase the yield and to improve the performance of a crystallization unit if limiting factors are known.

For a fast validation, an experimental stage gate process is developed to come up with the required information of each stage at a minimum work load. The developed stage gate process bases completely on thermal analysis using Differential Scanning Calorimetry.

The solvent screening approach and the stage gate process are successfully adopted to investigate the yield maximization of an acrylic acid crystallization from an aqueous melt by adding a third component. For three possible components complete ternary solid-liquid equilibrium diagrams are measured and evaluated.

Accepted for publication in Chemical Engineering Data on 08-26-2010

5.1 Introduction

The recovery of acrylic acid by melt crystallization is limited in different ways. The yield is limited by the eutectic point at 62 wt% acrylic acid and a temperature of -11°C. Additionally, the performance of the suspension crystallization unit is limited by the water content of the mother liquid. An increasing water content causes problems in the downstream solid-liquid separation as demonstrated in chapters 2 and 3 [1;2].

Hence, the general scope of the present work is to increase the yield by the addition of a third component and therefore by altering the eutectic limits. Further, the performance of the crystallization should be improved in that way that the maximum recovery of acrylic acid should be achieved at low water content in order to reduce compressibility problems.

The work flow is divided into two stages to save time and money. This results in a dedicated solvent screening for the component identification and ends in a concerted experimental work flow using fast thermal analysis methods.

5.2 Solid-liquid equilibrium

5.2.1 Theoretical prediction of a solid-liquid phase equilibrium

At thermodynamical equilibrium, the chemical potentials of all components in all coexisting phases have to be equal. For the crystallizing component i this equilibrium is defined as:

$$\mu_i^L = \mu_i^S \quad \text{eq. 5-1}$$

Where the superscript L and S stand for the liquid phase and for the solid phase, respectively. Two concepts exist to take the nonideality of a solution into account. The model of Oonk [3] uses the activity coefficients and the model of Walas [4] uses the excess function concept. Subsequently, the model by Oonk [3] based on activity coefficients is used because it considers vapor-liquid data which are available for many components.

The equality of the chemical potential of each component in every phase can be reformulated as the isofugacity criterion:

$$f_i^L = f_i^S \quad \text{eq. 5-2}$$

The fugacities of the solid and the liquid phase are formulated using activity coefficients:

$$f_i^L = x_i^L \cdot \gamma_i^L \cdot f_{0i}^L \quad \text{eq. 5-3}$$

$$f_i^S = x_i^S \cdot \gamma_i^S \cdot f_{0i}^S \quad \text{eq. 5-4}$$

where f_{0i}^S and f_{0i}^L are the (pure component) standard fugacities of the solid and the liquid, γ_i^S and γ_i^L are the respective activity coefficients. Rearranging eq. 5-2 and eq. 5-3, one obtains the solubility of component i in the liquid phase

$$x_i^L = \frac{x_i^S \cdot \gamma_i^S \cdot f_{0i}^S}{\gamma_i^L \cdot f_{0i}^L} \quad \text{eq. 5-5}$$

Unfortunately, the standard fugacities are not readily available, especially when the system temperature lies above the triple point of the crystallizing component and below the one of the other component. In this case 'pure solid' and 'pure liquid' represent hypothetical states. However, for the calculation of the solubility only the ratio f_{0i}^S / f_{0i}^L is of importance. One harnesses a thermodynamic cycle as illustrated in figure 5-1

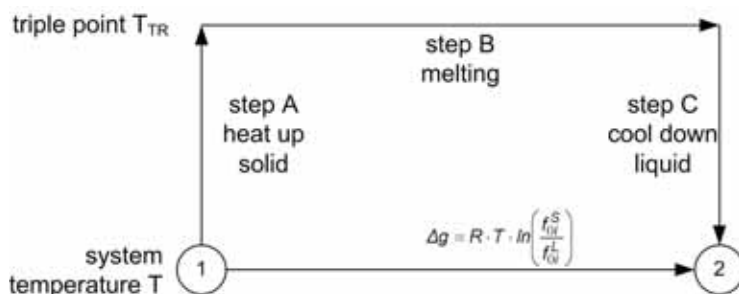


Figure 5-1 Thermodynamic cycle for the calculation of the ratio f_{0i}^S / f_{0i}^L .

The Gibbs enthalpy change for the transition from pure solid 1 to supercooled liquid 2 at temperature T is given by

$$\Delta g = R \cdot T \cdot \ln \frac{f_{0i}^S}{f_{0i}^L} \quad \text{eq. 5-6}$$

In a closed system

$$\Delta g = \Delta h - T \Delta s \quad \text{eq. 5-7}$$

where the change in enthalpy Δh and entropy Δs can be expressed as the sum of the changes for step A, step B, and step C:

$$\begin{aligned}\Delta h &= \int_T^{T_{0i}^{Tr}} c_{p,i}^S dT + \Delta h_{0i}^{Tr} + \int_{T_{0i}^{Tr}}^T c_{p,i}^L dT \\ &= \Delta h_{0i}^{Tr} + \int_{T_{0i}^{Tr}}^T c_{p,i}^L dT\end{aligned}\quad \text{eq. 5-8}$$

$$\begin{aligned}\Delta s &= \int_T^{T_{0i}^{Tr}} \frac{c_{p,i}^S}{T} dT + \frac{\Delta h_{0i}^{Tr}}{T_{0i}^{Tr}} + \int_{T_{0i}^{Tr}}^T \frac{c_{p,i}^L}{T} dT \\ &= \frac{\Delta h_{0i}^{Tr}}{T_{0i}^{Tr}} + \int_{T_{0i}^{Tr}}^T \frac{c_{p,i}^L}{T} dT\end{aligned}\quad \text{eq. 5-9}$$

Here, $\Delta c_{p,i}$ is the difference between the specific heat capacities of the solid and the liquid, respectively, i. e. $\Delta c_{p,i} = c_{p,i}^S - c_{p,i}^L$, and Δh_{0i}^{Tr} is the melting enthalpy at the triple point. Provided that the heat capacities are temperature independent between T and T_{0i}^{Tr} one obtains:

$$\ln \frac{f_{0i}^L}{f_{0i}^S} = \frac{1}{R \cdot T} \cdot \Delta h_{0i}^{SL} \left(1 - \frac{T}{T_{0i}^{Tr}} \right) - \frac{1}{R \cdot T} \cdot \Delta c_{p,i} \cdot (T_{0i}^{Tr} - T) + \frac{\Delta c_{p,i}}{R \cdot T} \cdot \ln \frac{T_{0i}^{Tr}}{T} \quad \text{eq. 5-10}$$

Eq. 5-10 can be simplified assuming that the first term is the predominant one and that the others cancel out. Further, the triple point temperature is often substituted by the melting temperature T_{0i}^{SL} , hence Δh_{0i}^{Tr} becomes the melting enthalpy Δh_{0i}^{SL} at T_{0i}^{SL} . Finally one obtains an equation for the calculation of solubilities.

$$-\ln \frac{f_{0i,L}}{f_{0i,S}} = \ln \frac{x_{i,L} \cdot \gamma_{i,L}}{x_{i,S} \cdot \gamma_{i,S}} = -\frac{1}{R \cdot T} \cdot \Delta h_{0i}^{SL} \cdot \left(1 - \frac{T}{T_{0i}^{SL}} \right) \quad \text{eq. 5-11}$$

In case of pure solids, the activity coefficients in the solid phase become unity and eq. 5-11 is rearranged to directly yield the solubility:

$$x_i^L = \frac{1}{\gamma_i^L} \cdot \exp \left[-\frac{1}{R \cdot T} \cdot \Delta h_{0i}^{SL} \cdot \left(1 - \frac{T}{T_{0i}^{SL}} \right) \right] \quad \text{eq. 5-12}$$

The activity coefficients can be calculated by well-known thermodynamic models, e.g. NRTL or UNIQUAC. For ideal systems eq. 5-12 simplifies to the Van't Hoff equation:

$$\ln x_i^L = \frac{\Delta h_{0i}^{SL}}{R} \left(\frac{1}{T^{SL}} - \frac{1}{T} \right) = \frac{\Delta_{fus} h_i}{R} \left(\frac{1}{T_m} - \frac{1}{T} \right) \quad \text{eq. 5-13}$$

For the prediction of the solid-liquid equilibrium of acrylic acid and water, it is important to consider the aqueous milieu. Therefore, it is not possible to use the reduced ideal Van't Hoff equation without including the activity coefficients. For mixtures of acrylic acid and water the eq. 5-12 is used to predict solid-liquid equilibrium temperatures. The activity coefficients are calculated from ASPEN Software. The UNIQUAC model combined with the Hayden-O'Connell method was used. The results are presented in figure 5-2.

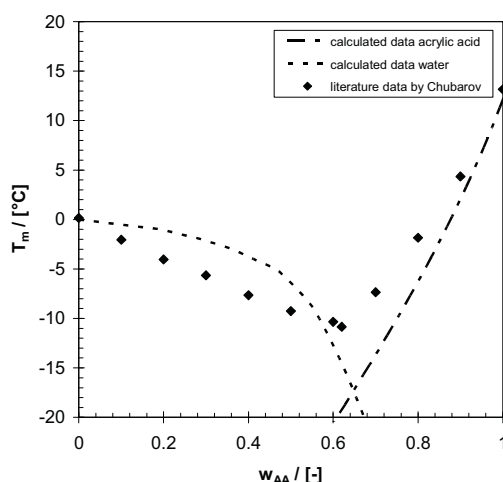


Figure 5-2 Solid-liquid equilibrium for acrylic acid and water - literature [5] and calculated data.

It is obvious that the predicted solid-liquidus lines which are represented by the dashed lines, differ significantly from literature data measured by Chubarov [5]. The temperature level of the liquidus line for water is much higher than the measured values, whereas the acrylic acid one is lower. Finally, the composition and temperature of the predicted eutectic point does not match reality.

This implies that the presented equation eq. 5-12 based on activity coefficients is not useful to predict the solid-liquid equilibrium for the aqueous acrylic acid system. In the near future experimental measurements of solid-liquid equilibria will still remain the preferred way to ensure reliable data for designing industrial applications. Therefore, this work is focused completely on rapid experimental procedures.

5.2.2 Thermal analysis methods for determination of thermodynamical properties

Thermal analysis methods are generally used to quantify and qualify several kinds of phase changes and recalescence actions. For the design and the control of crystallization processes at a maximum yield, the knowledge of phase diagrams is essential. These limitations are given by the necessary operating temperature, the eutectic and peritectic points, respectively [6].

In the past several techniques have been used to determine the solid-liquid equilibria:

- Thermal microscopy
- Thermal analysis
- Zone melting
- Single crystal growth

These techniques are not all universally applicable and some have only limited utility. The choice depends on a number of factors: availability of instrumentation, amount of material and time available, environmental sensitivity of the components and temperature range [6]. In the present work, the thermal analysis, more precisely the Differential Scanning Calorimetry (DSC), is used as a rapid measurement for temperatures and enthalpies of phase changes requiring only very small amounts of chemical samples. This opens up a new high-throughput method to determine complete binary and ternary solid-liquid equilibrium phase diagrams.

Differential scanning calorimetry principle

The Differential Scanning Calorimetry (DSC) is a thermo-analytical technique. Two crucibles – one containing the sample, the other one as a reference – are heated or cooled with the same rate. When the sample undergoes a (isothermal) phase change, unlike the reference it will not follow the heating/cooling program of the DSC device. In order to compensate the appearing temperature difference between sample and reference, the DSC device has to increase or decrease the heat flow to the sample crucible.

The result of a DSC experiment is a curve of heat flux versus temperature or versus time. The melting point and enthalpy of fusion of the sample material can be determined simultaneously from the DSC curve. An endothermic phase change gives a negative peak, whereas an exothermic phase change results in a positive peak. The peak area quantifies the enthalpy of fusion. A pure sample gives a sharp peak, while an impure sample could show a broader peak, overlapping peaks, an indefinite start, and an unincisive maximum. As an example figure 5-3 represents a schematic plot of an exothermic heat flow versus temperature. The temperature boundaries of the melting process are represented by $T_{m,on}$ and $T_{m,off}$. Whereas the index “m” represents the melting process, “on” represents the on-set

and “end” the end-set, respectively. The peak represents the melting temperature T_m of the sample.

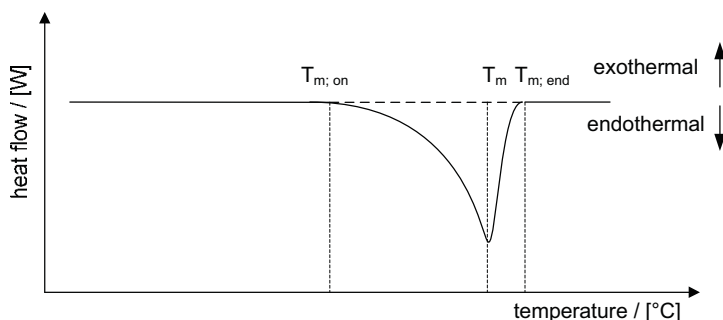


Figure 5-3 Heat flow of a solid to liquid phase change.

T_m stands of course also for the equilibrium crystallization temperature. However, due to metastability effects which are intrinsic to crystallization processes, it is not possible to measure the correct phase change temperature by cooling the sample. Keeping all these conditions in mind, the DSC provides a suitable technique to measure rapidly and exactly complete solid-liquid equilibrium phase diagrams, using the melting points of several samples at different concentrations. Additionally, the latent enthalpy of fusion can be obtained by measuring the area of the peak over time.

5.2.3 Determination of the binary eutectic point and equilibrium diagram

For the industrial application of crystallization it is important to know two aspects of a solid-liquid system:

1. The maximum achievable yield
2. The minimum operation temperature to reach an economical recovery yield

These limits are given by the eutectic point. The eutectic point represents the minimum temperature at which a solid-liquid equilibrium exists. On the other hand, the eutectic concentration limits the possible yield of pure crystals. This becomes clear when applying the lever rule for calculating the yield of a crystallization step close to the eutectic temperature as shown in figure 5-4. The mass yield Y of component A is then given by

$$Y = \frac{w_{F,A} - w_{EP,A}}{w_{F,A}(1 - w_{EP,A})} \quad \text{eq. 5-14}$$

where A is the mass of pure crystals A , F is the mass of the feed with concentration $w_{F,A}$, and $w_{EP,A}$ is the mass fraction of A at the eutectic point. It is obvious that the higher $w_{EP,A}$ the more component A will remain in the mother liquor, hence the yield will decrease.

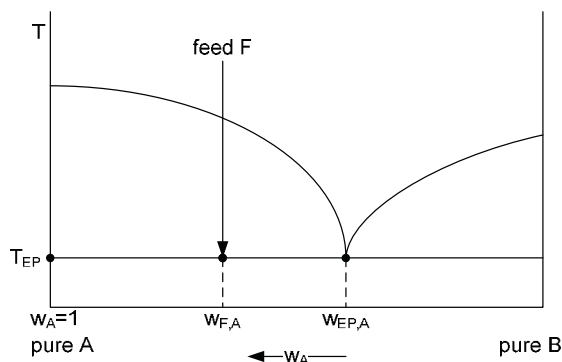


Figure 5-4 Calculation of the maximum yield of a crystallisation unit.

For an extensive solvent screening it is necessary to identify the eutectic point by a standardized method. The determination of the eutectic temperature is possible by a single simple DSC experiment with only one composition of the binary system. Because of subcooling effects due to metastability, phase changes are performed from the completely solid state, hence heating up the sample.

In a binary mixture two exothermal peaks will occur. The first peak is caused by the phase change from a complete solid state into a two-phase system with solid A and liquid of eutectic composition. The second peak represents the transition from a solid-liquid mixture to a complete melt.

For determination of the eutectic composition of a binary system Burger [7] proposed a simple and rapid method. The melting of samples at eutectic composition always occurs at the same temperature, but the enthalpy of fusion associated to the composition will increase with the amount of solids that can form at this certain point. For a mixture of eutectic composition, the DSC curve is similar to that of a pure component, i.e. it shows only one peak. The enthalpy of fusion can be evaluated by integrating the peak area between the measured curve and a virtual or true baseline of a DSC plot.

The method of Burger [7] can be performed either via the isobaric phase diagram or via the mass related enthalpy of fusion of the eutectic peak. In the first case, the end melting temperature of the mixture is plotted against its composition. In the second case, the enthalpy of fusion per mass unit of the first peak [J/g] is plotted against the molar concentration [mol%]. The second method proved to be the favorable one, because there is a linear relationship between the specific enthalpy of fusion and the concentration. Further,

the integration of the first peak is easily possible for all mixtures. The end-set of the melting of those mixtures which composition lie near the eutectic can be determined only with difficulty and with little accuracy.

Figure 5-5 shows an example of the second method. The specific enthalpy of fusion of the first peak is plotted against the molar composition. The eutectic composition is then determined by a linear extrapolation. The intersection point characterizes the eutectic composition giving an additional point of the two-component phase diagram [7].

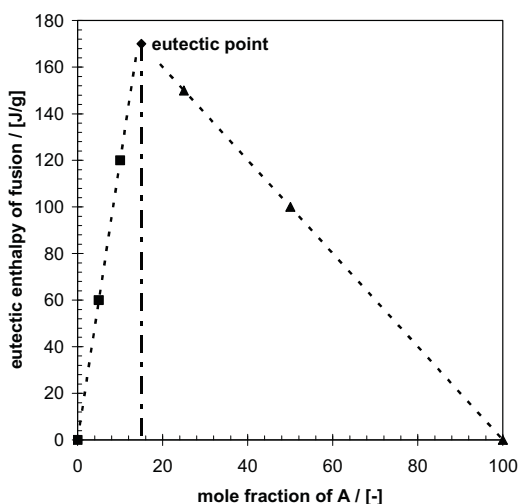


Figure 5-5 Eutectic enthalpy of fusion of the system methyl-4-hydroxy benzoate with p-hydroxy benzoic acid [7].

5.2.4 Approach to determine the ternary eutectic point and solid-liquid equilibrium

In analogy to a binary system, the feasibility of an industrial crystallization step depends mainly on the temperature level and limitation by the ternary point (TEP). Therefore, the proceeding described above to get rapid knowledge of the limits of a crystallization process is adapted to ternary systems.

The temperature level of the ternary eutectic point can also be determined by the DSC. Figure 5-6 shows qualitatively a typical DSC plot of a melting process of a ternary solid system. The temperature level of the ternary point is marked with $T_{m; TEP}$.

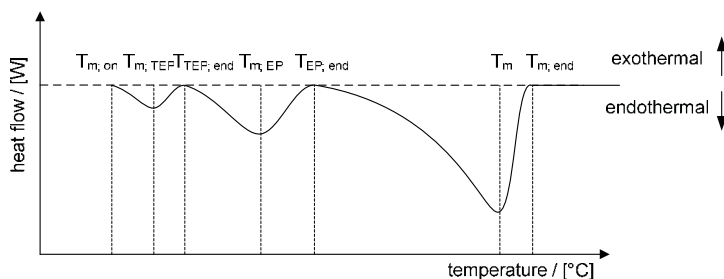


Figure 5-6 Enthalpy flow of a ternary system at solid to liquid phase changes.

As it is the case with the binary system, it is possible to calculate the enthalpy of fusion of the ternary eutectic point. The ternary eutectic point is obtained as follows and demonstrated in figure 5-7:

1. $\Delta_{fus}h_{TEP}$ reaches its maximum at the ternary eutectic composition (TEP).
2. For pure components and binary mixtures $\Delta_{fus}h_{TEP}$ is zero, because in these cases the ternary eutectic point does not exist! Therefore, $\Delta_{fus}h_{TEP}$ is zero for compositions at the sides of the triangle.
3. Mixtures with compositions on the apparent lines between the ternary eutectic point and the pure components (represented by the lines A-TEP, B-TEP and C-TEP) will exhibit only two peaks belonging to the crystallization of the pure components A, B, and C, respectively, and one peak representing the ternary eutectic point.
4. The maximum $\Delta_{fus}h_{TEP}$ of the pseudo-binary system B-C at constant mass fraction of A, e.g. along AC-AB, is determined as described in section 5.2.3. The connection between the respective composition and the pure component A results in a straight line. The same is done for the pseudo-binary systems A-C and B-C. The intersection of the connecting lines represents the ternary eutectic point.

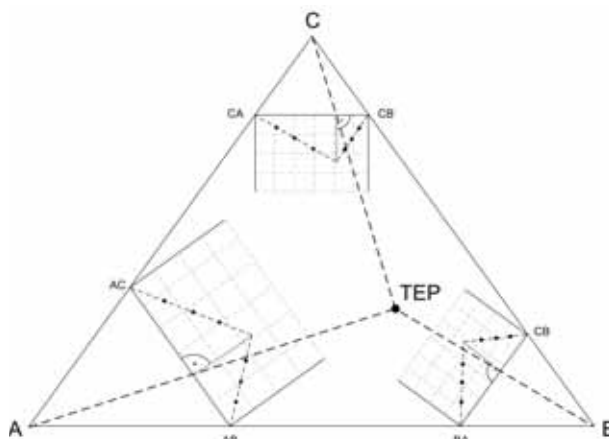


Figure 5-7 Determination of the triple eutectic point by adaption of the binary method of Burger [7].

The approach is valid only for ternary systems, where the binary systems do not show any peritectic points. The melting behavior of peritectic systems is different from eutectic ones.

5.3 Approach to a fast solvent screening method

5.3.1 Approach to a data base request for fast solvent screening

In general the search for an additional solvent as a component to increase the yield of a crystallization process is quite difficult, because of the huge numbers of requirements and properties which have to be fulfilled, e.g. non-toxicity, chemically inertness, crystalline behavior, etc.

Based on the scope of this chapter and the mentioned requirements, a two-stage solvent screening method was designed with the following objectives:

1. Reduce the number of necessary experiments to a minimum.
2. Consider the downstream requirements due to toxicity, product specifications, etc.
3. Use physical and chemical data to prepare a first rough estimation of the potential benefit.
4. Use of solid-liquid binary data for a first rough estimation of the location of the ternary eutectic point.

Mainly based on these four objectives a decision tree is developed for an automatic data base request. The structure is shown in figure 5-8.

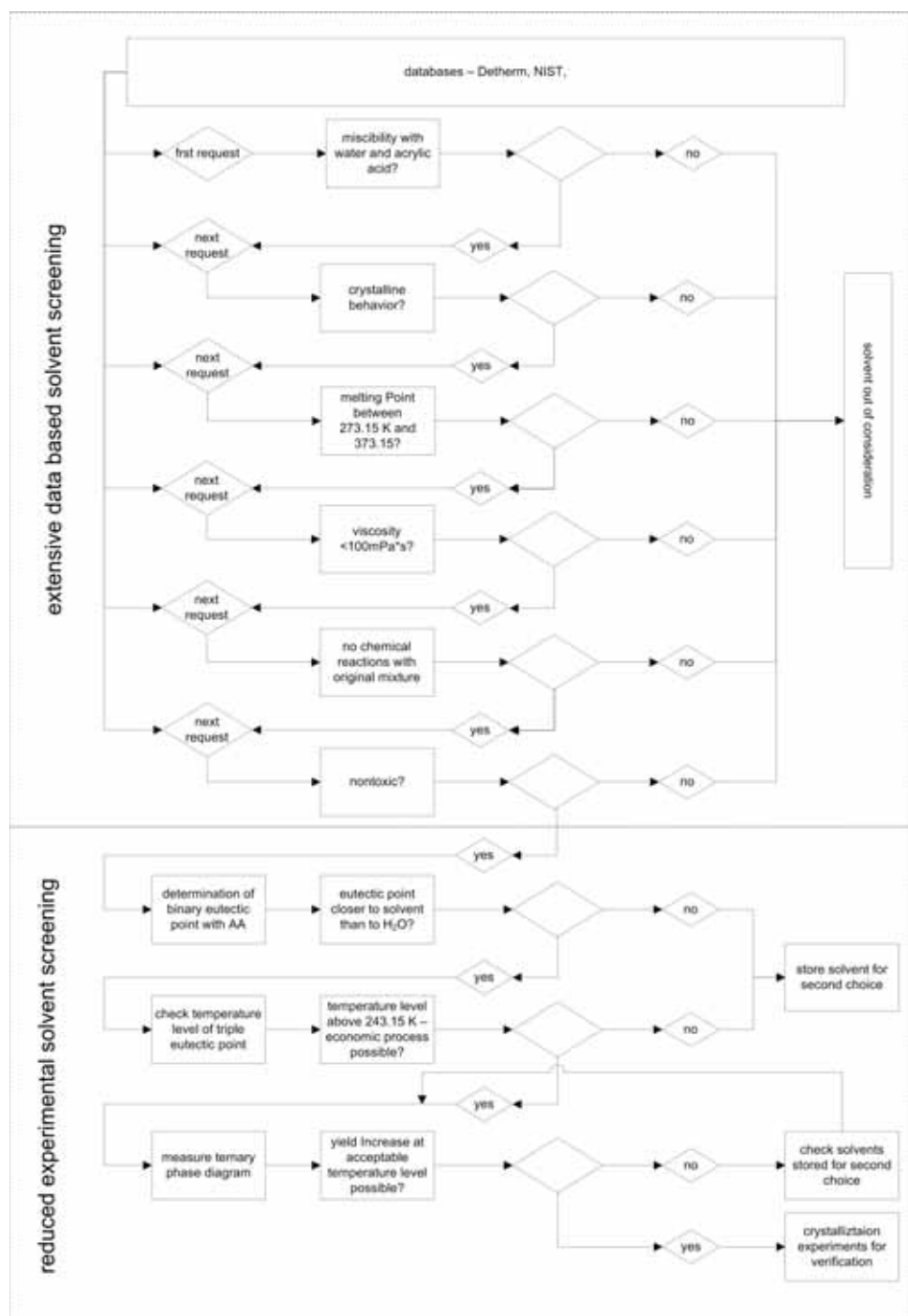


Figure 5-8 Data base request for fast solvent screening.

5.3.2 State of the art

The idea to increase the yield of a crystallization unit is a common industrial need. Within the next two sections two well-known approaches will be presented shortly. There are many possible processes and substances published in patents and literature for aqueous systems of acrylic acid. However, due to the resulting process complexity, industrial applications using any of these processes are not known. Therefore, they will be presented for the sake of completeness but the substance classes will not be considered in the solvent screening for acrylic acid.

5.3.2.1 Salting out

Several approaches to increase the yield of an acrylic acid crystallization from aqueous solutions have been described in the past. In some cases, the limiting eutectic point has been removed successfully by the addition of certain salts to the aqueous solution.

Faerber [8] disclosed in 1957 that calcium chloride (CaCl_2), sodium sulfate (Na_2SO_4), and dry metal salts such as nickel chloride (NiCl_2) and nickel bromide (NiBr_2) can be used as drying agents in combination with an aliphatic ketone. The salt dissolves in the aqueous phase and reduces the solubility of acrylic acid. The acrylic acid is transported into the organic phase. This displacement is called salting out. It was demonstrated that the acrylic acid could be concentrated from the aqueous solution up to maximal 80% in the organic phase.

Otsuki Susumu et al. [9] showed a method to accelerate the separation of an organic solvent phase from an aqueous phase to recover acrylic acid. They suggested to add an alkali metal salt or an ammonium salt $[\text{NH}_4]^+$ to the aqueous solution for accelerating the solvent separation. Rather than accelerating the phase separation or drying the aqueous solution, this patent discloses that the addition of such salts removes the eutectic point between acrylic acid and water. In this case the eutectic limitation can be overcome by forming a system of solid solutions.

One salt that eliminates the eutectic is sodium chloride. Other alkali metal salts like halides, nitrates and sulfates, and ammonium salts can remove the eutectic as well. However, it has been found that barium chloride, ferric chloride, and tin chloride have no significant effect on the acrylic acid-water SLE [10].

At the end, salts can be used to shift and remove the eutectic point, respectively. Therefore, it is possible to draw the following conclusion. The addition of salts opens up two types of processes: The first possibility is to use the salting out effect in a liquid-liquid extraction. Salts push acrylic acid into the organic phase which it can be crystallized from. This requires further downstream units to recover and recycle at least the organic phase.

Second, salts can make the binary eutectic system become a solid solution. This always requires an extensive, economically unattractive multi-stage fractional crystallization. Hence, salts will be disregarded as potential third compounds.

5.3.2.2 Ionic liquid

Ionic liquids (ILs) are defined as liquid salts which are liquid below 100°C [11]. Ionic liquids are organic salts and consist of large bulky and asymmetric organic cations and anions such as tetrafluoroborate $[\text{BF}_4]^-$, halides, nitrate $[\text{NO}_3]^-$, sulphate $[\text{SO}_4]^-$, aluminum chloride $[\text{AlCl}_4]^-$, etc.

The group of the cation is variable; typical cations are alkyl chains such as methyl, ethyl, butyl, etc., or other functional groups (e.g. fluoroalkyl, alkenyl, methoxy). The variability of the anions and residual groups in the imidazolium, pyridinium, pyrrolidinium, ammonium, or phosphonium cations are utilized to adjust the physical properties of the ionic liquids such as melting point, viscosity, and density as well as the miscibility with water or organic solvents. Furthermore, they can be functionalized to act as acids or bases. The change of the anion dramatically affects the chemical behavior and stability of the ionic liquid.

The vast range of possible ionic liquids makes a dedicated screening quite extensive. Additionally, in contrast to the use of common organic bulk chemicals a complete recovery of the ionic liquid is required due to the high specific costs. Therefore, also ionic liquids will be excluded from the solvent screening for a potential third component.

5.3.3 Screening results

The increase of the crystallization yield requires certain properties as listed in paragraph 5.3.1. Especially organic components can fulfil these features. The screening shows that especially alcohols, ketones, and carboxylic acids should be considered. Especially carboxylic acids with a low number of carbons (1-4) could be attractive for the installation in an industrial process. In the end, the screening approach comes up with three components which have to be investigated by simple lab experiments: propionic acid, butanoic acid, and acetic acid. Propionic and acetic acid are typical by-products of the two-stage acrylic acid oxidation process [12], so that a possible use would not generally change the complete production process:

- Acetic acid shows properties in agreement with the requirements ($T_{EP} = -27^\circ\text{C}$; $x_{EP} = 58 \text{ wt\%}$ acetic acid; $T_{m,AcA} = 16.5^\circ\text{C}$).
- Butanoic acid shows good properties regarding the eutectic temperature and the eutectic composition in the binary system with water. The eutectic temperature is not too low ($T_{EP} = -13.4^\circ\text{C}$) and the eutectic composition is $x_{EP} = 87 \text{ wt\%}$ butanoic acid.

The binary system with water shows a miscibility gap which is not a fundamental problem, because the process would be operated at high acrylic acid concentrations.

- Propionic acid shows good properties regarding the eutectic temperature and the eutectic composition in the binary system with water ($T_{EP} = -29.4^{\circ}\text{C}$; $x_{EP} = 87$ wt% propionic acid), as required. Besides, some SLE data of acrylic acid and propionic acid [14] are available ($T_{EP} = -11^{\circ}\text{C}$, $x_{EP} = 74.87$ wt% propionic acid). However, propionic acid exhibits one major disadvantage. The system propionic acid – acrylic acid has a peritectic point [10] ($T_{PP} = -17.1^{\circ}\text{C}$ and $x_{PP} = 44.4$ wt% propionic acid). A crystallization could result in the formation of a solid solution. Nevertheless, propionic acid will be considered as a possible component to increase the acrylic acid yield, even if a two-stage process would be necessary.

5.4 Experimental

5.4.1 Objectives

The objectives of the experiments are the general check, if the identified components of the screening approach from section 5.3.1 allow an increase of the crystallization yield of the binary system acrylic acid and water. One requirement for this purpose is that the location of the existing ternary eutectic point is far from pure acrylic acid hence at a low water content. This would offer the opportunity to separate pure acrylic acid at a high yield without getting in trouble with highly compressible acrylic acid crystals.

The temperature level of the ternary eutectic point is very important regarding crystallization and solid-liquid separation conditions like liquid viscosity and density. A temperature below (-30°C) makes an industrial crystallization process uneconomical. Crystal growth at low temperatures often leads to kinetic problems induced by limited heat and mass transfer. This may results in impure crystals, what could necessitate a two-stage process. A high difference between the operation temperature and the melting point could also lead to operating problems of wash column units for crystal separation and purification.

Therefore, the experiments are dived into three steps. First, the temperature level of the ternary eutectic point will be determined by simple and fast DSC measurements. For each system five mixtures at different composition will be analyzed. Further, the ternary eutectic point and region will be determined via the advanced approach presented in paragraph 5.2.4. Finally, if the temperature of the ternary eutectic point is higher than (-30°C), the complete phase diagram will be measured.

5.4.2 Experimental setup and procedure

The experiments were carried out on a Differential Scanning Calorimeter DSC 1 400W combined with an automatic probe sampler and an external Intra Cooler from Mettler Toledo. The used DSC setup allows measurements in a temperature range from -85°C up to 700°C with a precision of 0.02 K. The generated raw data were evaluated with the Mettler Toledo Software STARe. The software allows the calculation and analysis of all system data like phase change temperatures (ternary, binary, and melting temperature) and specific enthalpy of fusion. The ternary mixture samples were prepared from the pure components. The exact compositions were calculated after weighing. The measurements were carried out with hermetically closed crucibles to avoid changes of the sample compositions due to evaporation of the sample or inclusion of moisture. Additionally, the measuring cell was flushed continuously with nitrogen. All experiments were carried out with defined temperature programs using temperature gradients of 1 K/min or 5 K/min, respectively. Generally, 5 K/min is the preferred heating rate. If an overlap of peaks occurs, a slower temperature gradient of 1 K/min is required to obtain a decent base line and distinct peaks. The used temperature programs of the different compositions are summarized in table 5-1.

Table 5-1 DSC temperature programs.

segment	time period	AA / H ₂ O / AcA	AA / H ₂ O / PA	AA / H ₂ O / BA
1	10 min	(-70°C)	(-40°C)	(-50°C)
2	varied	$(-70^{\circ}\text{C}) - (20^{\circ}\text{C})$	$(-40^{\circ}\text{C}) - (20^{\circ}\text{C})$	$(-50^{\circ}\text{C}) - (20^{\circ}\text{C})$
3	5 min	(20°C)	(20°C)	(20°C)
4	10 min	(-70°C)	(-40°C)	(-50°C)
5	varied	$(-70^{\circ}\text{C}) - (20^{\circ}\text{C})$	$(-40^{\circ}\text{C}) - (20^{\circ}\text{C})$	$(-50^{\circ}\text{C}) - (20^{\circ}\text{C})$

5.4.3 Results

5.4.3.1 Determination of the ternary eutectic temperature

For all three ternary systems different samples were analyzed by the presented DSC measurement programs. Afterwards, the occurring curves were interpreted and the peaks were related to the possible phase changes. As assumed, during the heating up almost all samples of each system showed a first peak at a certain temperature. This peak was

identified to be the temperature of the ternary eutectic point called afterwards “ternary peak temperature”.

The ternary mixture containing acetic acid shows an average ternary peak temperature of -36.1°C with a standard deviation of 0.5°C. The results for different concentrations are presented in table 5-2.

Table 5-2 Ternary peak temperatures acrylic acid / water / acetic acid.

w_{AA} / [wt%]	w_{H_2O} / [wt%]	w_{AcA} / [wt%]	ternary peak temperature
10%	50%	40%	-35.5°C
20%	60%	20%	-35.8°C
32%	20%	48%	-36.5°C
37%	20%	43%	36.2°C
51%	40%	9%	-36.7°C
average ternary peak temperature			-36.1°C
standard deviation			0.5°C

If butanoic acid is used as a third component, the average ternary peak temperature is around -33.2°C with a standard deviation of 0.6°C. The results for different concentrations are presented in table 5-3.

Table 5-3 Ternary peak temperatures acrylic acid / water / butanoic acid.

w_{AA} / [wt%]	w_{H_2O} / [wt%]	w_{BA} / [wt%]	ternary peak temperature
12%	58%	30%	-32.9°C
15%	5%	80%	-32.9°C
42%	8%	50%	-32.5°C
46%	44%	10%	-33.9°C
62%	28%	10%	-33.8°C
average ternary peak temperature			-33.2°C
standard deviation			0.6°C

The system with propionic acid as a third component shows an average of around -31.2°C with a standard deviation of 0.9°C . Table 5-4 shows the concentration of the samples and the corresponding temperatures.

Table 5-4 Ternary peak temperatures acrylic acid / water / propionic acid.

w_{AA} / [wt%]	w_{H_2O} / [wt%]	w_{PA} / [wt%]	ternary peak temperature
8%	7%	85%	-30.2°C
13%	57%	30%	-31.8°C
12%	23%	65%	-30.3°C
29%	6%	65%	-31.7°C
38%	7%	55%	-32.0°C
average ternary peak temperature			-31.2°C
standard deviation			0.9°C

5.4.3.2 Determination of the ternary eutectic concentration (TEP)

For all three systems the determination of the Ternary Eutectic Points (TEP) has been carried out as described in paragraph 5.2.4. The analysis of all three systems shows good and clear results. The graphical constructions of the lines between the pure components and the local maxima of the enthalpy of fusion of the ternary eutectic point and their extrapolation result in one point. The absolute deviation of the intersection of the three lines of each system was about 5 wt%. Therefore the precision of the determined ternary point is in a circular concentration range with a diameter of 10 wt%.

Figure 5-9 represents the results of the system acrylic acid, water, and acetic acid. The ternary eutectic point was identified at a concentration of 32 wt% acrylic acid, 30 wt% water and 38 wt% acetic acid.

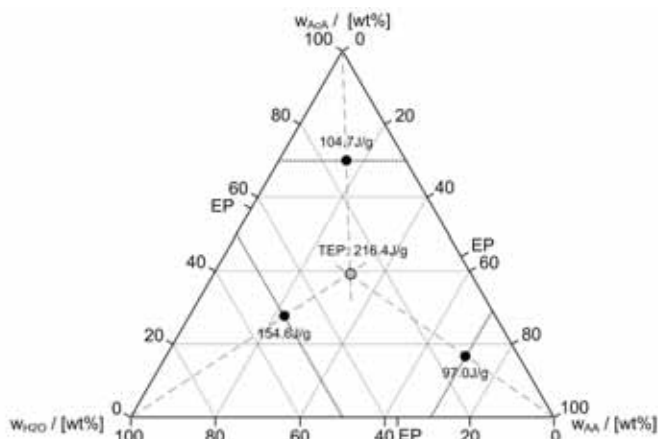


Figure 5-9 Determination of ternary eutectic point; acrylic acid - water - acetic acid.

The system acrylic acid, water, and butanoic acid possess the ternary eutectic point with the lowest water concentration. Figure 5-10 shows the graphical construction of the ternary eutectic point at 35 wt% acrylic acid, 8 wt% water, and 57 wt% butanoic acid.

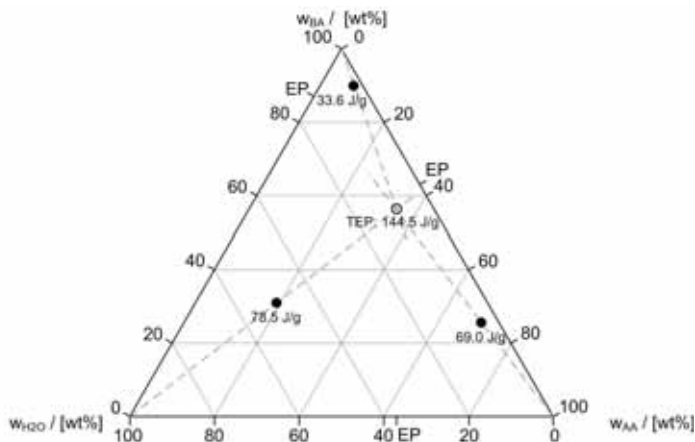


Figure 5-10 Determination of ternary eutectic point; acrylic acid - water - butanoic acid.

Propionic acid shifts the ternary eutectic point away from acrylic acid and water. Figure 5-11 shows its location at 20 wt% acrylic acid, 17 wt% water, and 63 wt% propionic acid.

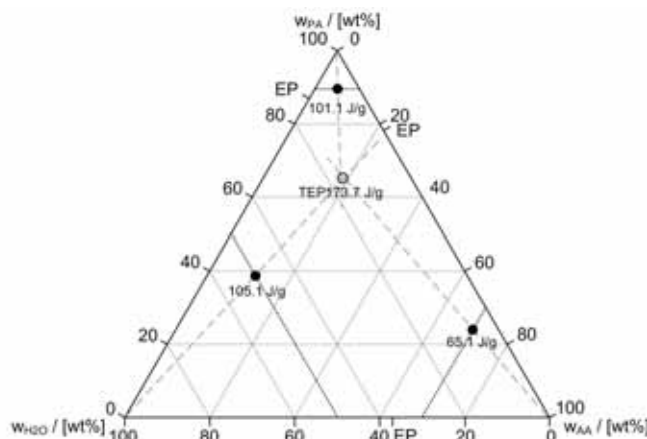


Figure 5-11 Determination of ternary eutectic point; acrylic acid - water - propionic acid.

The values in each diagram represent the values of the specific enthalpy of fusion of the ternary points. For all three systems, the extrapolated enthalpy of fusion of the ternary point seems to be a function of the water content of this point. The higher the water content of the ternary eutectic points, the higher the corresponding enthalpy of fusion. This goes along with the fact that the enthalpy of fusion of water (333 J/g) is around twice the value of a typical organic component (150 J/g).

The determination of the ternary eutectic point of each system has to be verified by the measurements of the complete solid-liquid equilibrium diagrams.

5.4.3.3 Phase diagrams

With the knowledge about of the approximate location of the ternary eutectic point, it was possible to perform selective DSC experiments to measure the complete ternary phase diagram. For each system a dedicated sample table with at least 36 samples was worked out. With this number of experiments the complete ternary diagram could be covered with a concentration raster having width of 10 wt%. The repetition of certain experiments shows an accuracy of the determination of phase changes temperatures by DSC of 0.05 K.

Subsequently, the temperatures were plotted against the concentration with the help of a contour diagram. The calculation software MINITAB was used for this graphical evaluation. The software classifies the temperatures into 12 intervals. This limited number of temperature levels obviously restricts the level of detail of the graphical demonstration. However, the graphical demonstration provides useful information on the solid-liquid equilibria of the investigated systems. For all three systems a selection of the numerical

data are listed in the appendix. The literature values of the binary systems [5;13] is not listed in the tables.

Figure 5-12 shows the ternary solid-liquid equilibrium of the system acrylic acid, water, and acetic acid. The region of the ternary eutectic point is represented in dark blue. This region coincides with the results of paragraph 5.4.3.2. There are two discrepancies in the diagram. The binary eutectic point of water and acetic acid shows a lower temperature than the temperatures from this point towards the internal of the system. The second discrepancy is at 80 wt% acrylic acid, where the same phenomena appears.

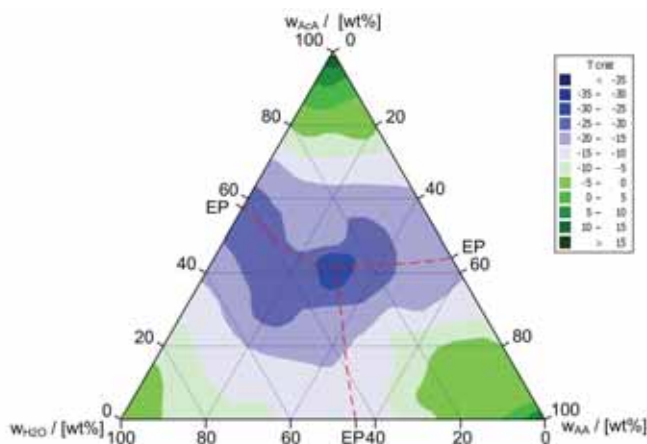


Figure 5-12 SLE diagram acrylic acid - water - acetic acid.

Figure 5-13 shows the graphical representation of the DSC results of acrylic acid, water, and butanoic acid. Also for this system the region of the ternary eutectic point corresponds to results of the previous section. The shape of the temperature regions is conclusive without any discrepancies.

The results of the ternary system of acrylic acid, water, and propionic acid, shown in figure 5-14, are coherent with the results of the previous section. However, the diagram shows also two irregularities regarding the equilibrium temperature. Both discrepancies are close to the ternary eutectic point, with the lowest temperature.

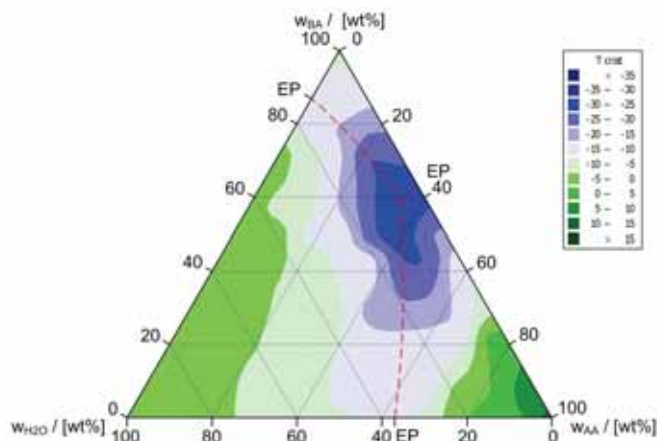


Figure 5-13 SLE diagram acrylic acid - water - butanoic acid.

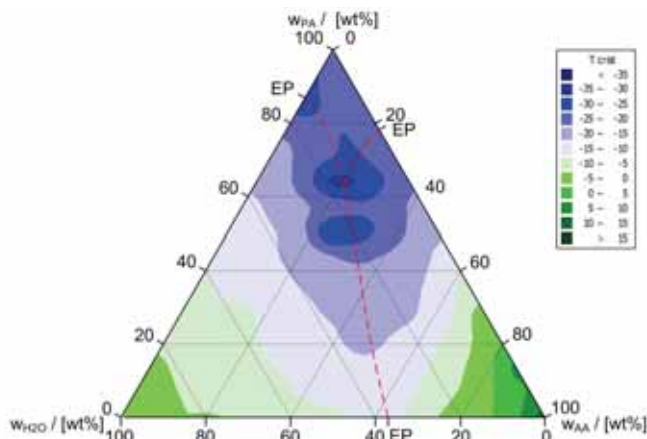


Figure 5-14 SLE diagram acrylic acid – water - propionic acid.

5.5 Discussion

The solvent screening – with the aim of finding a third component to increase the yield of an acrylic acid crystallization from aqueous mixtures – results in three potential components: acetic acid, propionic acid, and butanoic acid. All identified components reveal similar molecular structures. It is known that propionic acid forms a peritectic system. For further investigations, it would be useful to differ the screening criteria, so that components with higher melting points would be considered as well.

The determination of the ternary eutectic temperature by using the rapid technique explained in paragraph 5.2.4 shows results well corresponding to DSC measurements. There are deviations in the temperature values of up to 1 K. It was found by the analysis of the DSC

plots that the determination of the eutectic temperature becomes more difficult with increasing distance from the TEP. This is due to the decreasing peak area.

The determination of the ternary eutectic concentration by the approach based on a method for binary eutectic systems shows apparently good results. It was found that the precision of this method is depending mostly on the accuracy of the pseudo binary measurements at constant concentration of one of the three components. For both approaches, it is necessary that the DSC plots show a defined peak of the ternary eutectic point in relation to temperature determination and the calculation of the relative enthalpy of fusion. The best results are found, if the measurements are carried out at concentrations closer to the ternary eutectic point than to the pure components. A practical approach to ensure this was to set the constant concentration of one component close to one of its binary eutectic points.

The measurement of the full ternary liquid-solid equilibrium by DSC measurements is quite comfortable once the samples are prepared. There are some discrepancies regarding the presented equilibrium temperatures. It was found that these mistakes are caused by only small deviations of the detected temperatures (0.5 K). If the set temperature ranges differ a little bit, the existing discrepancies disappear and others appear. Therefore, the graphical presentation requires a gliding temperature representation and a post control of all measured equilibrium temperatures.

5.6 Conclusion and outlook

In consideration of the results presented in section 5.4 the following conclusions are drawn:

1. All three components could be used to modify the crystallization process from an aqueous solution. Crystallization is possible at a moderate and acceptable temperature level. For all cases it holds true that the ternary eutectic point offers the farthest distance to pure acrylic acid. This goes along with the highest achievable yield for each system. However, the possible modifications and resulting advantages and disadvantages are different for all three systems.
2. Compared to propionic and butanoic acid, acetic acid needs to be added at smaller concentrations to aqueous acrylic acid in order to achieve an increase in the crystallization yield. Nevertheless, if the crystallization process could be designed in that way that the mother liquor is at ternary eutectic composition, the crystals would grow from a water concentration of around 30 wt% water. This could cause problems due to high compressibility of the acrylic acid crystals [1; 2].
3. Butanoic acid allows to crystallize acrylic acid at a low water concentration (<10 wt%) because of the location of the ternary eutectic point. But this requires the addition of a lot of butanoic acid in comparison to acetic acid.

4. The performance of propionic acid ranks in-between the ones of acetic acid and butanoic acid regarding the required concentration range and the water content of the mother liquor. Unfortunately, the peritectic point at 55.6 wt% acrylic acid cripples all advantages. Additionally, the further downstream processing could turn out to be very difficult, since the binary vapor-liquid equilibrium data are unfavourable. It will be quite impossible to separate the components by distillation because of an azeotropic point and a very close-boiling behavior.

With regard to the listed advantages and disadvantages, propionic acid can be neglected for further considerations. For the other two components a theoretical process should be designed, simulated, and benchmarked afterwards in terms of the possible overall yield, energy consumption, and apparatus complexity.

Nomenclature**Symbols**

C_P	heat capacity at constant pressure	[J/(mol·K)]
f_i	fugacity of component i	[Pa]
g	molar Gibbs enthalpy	
$\Delta_{fus}h_i$	molar enthalpy of fusion of component i	[J/mol]
h	molar enthalpy	[J/mol]
R	gas constant	[J/(mol·K)]
s	molar entropy	[J/(mol·K)]
T	temperature	[K]
w	mass fraction	[wt%]
x	mole fraction	[mol%]
Y	yield	%

Greek Symbols

γ	activity coefficient	[-]
μ	chemical potential	[J]

Subscripts

end	end-set
i	component i
L	liquid phase
m	solid-liquid equilibrium / melting
on	on-set
S	solid phase
0	standard state

Abbreviations

A	component A
AA	acrylic acid
AcA	acetic acid
B	component B
BuA	butanoic acid
C	component C
EP	binary eutectic point
F	feed
H ₂ O	water
PA	propionic acid
PP	peritectic point
TEP	ternary eutectic point
Tr	triple point

References

- [1] Hengstermann, A.; Kadam, S.; Jansens, P.J.; Influence of water content and supercooling on crystal morphology of acrylic acid, *J. of Crystal Growth and Design*, 2009, Vol. 9 (4), pp2000–2007.
- [2] Hengstermann, A.; Harms, S.; Jansens, P.J.; The Influence of Water and Supercooling on Permeability and Compressibility of Crystal Beds formed out of Acrylic Acid Crystals, *Chemical Engineering Technology*, 2009, Vol. 33 (3), pp433-443.
- [3] Oonk, H.A.J.; *Phase Theory, The Thermodynamic of Heterogeneous Equilibria*, Elsevier, Amsterdam, The Netherlands, 1981.
- [4] Walas, S.M.; *Phase Equilibria in Chemical Engineering*, Butterworth, Boston, USA, 1985.
- [5] Chubarov, G.A.; Danov, S.M.; Liquid-Solid Equilibrium in the Systems Acrylic Acid - Water, Acrylic Acid - Acetic Acid, and Methacrylic Acid – Water, *J. Appl. Chem., USSR*, 1978, Vol. 51 (8), pp1796-1798.
- [6] Rosseau, R.W.; *Handbook of separation process technology*, John Wiley & Sons, Inc., Gerogia In-situte of Technology, 1987, Chap. 11.
- [7] Burger, A.; *DTA und DSC: Grundlagen, Methodik und Anwendung*, Pharm. Unserer Zeit, 1982, Vol. 11, pp177-189.
- [8] Faerber, G.; *Concentration of Aqueous Acrylic Acid*, Solvay Werke GmbH, Rheinberg, Germany, 1957, US-Patent US2922815.
- [9] Otsuki, S.; Hori, K.; Miyanoara, I.; *Accelerating Separation Rate of two liquid phases in the extraction of Aqueous Acrylic Acid*, Rohm and Haas Company, Philadelphia, USA, 1972, US-Patent US3846488.
- [10] Paspek, S.C.; Every, W.A.; *Process for purification of acrylic acid by fractional crystallization*, Standard Oil Company, USA, 1980, US-Patent US4230888.

- [11] Wasserscheid P.; Welton T.; *Ionic Liquids in Synthesis*, WILEY-VCH Verlag, Weinheim, Germany, 2003, Chap. 1.
- [12] Machhammer, O.; Dams, A.; Eck, B.; Proll, T.; *Verfahren zur Reinigung von Acrylsaeure und Methacrylsaeure*, BASF Aktiengesellschaft, 1996, German Patent DE 19606877A1.
- [13] Lohmann, J.; Roepke, T.; Gmehling, J.; *Solid-Liquid Equilibria of Several Binary Systems with Organic Compounds*, J. Chem. Eng. Data, 1998, Vol. 43 (5), pp856-860.
- [14] Faucon, M.A. ; *Annales de Chimie et de Physique*, 1910, Vol. 18, pp70-152.

Appendix

Table A-5 Equilibrium data for acrylic acid - water - acetic acid.

W_{AA}	W_{H_2O}	W_{AcA}	T_m	T_m
[wt%]	[wt%]	[wt%]	[°C]	[K]
29.9	25.3	44.8	-33.40	239.75
30.0	22.4	47.6	-31.60	241.55
31.7	28.3	40.0	-31.10	242.05
30.1	31.4	38.5	-30.40	242.75
16.4	43.7	39.9	-30.30	242.85
39.9	27.0	33.1	-28.20	244.95
21.8	38.1	40.1	-27.40	245.75
23.4	33.4	43.2	-27.00	246.15
32.4	30.5	37.1	-26.90	246.25
49.6	19.7	30.7	-24.80	248.35
22.7	27.1	50.2	-24.60	248.55
30.0	34.9	35.1	-22.50	250.65
3.6	36.4	60.0	-21.80	251.35
27.8	37.2	35.0	-21.60	251.55
24.0	39.9	36.1	-20.60	252.55
7.3	32.8	59.9	-20.60	252.55
27.0	25.0	48.0	-20.00	253.15
25.5	44.5	30.0	-18.80	254.35
25.0	25.0	50.0	-17.20	255.95
20.0	35.9	44.1	-13.10	260.05
6.6	63.0	30.4	-12.40	260.75
2.5	27.5	70.0	-12.30	260.85
14.6	65.4	20.0	-11.80	261.35
5.7	24.2	70.1	-11.00	262.15
15.0	38.2	46.8	-10.50	262.65
16.0	24.0	60.0	-9.80	263.35
43.8	36.3	19.9	-9.40	263.75
49.0	21.0	30.0	-6.50	266.65
29.5	60.5	10.0	-6.20	266.95
18.2	1.8	80.0	-1.40	271.75
73.0	7.1	19.9	-0.60	272.55
64.0	16.0	20.0	0.30	273.45
66.3	23.7	10.0	1.50	274.65

Table A-6 Equilibrium data for acrylic acid - water - butanoic acid.

w_{AA}	w_{H_2O}	w_{BA}	T_m	T_m
[wt%]	[wt%]	[wt%]	[°C]	[K]
31.9	8.0	60.1	-30.80	242.35
41.5	8.3	50.2	-29.30	243.85
48.0	12.1	39.9	-25.40	247.75
23.0	7.5	69.5	-24.50	248.65
33.1	16.6	50.3	-22.90	250.25
24.0	16.1	59.9	-22.40	250.75
15.0	5.0	80.0	-19.30	253.85
46.6	23.3	30.1	-18.40	254.75
58.3	11.6	30.1	-17.70	255.45
5.1	15.1	79.8	-14.50	258.65
15.0	15.0	70.0	-14.50	258.65
64.0	16.0	20.0	-13.50	259.65
48.0	32.1	19.9	-13.50	259.65
61.9	28.0	10.1	-13.40	259.75
36.0	24.0	40.0	-13.40	259.75
24.9	25.0	50.1	-11.30	261.85
16.8	33.2	50.0	-11.30	261.85
46.2	44.0	9.8	-10.90	262.25
35.0	35.0	30.0	-9.40	263.75
16.0	24.0	60.0	-9.00	264.15
7.5	22.2	70.3	-7.80	265.35
32.0	48.0	20.0	-7.00	266.15
8.1	32.0	59.9	-6.80	266.35
28.0	62.0	10.0	-5.80	267.35
23.3	46.6	30.1	-5.70	267.45
16.0	64.0	20.0	-4.40	268.75
12.0	47.9	40.1	-4.10	269.05
8.7	41.4	49.9	-3.90	269.25
11.6	58.4	30.0	-3.70	269.45
9.1	80.9	10.0	-3.40	269.75
80.9	9.1	10.0	-0.10	273.05

Table A-7 Equilibrium data for acrylic acid - water - propionic acid.

w_{AA}	w_{H_2O}	w_{PA}	T_m	T_m
[wt%]	[wt%]	[wt%]	[°C]	[K]
23.3	11.7	65.0	-31.40	241.75
25.0	25.0	50.0	-30.90	242.25
29.3	5.9	64.8	-29.50	243.65
12.5	12.5	75.0	-29.00	244.15
33.6	16.6	49.8	-29.00	244.15
18.7	6.3	75.0	-28.80	244.35
17.5	17.4	65.1	-27.50	245.65
31.3	13.7	55.0	-26.90	246.25
26.7	18.3	55.0	-26.30	246.85
6.3	18.8	74.9	-24.70	248.45
38.1	6.9	55.0	-24.20	248.95
41.9	8.3	49.8	-24.20	248.95
11.7	23.3	65.0	-23.30	249.85
7.6	7.5	84.9	-23.10	250.05
22.6	22.4	55.0	-23.10	250.05
46.9	23.1	30.0	-22.80	250.35
35.9	24.1	40.0	-21.30	251.85
18.3	26.7	55.0	-20.30	252.85
16.6	33.2	50.2	-19.50	253.65
48.0	32.0	20.0	-19.20	253.95
5.9	29.1	65.0	-18.10	255.05
48.1	12.0	39.9	-17.40	255.75
35.0	35.0	30.0	-16.30	256.85
24.0	36.1	39.9	-15.40	257.75
58.2	11.6	30.2	-15.00	258.15
62.1	27.9	10.0	-12.90	260.25
8.4	41.6	50.0	-12.40	260.75
64.1	16.0	19.9	-11.60	261.55
45.2	44.8	10.0	-11.30	261.85
23.3	46.7	30.0	-10.70	262.45
12.1	47.9	40.0	-10.60	262.55
32.1	48.0	19.9	-10.30	262.85

BENCH MARK STUDY FOR A NOVEL ACRYLIC ACID RECOVERY

Abstract

A new approach to recover acrylic acid comprises an early stage eutectic crystallization of acrylic acid and water (ice) in combination with a conventional hydraulic wash column for crystal separation and purification. For an industrial implementation, the economical advantages of the new recovery process have to be figured out. For the comparison of the conventional and the novel recovery process, both have been simulated.

The early-stage separation of acrylic acid and ice recovers 78% of the acrylic acid without any thermal load. This decreases the loss of acrylic acid caused by dimerization and polymerization by 78%. The novel recovery process reduces the overall energy demand to 42%. Due to the water removal by the aqueous product itself, the amount of wastewater to be incinerated is reduced to 23%. This comes along with a reduction of the natural gas required for the wastewater incinerator of 77%. Based on specific design parameters of the simulations, it was possible to estimate the differences of the main equipment dimensions. The dimension of the distillation units is reduced to around 50%, whereas the dimension of the melt crystallization units is double.

The presented results show that the novel recovery process is an innovative and promising process considering sustainable requirements like reduced overall specific energy demand and an improved yield due to the charge material.

6.1 Introduction

The conventional acrylic acid recovery process needs at least three distillation units to purify the acrylic acid coming from the two-stage oxidation reaction. The limited purification potential of the distillation sequence requires the ultra-purification of acrylic acid by an end-of-pipe melt crystallization. In the recent past, the main investigation activities have been focused on the separation of pure acrylic acid by melt crystallization from the aqueous bottom stream of the absorption column. However, the morphology of acrylic acid is mainly influenced by water in the melt as found in chapter 2 [1]. These morphology changes lead in a difficult solid-liquid separation of acrylic acid from aqueous solutions as shown in chapter 3 [2].

Hence, the idea came up to crystallize acrylic acid and water simultaneously from the aqueous bottom stream of the absorption column combined with a separation and a purification step [3;4]. Due to the yield limitation of the eutectic crystallization process by the ternary eutectic point of the system detected in chapter 5 [5], the effluent mother liquid has to be fed to a conventional distillation sequence to separate the remaining acrylic acid to increase yield of the recovery process.

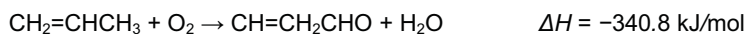
Therefore, the scope of this work is a detailed simulation based comparison of the novel process with the conventional one. The first one represents the conventional recovery process as a benchmark and the second one represents the novel recovery process using the eutectic crystallization as a cold separation step. Based on the results generated from the two simulations – like the specific energy demand, the qualitative dimension of the main separation units, and the amount of wastewater – the advantages of the novel acrylic acid recovery process are evaluated.

6.2 State of knowledge

6.2.1 Reaction – acrylic acid from propene

Commercial acrylic acid is mostly produced from propene by a two-stage oxidation. Some other process routes were developed in the past but their industrial use is negligible [6]. The two-stage oxidation process is explained with the help of figure 6-1. Before entering the first oxidation reactor R1, the propene feed stock is mixed with steam, air, and with recycled waste gas of the absorption column A1. Both oxidation reactors R1 and R2 are fixed catalyst bed shell-and-tube reactors. The reactor beds are packed with different metal oxide catalysts. In the first oxidation stage R1, the propene is catalytically reacted at a temperature of 300°C with air oxygen to form mainly acrolein as an intermediate. In the second oxidation reactor R2, the acrolein is further oxidized at a temperature of 250°C to form acrylic acid. The

contact time for both reactions is around 2 seconds. The several oxidation reaction equations are:



The selectivity of both oxidation stages is similar and at around 95%. Both oxidation steps are exothermic reactions and require an intensive heat removal to avoid hot spots in the reaction zones which reduce the activity of the catalysts. The reactors are equipped with co-current cooling circuits using molten salts as coolants. Finally, the heat is removed from the cooling circuit by cooling water producing steam of 11 bar. The steam is used in the further downstream to provide the heat duty of the reboilers of the distillation columns.

The effluent gas reaction unit is cooled to about 200°C. The cooled gas is fed to the absorption column A1 to be quenched with water. The water is taken from the recovery section to reduce the amount of wastewater and to evaporate low boilers for disposing via the waste gas incinerator. The effluent gas contains a large amount of steam from the reaction and the induced moist air for the first stage. Therefore, the quench liquid is usually obtained as an aqueous solution of 60 wt% acrylic acid, 37 wt% water, 2 wt% acetic acid, and 1 wt% high boilers [7]. Additionally the oxidation reaction comes up with a lot more low and high boilers like acrolein or maleic anhydride. However, for the sake of simplicity, the small amount of low and high boilers is represented in this study by acetic acid and the general notation high boilers.

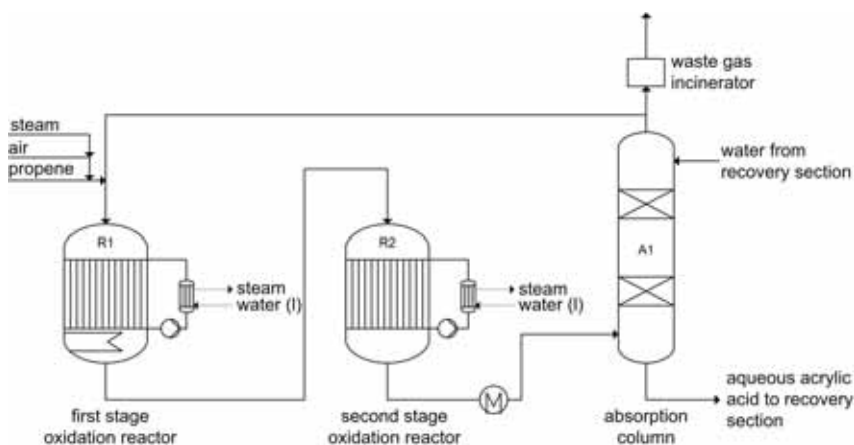


Figure 6-1 Two stage reaction process [6].

Alternatively, the acrylic acid can be absorbed by a high boiling organic solvent with a boiling point higher than 160°C such as biphenyl, diphenyl ether, or a carboxylic ester [6]. The advantage of a high boiling solvent is the less absorption of steam in the absorbing column. This goes along with a lower energy demand of the subsequent purification step, but it also increases the loss of acrylic acid at the absorption column top. Subsequently, only the downstream recovery of acrylic acid from an aqueous solution is subject of the description.

6.2.2 Recovery of acrylic acid

The separation of acrylic acid from an aqueous solution is quite complex. A conventional distillation is not possible because of a tangential azeotropic behavior in the region of high water concentrations [8]. The remaining acrylic acid concentration is around 10 wt% and makes a separation a by simple distillation uneconomic.

Therefore, two possibilities are established in industrial processes to recover acrylic acid from an aqueous solution [6;7]. The dehydration of acrylic acid is possible by a cold extraction step using high or low boiling solvents. Several distillation units for the further purification of acrylic acid and a solvent recycling follow the extraction. The second possibility of dehydration is an azeotropic distillation using an azeotroping agent like toluene [7]. Both recovery processes are established on industrial scale. In this study, the recovery by an azeotropic distillation using toluene is the benchmark for a new acrylic acid recovery section using a eutectic crystallization.

The description of the complete recovery process using an azeotropic distillation first, will follow the process scheme presented in figure 6-2. The description and figure 6-2 are prepared in accordance to the PERP report on acrylic acid [7] and the US patent 5910607 [9].

The aqueous solution is fed to the azeotropic distillation column K1 to remove mainly water, and low boilers. Toluene is used as an azeotropic solvent to form an azeotropic mixture with water and acetic acid. The resulting azeotropic mixture provides a lower boiling point than the one of acrylic acid. The condensed liquid at the top of the distillation column K1 is fed to a liquid-liquid phase separator. The heavier aqueous phase leaves the recovery section. The lighter phase, containing toluene is fed back as solvent reflux to the distillation column K1. The bottom stream of the azeotropic distillation column contains acrylic acid, toluene, acetic acid, and high boilers. The separation in the stripping section can be operated smooth to prevent high bottom temperatures and smaller boil-up ratios to minimize the apparatus dimensions.

The bottom stream of column K1 is feed to the acetic acid distillation column K2. The acetic acid distillation K2 is operated at a lower pressure than the azeotropic distillation column K1. This allows high acrylic acid concentrations in the bottom stream of the column. In contrast to the azeotropic distillation, where it is hard to come up with a high acrylic acid concentration in the stripping section, whereas the conditions the rectifying section are smooth. Considering the VLE data [10] of acrylic acid and acetic acid, the reason for this is obvious. In the region of the pure components, the distances between the vapour and the liquid lines become quite small. A complete separation would lead to a high number of theoretical stages and an according tall apparatus dimension. Therefore, acetic acid and toluene are enriched only in the rectifying section of column K2. For a further separation of acetic acid, the distillate is recycled to the azeotropic distillation K1, providing an outlet for acetic acid. Remaining acrylic acid in the distillate is not critical to the recycling operation. The bottom stream of the column K2 contains mainly acrylic acid, the remaining high boilers, and a low concentration of low boilers.

The crude bottom liquid of K2 is fed to the high boiler distillation K3. The high boiler distillation is operated at the same pressure like the acid distillation column K2. Due to the high differences in the boiling points of acrylic acid and the containing high boilers, the column needs only a small number of theoretical stages. There are several patents and publications disclosing the use of thin-film or short-path evaporators for this separation. Other patents disclose to feed the crude bottom liquid of the column K2 directly to a crystallization unit for ultra purification.

However, the high boiler distillation K3 is operated at a high boil up ratio to ensure a low acrylic acid concentration in the residue stream. The residue stream is passed to an incinerator unit. The reflux ratio at the top of the column K3 is very small. The distillate of the column K3 already contains mainly acrylic acid.

For different applications, the acrylic acid quality of the boiler distillation K3 is sufficient and a part of the stream leaves the process at this point. For special applications, an ultra-pure acrylic acid quality is required. Therefore, the remaining stream is fed to a melt crystallization unit for further purification. Several melt crystallization techniques are available on industrial scale. The major differences of these techniques are the crystallization modes themselves. The two different crystallization modes layer and suspension mode show major differences in the occurring solid handling, the washing device, and the specific energy demand. However, in this study, it is assumed that the installed crystallization unit C1 is a one-stage suspension crystallization unit composed of a crystallizer and a washing device. The effluent product stream contains more than 99.95 wt% acrylic acid and is called fine glacial acrylic acid

(FGAA). The yield is limited by the eutectic composition. The remaining components are acrylic acid dimers representing the high boilers and acetic acid representing the low boilers. The remaining mother liquid is passed to the incinerator.

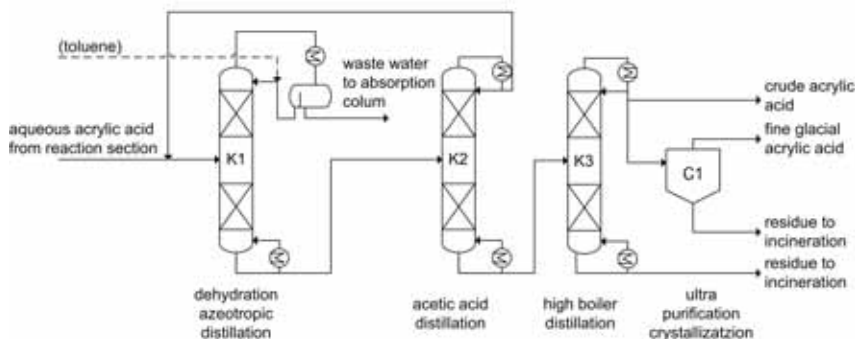


Figure 6-2 Recovery section by azeotropic distillation.

6.3 Simulation

6.3.1 Simulation tool

For the simulation study of the acrylic acid recovery process the Aspen Simulation Engine Software Version V7.1 from AspenTech Inc. is used. All simulation results for streams, heat duties, column profiles, and heat exchangers will be on a mass base. The model uses thermodynamic data from the conventional AspenTech database and the NRTL-HOC property method.

6.3.2 Simulation of crystallization units

Due to the missing ability of the simulation tool to represent melt crystallization units, the following simplifications and assumptions will be made. All melt crystallization units will be designed as follows:

- The crystallizer unit will be represented by a single heat exchanger. The heat balance of this apparatus will be enhanced by the removed heat of fusion.
- The solid-liquid separation unit will be represented by a separator block. This block uses separation coefficients. By using a dedicated solver model for the separator block, the separation coefficients are adjusted to come up with a specific concentration of the stream representing the crystal fraction. Additionally, with the help of the solver model, the solid fraction representing the product mass stream can be adjusted, too.

- The melt crystallization unit possesses a heat exchanger for crystal melting. This heat exchanger will be represented by a conventional heat exchanger, too. The heat balance of this apparatus will also be enhanced by the required heat for melting.
- For the conventional crystallization unit, the thermodynamic description of the temperature level and maximal yield will base on the binary solid-liquid equilibrium of acrylic acid and acetic acid.
- For the novel crystallization unit operating under eutectic conditions, the ternary solid-liquid equilibrium of acrylic acid, water, and acetic acid determined in chapter 5 [5] will be used.

It is assumed that the crystallization units operate in suspension mode with a single stage. Due to the use of wash columns a product recycle of 15 wt% is assumed. The product recycle has to be crystallized again. This has to be taken into account adding the heat of fusion to the crystallizer units. This has to be considered for the preparation of the heat balance of a crystallization unit. The detailed design of a crystallization unit will not be represented in this simulation study.

6.3.3 Specification of utilities

The reflection of industrial conditions is quite important for a realistic benchmark of a new recovery process. Therefore, it is necessary to consider the conditions of available utilities like cooling water for the condensers and steam for the reboilers. The available cooling water for condensers will provide a supply temperature of 25°C so that the outlet streams of all condensers will be set to 35°C. For reboilers 4 bar steam is available which corresponds to a temperature of 144°C. For the operation of the melt crystallization units, a separate cooling circuit is available. The required cooling duty on a separate temperature level will be declared separately. The outlet temperature for the melters of the crystallization unit is set to a value of 25°C.

6.3.4 Simulation margin and feed composition

For the benchmark of a new recovery process the simulation will be limited to the recovery process only. The reaction section will be left out of consideration. The bottom outlet of the absorption column will be the feed for the two simulation studies. The defined feed composition is presented in table 6-1. The overall mass stream of the feed will be set to 10,000 kg/h. The temperature of the feed will be set to a constant value of 70°C for both simulations.

Table 6-1 Feed composition for recovery section.

component	mass fraction / [wt%]
acrylic acid (AA)	60.0 wt%
acetic acid (ACA)	2.0 wt%
water (H ₂ O)	36.5 wt%
toluene (TOL)	0 wt%
high boiler (HIBOI)	1.5 wt%

6.3.5 Conventional acrylic acid recovery process

One of the industrial relevant recovery processes has already been explained in section 6.2.2. According to this process design, the simulation of the recovery process was prepared. The flow sheet created with AspenTech is shown in figure 6-3 and is used for the simulation. A literature and patents research was done to gain reference values for various processes and design parameters like number of theoretical stages, feed stages, temperature limits, stream concentrations, etc. All design parameters for the different units are presented in the following tables. The majority of the design and operation parameters are taken from the patent US 5910607 [9] including a detailed description of the process.

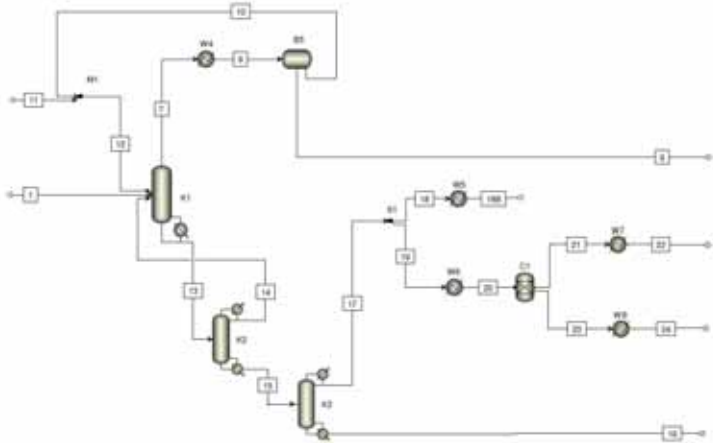


Figure 6-3 AspenTech flow sheet of the conventional recovery process.

Table 6-2 Design and operation parameters azeotropic distillation K1.

	literature [9]	chosen for simulation
condenser pressure	150 – 400 mbar	150 mbar
bottom temperature	<100°C	95°C
no. of theo. stages	5 - 30	28
feed stage (no.1 = top condenser)	-	10
stage for recycle stream from K2	-	10
reflux stage	-	2
reflux ratio	-	fixed, toluene from phase separator B6
design parameter:	-	H ₂ O content in bottom stream no. 13
design specification	-	<0.01 wt%
operation variable	-	distillate rate

Table 6-3 Design and operation parameters acetic acid distillation K2.

	literature [9]	chosen for simulation
condenser pressure	50 – 250 mbar	50 mbar
bottom temperature	<100°C	65°C
no. of theo. stages	5 - 20	20
feed stage (no.1 = top condenser)	-	5
reflux stage	-	2
reflux ratio	-	1.3
design parameter:	-	ACA content in bottom stream no. 15
design specification	-	<0.01 wt%
operation variable	-	distillate rate

Table 6-4 Design and operation parameters high boiler distillation K3.

	literature	chosen for simulation
condenser pressure	no data available	50 mbar
bottom temperature	no data available	max. 105°C
no. of theo. stages	-	4
feed stage (no.1 = top condenser)	-	3
reflux stage	-	2
reflux ratio	-	1.4
design parameter:	-	AA content in bottom stream no. 16
design specification:	-	<15 wt%
operation variable:	-	bottom flow rate

The rigorous simulation of the melt crystallization under realistic conditions is not possible using the AspenTech Simulation Tool. However, as already explained in section 6.3.2, separation blocks using split fractions are used within this study. The separator block was used with the following parameters.

Table 6-5 Design and operation parameters melt crystallization W6, C1, W7, and W8.

	literature [3,11]	chosen for simulation
design parameter	-	AA-content in mother liquid
design specification	-	52 wt% AA
distribution coefficient ACA	0.05	0.05
distribution coefficient H ₂ O	0.02	0.02
distribution coefficient TOL	-	0,05
distribution coefficient HIBOI	0.013	0.013
crystallization temperature	-20°C	-20°C
outlet temperature for product and mother liquid	-	25°C

6.3.6 Novel acrylic aid recovery process using eutectic crystallization

The new acrylic acid recovery process follows the idea of crystallizing acrylic acid and water simultaneously at the eutectic point directly from the bottom outlet of the absorption column. The feed composition is already presented in section 6.3.4. The general feasibility of this operation has been demonstrated by Patent WO 2009130085 [4]. The authors demonstrated the possibility to use the known purification technologies, like wash columns, for the separation and the purification of a crystal mixture from water and acrylic acid simultaneously. Additionally, in chapter 4 [12] it was found that the in-situ formation of ice and acrylic acid crystals improves the permeability and the compressibility of the acrylic acid crystal bed during filtration and purification. The thermodynamic limit of the ternary system of acrylic acid, water, and acetic acid is described in chapter 5. [5]. The ternary eutectic point was identified at a concentration of 32 wt% acrylic acid, 30 wt% water, and 38 wt% acetic acid at a temperature of around -35°C.

Therefore, a novel recovery process with an acrylic acid recovery at an early stage is designed with respect to all results found in the previous chapters of this thesis. The description of the novel process will be done with the help of figure 6-4.

The stream coming from the bottom outlet of the absorption column with a temperature of 70°C will be cooled within the installed heat exchanger W1A to a temperature of 35°C. Afterwards the cooled stream is fed to the crystallization unit made up of the heat exchanger W1B representing a crystallizer and the separation and purification unit C1 representing a wash column. For the sake of simplicity, the design and connection of the crystallization unit will not be shown within this study. Based on the resulting mother liquid composition represented by stream no. 5, the outlet temperature of the heat exchanger W1B is set afterwards to app. -15°C. The separation unit C1 is a conventional AspenTech separator block using split fraction values for the different components. The split factors are calculated by the required amount of acrylic acid crystals and the distribution coefficients for the by products. The amount of acrylic acid crystals to be separated is set to the mass equal the FGAA stream no. 22 of the conventional recovery process presented in section 6.3.5. With regard to the binary eutectic composition of 62 wt% acrylic acid and 38 wt% water the amount of water crystals which will be crystallized and separated in W1B and C1 is calculated. The heat exchanger W3 represents the product melter. The outlet temperature of the “aqueous FGAA” represented by stream no. 4 is set to 25°C.

The effluent mother liquid presented by stream no. 5 will be heated up to 70°C by the installed heat exchanger W2. The warmed up mother liquid will be fed to a further distillate recovery process to come up with the production of acrylic acid of around 99 wt%. The setup and parameters of the distillate recovery process are equal to the values presented in section

6.3.5. Table 6-6 shows the used process parameters for the novel crystallization unit implemented to the conventional recovery process.

Table 6-6 Design and operation parameters melt crystallization W1B, C1, W2, and W3.

	literature	chosen for simulation
design parameter 1	-	AA product mass stream no. 3
design specification 1	-	app. 4600 kg/h AA
design parameter 2	-	AA / H ₂ O concentration in product stream no. 3
design specification 1	-	62 wt% / 38 wt%
distribution coefficient ACA	-	0.05
distribution coefficient TOL	-	0.05
distribution coefficient HIBOI	-	0.013
crystallization temperature	-	-25°C
outlet temperature for product and mother liquid	-	25°C

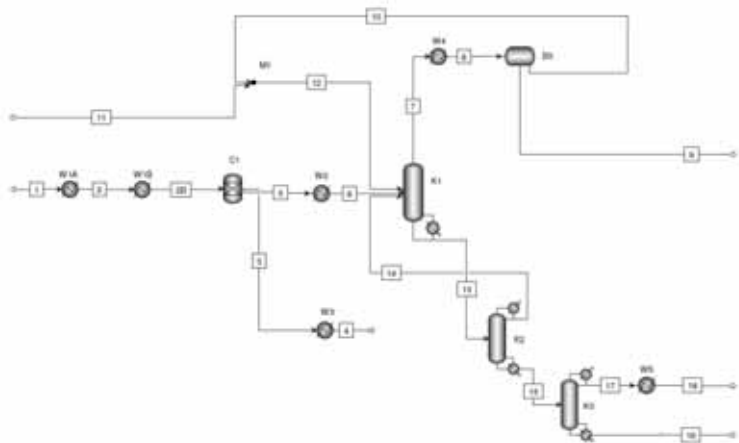


Figure 6-4 AspenTech flow sheet of the novel recovery process using eutectic crystallization.

6.4 Results

The generated results show a coherent and plausible behavior. The detailed stream tables of both processes are presented in table 6-7, table 6-8, table 6-9, and table 6-10.

Table 6-7 Stream table from simulation study of the conventional acrylic acid recovery process (part I).

From	1	7	8	9	10	11	12	13	14	15
To	K1	W4	B5	B5	M1	M1	K1	K2	K1	K2
Component Mass Flow										
AA	6000	157.118	157.118	46.003	111.115	0	111.115	6501.96	548.058	5953.902
ACA	200	365.481	365.481	193.946	171.551	0	171.551	297.755	291.679	6.076
H2O	3650	3674.229	3674.229	3650	24.229	0	24.229	0	0	0
TOL	0	26803.17	26803.17	3.903	26799.23	4.038	26803.27	365.678	365.678	0
DAA	50	0	0	0	0	0	0	50	0	50
MSA	0	0	0	0	0	0	0	0	0	0
HIBOI	100	0	0	0	0	0	0	100	0	100
Component Mass Fraction										
AA	60.0%	0.5100%	0.5100%	1.1800%	0.4100%	0.0000%	0.4100%	88.8800%	45.4700%	97.4500%
ACA	2.0%	1.1800%	1.1800%	4.9800%	0.6300%	0.0000%	0.6300%	4.0700%	24.2000%	0.1000%
H2O	36.5%	11.8500%	11.8500%	93.7400%	0.0900%	0.0000%	0.0900%	0.0000%	0.0000%	0.0000%
TOL	0.0%	86.4600%	86.4600%	0.1000%	98.8700%	100.0000%	98.8700%	5.0000%	30.3400%	0.0000%
DAA	0.5%	0.0000%	0.0000%	0.0000%	0.0000%	0.0000%	0.0000%	0.6800%	0.0000%	0.8200%
MSA	0.0%	0.0000%	0.0000%	0.0000%	0.0000%	0.0000%	0.0000%	0.0000%	0.0000%	0.0000%
HIBOI	1.5%	0.0%	0.0%	0.0%	0.0%	0.0%	0.0%	2.1%	0.0%	2.5%
Mass Flow	10000	31000	31000	3893.85	27106.13	4.04	27110.16	7315.39	1205.42	6109.98
Volume Flow	10.34	66652.37	35.63	3.97	31.66	0	31.67	7.63	1.22	6.11
Temperature	69.05	48.99	35	35	35	20	35	93	40.05	63.86
Pressure	1	0.2	1	1	1	1	1	0.27	0.05	0.05
Mass Density	967	0.47	870	981.22	856.06	866.77	856.06	958.82	985.88	1000.37

Table 6-8 Stream table from simulation study of the conventional acrylic acid recovery process (part II).

From	16	17	18	18B	19	20	21	22	23	24
To		S1	W5	W5	W6	C1	W7	W7	C1	W8
Component Mass Flow										
AA	26.105	5927.797	1334.94	1334.94	4592.857	4592.857	4583.671	4583.671	9.186	9.186
ACA	0.004	6.072	1.367	1.367	4.705	4.705	0.376	0.376	4.328	4.328
H2O	0	0	0	0	0	0	0	0	0	0
TOL	0	0	0	0	0	0	0	0	0	0
DAA	49.068	0.932	0.21	0.21	0.722	0.722	0.058	0.058	0.664	0.664
MSA	0	0	0	0	0	0	0	0	0	0
HIBOI	98.996	1.004	0.226	0.226	0.778	0.778	0.062	0.062	0.715	0.715
Component Mass Fraction										
AA	14.9900%	99.8700%	99.8700%	99.8700%	99.8700%	99.8700%	99.9900%	99.9900%	61.6800%	61.6800%
ACA	0.0000%	0.1000%	0.1000%	0.1000%	0.1000%	0.1000%	0.0100%	0.0100%	29.0600%	29.0600%
H2O	0.0000%	0.0000%	0.0000%	0.0000%	0.0000%	0.0000%	0.0000%	0.0000%	0.0000%	0.0000%
TOL	0.0000%	0.0000%	0.0000%	0.0000%	0.0000%	0.0000%	0.0000%	0.0000%	0.0000%	0.0000%
DAA	28.1700%	0.0200%	0.0200%	0.0200%	0.0200%	0.0200%	0.0000%	0.0000%	4.4600%	4.4600%
MSA	0.0000%	0.0000%	0.0000%	0.0000%	0.0000%	0.0000%	0.0000%	0.0000%	0.0000%	0.0000%
HIBOI	85.0%	0.0%	0.0%	0.0%	0.0%	0.0%	0.0%	0.0%	9.3%	9.3%
Mass Flow	174.17	5935.8	1336.74	1336.74	4599.06	4599.06	4584.17	4584.17	14.89	14.89
Volume Flow	0.16	5.94	1.34	1.29	4.6	4.25	4.24	4.39	0.01	0.01
Temperature	103.11	63.48	63.48	35	63.48	-11	-11	25	-11	25
Pressure	0.05	0.05	0.05	1	0.05	1	1	1	1	1
Mass Density	1056.34	1000.11	1000.11	1032.28	1000.11	1081.92	1081.86	1043.24	1103.2	1062.61

Table 6-9 Stream table from simulation study of the new acrylic acid recovery process using eutectic crystallization (part I).

		1	2	3	4	5	6	7	8	9
From			W1A	C1	W3	C1	W2	K1	W4	B5
To		W1A	W1B	W3		W2	K1	W4	B5	
Component Mass Flow										
AA	KG/HR	6000	6000	4620	4620	1380	1380	93.525	93.525	22.801
ACA	KG/HR	200	200	2.5	2.5	197.5	197.5	423.197	423.197	196.112
H2O	KG/HR	3650	3650	2810.5	2810.5	839.5	839.5	850.797	850.797	839.504
TOL	KG/HR	0	0	0	0	0	0	8632.481	8632.481	3.008
DAA	KG/HR	50	50	0.625	0.625	49.375	49.375	0	0	0
MSA	KG/HR	0	0	0	0	0	0	0	0	0
HIBOI	KG/HR	100	100	1.25	1.25	98.75	98.75	0	0	0
Component Mass Fraction										
AA		60.000%	60.000%	62.140%	62.140%	53.800%	53.800%	0.940%	0.940%	2.150%
ACA		2.000%	2.000%	0.030%	0.030%	7.700%	7.700%	4.230%	4.230%	18.480%
H2O		36.500%	36.500%	37.800%	37.800%	32.730%	32.730%	8.510%	8.510%	79.090%
TOL		0.000%	0.000%	0.000%	0.000%	0.000%	0.000%	86.320%	86.320%	0.280%
DAA		0.500%	0.500%	0.010%	0.010%	1.920%	1.920%	0.000%	0.000%	0.000%
MSA		0.000%	0.000%	0.000%	0.000%	0.000%	0.000%	0.000%	0.000%	0.000%
HIBOI		1.000%	1.000%	0.020%	0.020%	3.850%	3.850%	0.000%	0.000%	0.000%
Mass Flow	KG/HR	10000	10000	7434.88	7434.88	2565.13	2565.13	10000	10000	1061.43
Volume Flow	CUM/HR	10.34	9.94	6.94	7.31	2.4	2.6	19693.92	11.45	1.09
Temperature	C	69.05	35	-25	25	-25	50	51.91	35	35
Pressure	BAR	1	1	1	1	1	1	0.2	1	1
Mass Density	KG/CUM	967	1005.75	1070.77	1017.52	1069.14	987.57	0.51	873	975.39

Table 6-10 Stream table from simulation study of the new acrylic acid recovery process using eutectic crystallization (part II).

From	10	11	12	13	14	15	16	17	18
To									
Component Mass Flow									
AA	70.724	0	70.724	1470.264	112.205	1358.06	25.977	1332.082	1332.082
ACA	227.085	0	227.085	127.61	126.123	1.487	0.004	1.483	1.483
H ₂ O	11.293	0	11.293	0	0	0	0	0	0
TOL	8629.474	3.075	8632.549	91.85	91.85	0	0	0	0
DAA	0	0	0	49.375	0	49.375	48.935	0.44	0.44
MSA	0	0	0	0	0	0	0	0	0
HIBOI	0	0	0	98.75	0	98.75	98.266	0.484	0.484
Component Mass Fraction									
AA	0.790%	0.000%	0.790%	80.000%	33.980%	90.080%	15.000%	99.820%	99.820%
ACA	2.540%	0.000%	2.540%	6.940%	38.200%	0.100%	0.000%	0.110%	0.110%
H ₂ O	0.130%	0.000%	0.130%	0.000%	0.000%	0.000%	0.000%	0.000%	0.000%
TOL	96.540%	100.000%	96.540%	5.000%	27.820%	0.000%	0.000%	0.000%	0.000%
DAA	0.000%	0.000%	0.000%	2.690%	0.000%	3.270%	28.260%	0.030%	0.030%
MSA	0.000%	0.000%	0.000%	0.000%	0.000%	0.000%	0.000%	0.000%	0.000%
HIBOI	0.000%	0.000%	0.000%	5.370%	0.000%	6.550%	56.740%	0.040%	0.040%
Mass Flow	8938.58	3.07	8941.65	1837.85	330.18	1507.67	173.18	1334.49	1334.49
Volume Flow	CUM/HR	0	10.37	1.91	0.33	1.51	0.16	1.33	1.29
Temperature	C	35	34.99	93.01	38.19	65.1	103.09	63.48	35
Pressure	BAR	1	1	0.27	0.05	0.05	0.05	0.05	1
Mass Density	KG/CUM	862.25	866.77	962.37	998.47	1001.63	1056.43	1000.13	1032.3

6.4.1 Heat balance

With the help of the simulation results, it is possible to calculate the specific energy demand of the different unit operations. The simulation of the melt crystallization units are enhanced by the heat of fusion for acrylic acid and water. It is assumed that acrylic acid and water are crystallized only once and a product recycle due to the wash column operation is required. Therefore, the product outlet streams of the melt crystallization units are used for the

calculation of the required heat streams for the crystallization and the melting operation. For acrylic acid the heat of fusion is set constant to $\Delta H_f = 154.9$ kJ/kg and for water to $\Delta H_f = 333.3$ kJ/kg. Figure 6-5 and figure 6-6 give a graphical representation of the specific energy demand for heating and cooling.

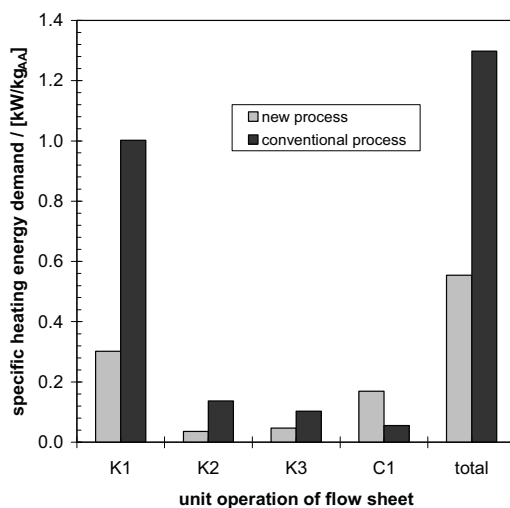


Figure 6-5 Comparison of the specific energy demand for heating.

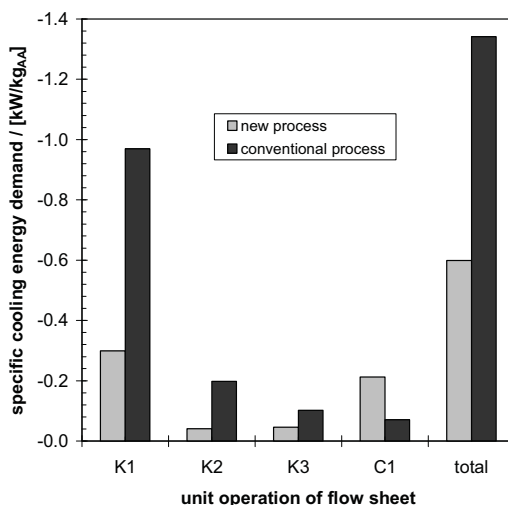


Figure 6-6 Comparison of the specific energy demand for cooling.

The differences in the calculated heat and cooling duties for the different unit operations are obvious from the figures. The relative deviation of the required energies for both recovery

processes are listed in table 6-11. There are differences in the energy savings between the different distillation units. However, if the absolute values are regarded, it is obvious that the energy saving of the eutectic crystallization is enormous in contrast to the azeotropic distillation. Whereas, the savings of the acetic acid and high boiler distillations are high in the relative deviation but small if the absolute savings are regarded.

The energy demand of the eutectic crystallization unit is quite high in comparison with the conventional acrylic acid crystallization. This is caused by the great feed stream consisting out of water and acrylic acid which is cooled down from 70°C to approximately -25°C. Additionally, water is crystallized with a heat of fusion which is double in comparison with the typical one of organics. However, the total energy saving is about 57.3% for heating and 55.3% for cooling.

Table 6-11 Deviation of the novel recovery process to the conventional recovery process.

	relative deviation to conventional process	
	heating	cooling
	[%]	[%]
K1	30.1%	30.8%
K2	26.1%	20.7%
K3	45.7%	45.4%
C1	305.0%	301.2%
total	42.7%	44.7%

For the energy management of a production plant and also for the cost estimation of variable utilities like steam, air, cooling water, and ammonia as coolant, it is important to get knowledge of the different energy transfer levels. Therefore, the calculated heat and cooling duties were divided into four classes:

- cooling water with a temperature level of 25°C for the condensers.
- coolant with a temperature level of -30°C for the melt crystallization units.
- heating water with a temperature level of 25°C for the melters (cp. cooling water).
- steam at a temperature level of 144°C for the installed reboilers.

The specific energy demand on the different temperature levels are shown in figure 6-7. Regarding the coolant of -30°C, the efficiencies of the installed refrigerating plants have to be considered.

The costs of the different specific energies are base on energy costs of a chemical site with a central energy supply. Due to confidential reasons, the specific costs are normalized to the overall energy demand of the conventional process which represents the sum of all energy streams. Figure 6-8 shows the different specific cost per kilogram acrylic acid.

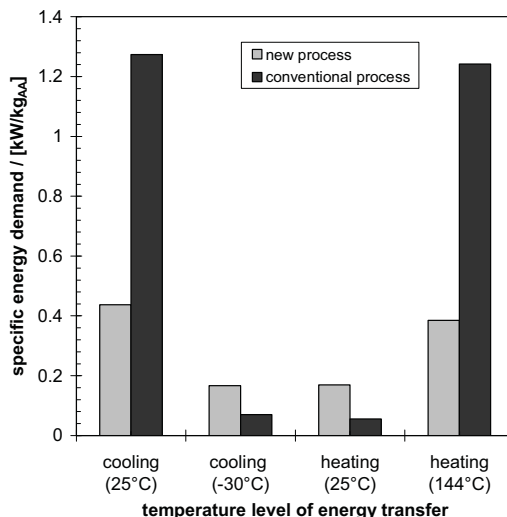


Figure 6-7 Classification of the specific energy demand by the temperature levels.

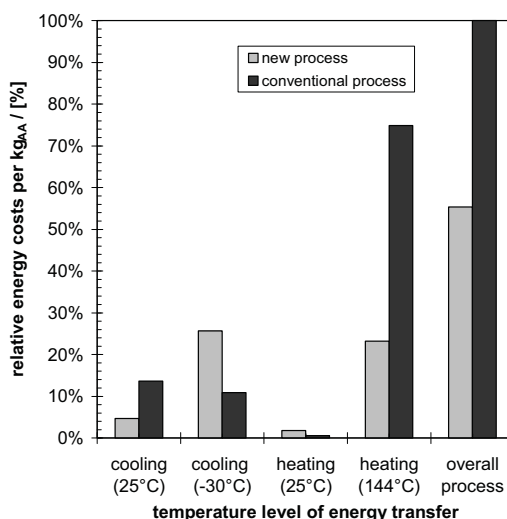


Figure 6-8 Relative energy costs classified by the temperature levels and in comparison to the energy costs of the overall process.

6.4.2 Dimension of main process units

For a first rough estimation of the differences in the investment costs of the different recovery processes, the dimensions of the main process units have been calculated. The calculation bases on significant parameters which will determine the main dimension of the units. Due to a limited access to cost estimation tools, the results of this section are limited to the dimensions of the main process units.

6.4.2.1 Distillation units

The dimensions of the distillation units are designed with the help of the tray sizing tool of the Aspen Simulation Engine Software V7.1. For acrylic acid, trays with a small hold-up are preferred due to the tendency of polymerization. In the literature [18] the use of sieve trays is suggested and tested successfully. For the design of sieve trays Aspen applies the shortcut method developed by Kister and Haas [19]. The shortcut method uses a flooding correlation for tray sizing. This method minimizes the amount of trial and error calculations. The first step is to determine the capacity Factor (CSB) at the most heavily loaded point in the column. The shortcut method for the calculation of the C-Factor bases upon an entrainment flooding correlation. The detailed equations of the shortcut method will not presented in this chapter. Next, the vapor velocity at flood based on the net column area minus the tray downcomer area needs to be calculated. This calculation is done for the top and bottom section of the column. Then, the bubbling area required for the top and bottom sections of the column needs to be calculate. Following a conventional rule of thumb, columns should be designed for 80% flood [19]. Afterwards, the downcomer top area needs to be dimensioned. This calculation is again performed separately for the top and the bottom section of the column. Once this has been completed the tower cross sectional area can be reckoned. The tower diameter is then given by the total tower area which is the sum of the tray bubbling area and the downcomer top area, minus the tower cross sectional area.

The tray and tower dimensions of the distillation units obtained with the help of the Aspen tray-sizing tool are listed in table 6-12 and table 6-13 below.

Table 6-12 Dimensions of the distillation units of the conventional recovery process.

	column diameter	downcomer area	bubbling area
	[m]	[m ²]	[m ²]
K1	2.98	0.70	6.28
K2	1.91	0.29	2.58
K3	1.55	0.19	1.70

Table 6-13 Dimensions of the distillation units of the novel recovery process.

	column diameter	downcomer area	bubbling area
	[m]	[m ²]	[m ²]
K1	1.6	0.20	1.81
K2	0.96	0.07	0.5
K3	1.0	0.08	0.71

The differences of the column dimensions are obvious. The diameter d_{DC} of the azeotropic distillation column K1 reduces from 2.98 m to 1.6 m. This is a dimension reduction of 46%. The diameter d_{DC} of the acetic acid distillation column K2 decreases from 1.91 m to 0.96 m which corresponds to a reduction of 49%. A reduction of 35% is achieved for the diameter d_{DC} of the high boiler distillation column K3 (from 1.55 m to 1.0 m).

The dimensions of the necessary utilities for the distillation units, like condensers and reboilers, increase proportionally to the differences in the heat balances. Therefore, a detailed design study will not be part of this dimension section.

6.4.2.2 Dimension of the melt crystallization units

For the dimension of the melt crystallization units, the specific parameters are the heat transfer coefficients of the scraped-surface crystallizers and the specific crystal load of the wash columns. Available data in the literature concerning the specific components are limited. Therefore, the following assumptions for the design of the crystallizer units and the hydraulic wash column units are made:

Scraped-surface crystallier (ssc):

- heat transfer coefficient $k = 2.5 \text{ kW}/(\text{m}^2 \cdot \text{K})$ [13]

- diameter of scraped-surface crystallizer $d_{SSC} = 0,305$ m [14]
- length of heat exchanger $l_{SSC} = 12,19$ m [14]

Hydraulic wash columns:

- specific crystal capacity $B_{HWC} = 5000 - 10000$ kg/(m³·h) [15]
- max. wash column diameter for p-xylene $d_{HWC} = 1$ m [16]

The dimension of the scraped-surface crystallizer is calculated from the removed heat duty as a result of the simulation study:

$$A_{SSC, req.} = \frac{q}{k \cdot \Delta T} \quad \text{eq. 6-1}$$

The number of required scraped-surface crystallizers units is readily obtained:

$$n_{SSC} = \frac{A_{req.}}{\pi \cdot d_{SSC} \cdot l_{SSC}} \quad \text{eq. 6-2}$$

The required area cross-section $A_{HWC, req.}$ for the use of wash columns is calculated from the crystal stream m_s which represents the crystal load of a wash column, and the crystal capacity of a wash column B_{HWC} :

$$A_{HWC, req.} = \frac{\dot{m}_{crystals}}{B_{HWC}} \quad \text{eq. 6-3}$$

The number of wash columns n_{HWC} is finally given by the ratio of required area cross-section $A_{req.}$ and specific area cross-section A_{HWC} of a single wash column with a defined diameter d_{HWC} :

$$n_{HWC} = \frac{A_{req.}}{A_{HWC}} = \frac{A_{req.} \cdot 4}{d_{HWC}^2 \cdot \pi} \quad \text{eq. 6-4}$$

The dimension of the scraped-surface crystallizer is obtained with the help of the presented equations eq. 6-1 and eq. 6-2. The number of scraped-surface heat exchangers is rounded up to the next integer number. The results are listed in table 6-14.

Table 6-14 Design parameters and dimensions of the scraped-surface crystallizer units.

		conventional process	novel process
crystal stream m_s	[kg/h]	4583	7430
heat duty q	[kW]	-389	-920
heat transfer coefficient k	[kW/(m ² ·K)]	2.5	2.5
ΔT	[K]	5	5
required heat exchanger surface A_{SSC}	[m ²]	31.12	73.6
diameter of heat exchanger d_{SSC}	[m]	0.305	0.305
length l_{SSC}	[m]	12.192	12.192
number of heat exchangers n_{SSC}	[-]	3	6

For the dimension of the wash column units, a specific crystal capacity of 7500 kg/(m²·h) is assumed. This matches the average value of the presented capacity range from the literature [15]. The diameter of the wash columns for the conventional recovery section is set in such a manner to come up with an integer number of wash columns. Therefore, the wash column diameter for the novel process is set to this diameter which could lead in sum to a different specific crystal capacity. The results are listed in table 6-15

Table 6-15 Design parameters and dimensions of the wash column units.

		conventional process	novel process
crystal stream m_s	[kg/h]	4583	7430
capacity of wash column B_{HWC}	[kg/(m ² ·h)]	7500	7500
required cross section $A_{req.}$	[m ²]	0.61	0.99
chosen column diameter d_{HWC}	[m]	0.9	0.9
cross section A_{HWC}	[m ²]	0.61	0.61
number of wash columns n_{HWC}	[-]	1	2 (1.6)
resulting capacity of wash column B_{HWC}	[kg/(m ² ·h)]	7500	6079

As expected from the mass and heat balance of the simulation, the melt crystallization unit of the novel recovery process is bigger than that of the conventional recovery process. The dimension results for the scraped-surface crystallizer show that the required number of apparatus is double for the novel recovery process, whereas the crystal stream is only 60% higher. This is caused by the higher value of the heat of fusion of water.

The increase of the crystal stream of 60% for the novel recovery process is reflected within the capacity of the wash column units. In general, the number of wash columns for the new process would be 1.6 considering the diameter of 0.9 m. Calculations show the possibility to manage the purification theoretically with a single wash column with a diameter of 1.0 m, but this results in a specific capacity of the wash column of around 9500 kg/(m²·h). This is close to the maximum capacity and the maximum known wash column diameter mentioned in the literature [15;16]. Due to uncertainties of the novel wash column operation to purify two crystals simultaneously, the two-column option is chosen which comes along with a higher investment, but with a lower specific crystal capacity.

6.4.3 Result summary

The general major advantages of the novel recovery process using the eutectic crystallization quantitatively are highlighted in percentage values.

The major amount (around 78%) of acrylic acid is separated via a cold separation step without any thermal load on the product. Only a small amount of the acrylic acid enters the hot separation steps. The cold separation comes along with an increasing overall yield, because the absolute amount of dimerization is reduced to at least 22% in comparison with the conventional recovery process. The tendency of dimerization is not considered in the simulation because of missing literature data.

The separation of acrylic acid and water via the eutectic crystallization reduces the amount of water which has to be removed in the azeotropic distillation and disposed by a wastewater incinerator. The amount of wastewater reduces to 22%. This reduction of 78% comes along with the saving of natural gas necessary for the evaporation of wastewater in the incinerator.

The energy demand of the novel recovery process is reduced drastically in comparison to the conventional recovery process. The specific energy demand for cooling is reduced to 45% and for heating to 42%. The total energy cost saving for all energy levels is 45%.

The rough estimation of the unit dimension shows that the diameters of the distillation columns will decrease by round about 40%. Due to the novel application of an early-stage eutectic crystallization, the dimensions of the melt crystallization unit will double its size as expected.

Despite all the advantages there is one disadvantage to be considered. The crystallization of acrylic acid and water under eutectic conditions increases the required equipment for storage

by 61%. If the aqueous acrylic acid has to be transported, the costs for transportation will also increase by 61%.

6.5 Discussion

The presented results of the simulation study come along with the expectation regarding the capacity reduction of the distillation units. The simulation study implies a few simplifications due to missing data from the literature or due to limitations of the used simulation tool:

The simulation of the melt crystallization is simplified to a once-through operation without any internal recycle streams. Additionally, it is assumed that the unit is a one-stage operation. Due to the high occurring temperature differences of 23 K of the melt crystallization unit of the conventional process and 15 K of the novel process, a two stage crystallization unit provides different advantages [15]. Therefore, the melt crystallization step should be scrutinized in detailed, considering a multi-stage process with all recycle streams.

The dimerization and polymerization of acrylic acid monomers is mentioned in the literature [7;9]. Both phenomena are caused by operations at high temperature, e.g. found in distillation columns. However, there are no data on the dimerization or polymerization conversion of acrylic acid at different temperature levels and residence times available in the literature. This tendency decreases the yield of all hot separation units. Due to the reduced amount of acrylic acid which passes the distillation units within the novel recovery process, the overall yield of the recovery section must be higher in comparison to the conventional one. However, the evaluation of this improvement is not possible yet but should be regarded by any model approach in further work.

The injection of inhibitor solutions in all installed unit operations has been left out of consideration. From the literature [9], it is known that the inhibitor is injected to the reflux of the distillation units. However, the required amount is not mentioned. For distillation units operating at high reflux ratios the required amount of inhibitor is quite high. In case of the novel recovery process, the amount of acrylic acid passing the distillation sequences is reduced to 23%. Due to similar distillation parameters this comes along with a decrease of the inhibitor demand of 77%. Further studies should consider the specific inhibitor demand and should compare it for the different recovery processes.

No optimization of the distillation sequences of the novel recovery process has been performed this study to ensure a direct comparison with the conventional recovery process. Therefore, an optimization of the distillation sequences should be done in the future to finalize the overall potential of the novel acrylic acid recovery process.

If the water of the aqueous product has to be separated in a downstream application, the overall energy demand has to be enhanced by this specific step.

6.6 Conclusion and outlook

The main objective of the simulation study was to come up with a novel acrylic acid recovery process using the melt crystallization method of a eutectic crystallization for the production of a fine glacial aqueous acrylic acid quality and a crude acrylic acid quality. AspenTech was used as simulation tool, keeping in mind that the simulation of a melt crystallization process is not possible without assumptions and simplifications. In spite of the limitations concerning the melt crystallization unit, it is possible to draw the following conclusion regarding the novel acrylic acid recovery process:

The required specific energy demand for the recovery section can be reduced to around 45%. The major energy savings are found in the azeotropic distillation for the dehydration of the acrylic acid. The specific energy demand for removing the heat of crystallization increases by a factor of three, but the absolute values are low compared with energy savings in the distillation sequence. The calculation of the total energy costs bases on estimated prices for the different energy levels. At this point, it has to be taken into account that these values differ significantly on the available utilities of a chemical site.

The specific dimensions of the distillation units, like column diameter, reduce to around 40%. This comes along with an estimated decrease in investment cost of around 25% according to simple cost estimation tools [17].

The specific dimensions of the melt crystallization unit increase by factor two. The number of scraped-surface crystallizers doubles, whereas the number of required utilities like residence vessels, pumps, and instrumentation are similar at an increasing dimension. Due to limited dimensions of the purification units, e.g. hydraulic wash columns, the number of main apparatus and utilities doubles. Therefore, it is assumed that the investment costs double, too.

78% of the acrylic acid will not be treated by any hot separation units which increases the yield of the recovery process by assumed 78% due to less loss caused by dimerization and polymerization.

The separation of water by the eutectic crystallization as a product compartment reduces the amount of wastewater to 23%. This reduction corresponds to a reduction of the natural gas demand of the wastewater incinerator.

The costs for transportation and storage will increase because of the additional amount of water. The product mass increases due to the water content by 61%.

Regarding all these conclusions, the novel acrylic acid recovery process turns out to be an innovative, powerful, and attractive alternative process with a high economical potential for the production of acrylic acid. A lower dimerization and polymerization rate increases the yield and reduces the raw material factor. Additionally, the novel process comes along with a reduced specific energy demand to preserve natural resources like coal or natural gas

required for the steam generation for the column reboilers and natural gas for the wastewater incinerator.

It appears path breaking that it is possible to design an innovative and an eco-friendly industrial recovery process by the use of one of the oldest known unit operations like melt crystallization. This shows that it is the responsibility of a process engineer to work continuously on process improvements and on the implementation of innovative processes on industrial scale.

Nomenclature**Symbols**

A	area cross-section	$[\text{m}^2]$
B_{HWC}	specific crystal load of a hydraulic wash column	$[\text{kg}/(\text{m}^2 \cdot \text{h})]$
d	diameter	$[\text{m}]$
ΔH_m	latent heat of fusion	$[\text{J}/\text{kg}]$
k	heat transfer coefficient	$[\text{kW}/\text{m}^2 \cdot \text{K}]$
l	length	$[\text{m}]$
m	mass rate	$[\text{kg}/\text{h}]$
n	number	$[-]$
q	heat flow	$[\text{kJ}/\text{s}]$
ΔT	temperature difference	$[\text{K}]$
V	volume flow rate	$[\text{m}^3/\text{s}]$
v	velocity	$[\text{m}/\text{s}]$

Greek Symbols

ρ	density	$[\text{kg}/\text{m}^3]$
--------	---------	--------------------------

Subscripts

DC	distillation column
HWC	hydraulic wash column
l	liquid phase
req.	required
SSC	scraped-surface crystallizer
s	solid phase

Abbreviations

AA	acrylic acid
ACA	acetic acid
FGAA	fine glacial acrylic acid
H ₂ O	water
HIBOI	high boiler
TOL	toluene

References

- [1] Hengstermann, A.; Kadam, S.; Jansens, P.J.; Influence of water content and supercooling on crystal morphology of acrylic acid, *J. of Crystal Growth and Design*, 2009, Vol. 9 (4), pp2000–2007.
- [2] Hengstermann, A.; Harms, S.; Jansens, P.J.; The Influence of Water and Supercooling on Permeability and Compressibility of Crystal Beds formed out of Acrylic Acid Crystals, *Chemical Engineering Technology*, 2010, Vol. 33 (3), pp433-443.
- [3] Nordhoff, S.; Balduf, T.; Bub, G.; Fornika, R.; Mosler, J.; Ratke, T.; Kobus, A.; Thong, D.; (Meth)Acrylsäurekristall und Verfahren zur Herstellung und Aufreinigung von wässriger (Meth)Acrylsäure, 2003, European Patent EP1492755A1.
- [4] Hengstermann, A.; Kuppinger, F.F.; Leistner, J.; Mosler, J.; Jansens, P.J.; Method for Producing and Purifying Aqueous Phases, 2008, WO-Patent WO2009130085A1.
- [5] Hengstermann, A.; Cameretti, L.; Solvent Screening and Measurement of Phase Diagrams for the Yield Maximization of an Acrylic Acid Crystallization, Submitted to *Chemical Engineering Data* on 01-09-2010.
- [6] Ullmann's Encyclopedia of Industrial Chemistry, Acrylic Acid and Derivatives, Wiley-VCH Verlag, Weinheim, Germany, 2010, 7th Edition, pp1-19.
- [7] PERP Product Reports, Nexant, Inc., San Francisco, California, USA, 1999.
- [8] ASPEN Plus, Thermo Analysis Tool, Binary VLE of Acrylic Acid and Water, Aspen Plus V7.1, 2010.
- [9] Sakakura, Y.; Yamagishi, M.; Hosaka, H.; Process for Producing Acrylic Acid, Mitsubishi Chemical Corp., 1999, US-Patent 5910607.

- [10] ASPEN Plus, Thermo Analysis Tool, Binary VLE of Acrylic Acid and Acetic Acid, Aspen Plus V7.1, 2010.
- [11] Chubarov, G.A.; Danov, S.M.; Liquid-Solid Equilibrium in the Systems Acrylic Acid - Water, Acrylic Acid - Acetic Acid, and Methacrylic Acid – Water, J. Appl. Chem., USSR, 1978, Vol. 51 (8), pp1796-1798.
- [12] Hengstermann, A.; Jansens, P.J.; Compressibility improvement of an acrylic acid crystal bed by the in-situ formation of ice crystals, submitted to AIChE on 02-11-2010.
- [13] Personal Conversation with Joe Armstrong 3rd, Achema, Frankfurt, Germany, 11th – 15th of May 2009.
- [14] Armstrong Engineering Associates, Company brochure, Scraped-surface Crystallizers, www.rmarmstrong.com, 2009.
- [15] Oord-Knol, L.; Hydraulic Wash Columns – Solid-liquid Separation in Melt Crystallization, PhD Thesis, Delft University of Technology, Delft, The Netherlands, 2000.
- [16] Arkenbout, G.F.; Melt Crystallization Technology, Technomic Publishing Company, Inc., Lancaster, 1995.
- [17] Vauck, W.R.A.; Mueller, H.A.; Grundoperationen chemischer Verfahrenstechnik, Issue 10, Wiley-VCH Verlag, Weinheim, Germany, 2000.
- [18] Smith, V.C.; Miller R.J.; First-Generation High-Capacity Trays still have what it takes, AIChE 2002 Annual Meeting, Session “Distillation Honors Session”, Indianapolis, Indiana, USA, 2002.
- [19] Kister, H. Z.; “Distillation Design”, McGraw-Hill Book Company Inc., New York, 1992.

APPENDIX

ENGLISH SUMMARY

A NEW APPROACH TO INDUSTRIAL MELT CRYSTALLIZATION OF ACRYLIC ACID

Axel Hengstermann

The quality standards for chemical substances have become higher in the recent past. Additionally, the specific energy consumption of chemical products and their production processes have become the focus of the public interest due to the contribution of the CO₂ emission to the global warming and finally to the predicted climate change. Therefore, the chemical industry is anxious to develop new innovative production processes to reduce the specific energy consumption and to improve the product quality.

The applications of acrylic acid require a very low level of side components. This concentration level is not possible to reach by a common distillation unit. Therefore, an end of pipe melt crystallization unit for the ultra purification of acrylic acid is well-known in literature. Despite of the installed melt crystallization units, the existing recovery processes for acrylic acid are quite energy intensive.

Hence, the aim of the research described in this thesis was to check if it is possible to purify acrylic acid via a suspension melt crystallization unit from an aqueous acrylic acid stream directly coming from the synthesis unit in order to reduce the specific energy demand. The early stage installation of a melt crystallization unit would lead to less thermal stress for the acrylic acid and would reduce the yield loss due to polymerization of acrylic acid in the distillation units.

For the development of a new melt crystallization unit the crystal morphology and its development at varying side component concentrations belongs to the field of major interest. Chapter 2 deals with the investigation of the crystal morphology of acrylic acid with respect to the water content in the melt and the driving force applicable in terms of supercooling β . The intention was to measure the dependence of absolute growth rates and aspect ratios. The results show that water in the melt induces the formation of a hollow cavity at the crystal faces {002} and provokes a needle-like crystal habit up to an aspect ratio of 4. It was found that the higher supercooling and water content, the higher the tendency to form needle-like crystals and the larger the length of the occurring cavity.

Afterwards, the growth rates of the developed faces were simulated by using the growth rate equation for the birth and spread mechanism. Additionally, a qualitative model to describe the formation of a hollow cavity at the crystal extremities was elaborated. Based on the measured data and the developed model, a general prediction of the crystal morphology in dependence of the water content and the supercooling of the melt was possible.

The performance of a solid-liquid separation process is often limited by the size distribution and the morphology of the crystals. For the prediction of the filtration behavior a robust and an applicable model based only on the crystallization process parameters is necessary. Chapter 3 deals with the modeling and the experimental investigation of the filtration behavior of acrylic acid crystals grown from aqueous melts. First, a model was developed to predict the compressibility and the permeability of a crystal bed at different water contents and supercooling of the melt. The model bases mainly on equations for non-spherical particles from Ouchiyama and the use of the chord length distribution obtained from an inline FBRM probe. Afterwards, experiments were carried out with a continuously operated scraped surface crystallizer equipped with an inline FBRM probe to measure the chord length distribution of the crystals. The permeability and compressibility of the resulting crystal beds were determined by simple filtration tests at various pressure drops to consider the influence of the mechanical stress on the crystal bed. It was found that the permeability decreases from around 10^{-10} m^2 to 10^{-12} m^2 with an increasing water content of 5 wt% to 15 wt% and supercooling of 0.02 to 0.1. Additionally, the compressibility coefficient increased in parallel from 0.3 to 0.37. Considering acceptable fault tolerances, with the help of the proposed model it was possible to reproduce the experimental results from a chord length distribution from FBRM as one main input parameter. With the help of the developed model, it will be possible to predict the performance of an industrial acrylic acid filtration unit or to adjust the crystallization parameters previous in operation.

The filtration performance can often be improved by the addition of filter aids. However, the use of filter aids within a melt crystallization process is not favored because of the additional solid-liquid separation. Therefore, the idea came up to crystallize acrylic acid and water at the eutectic point wherein the harder water crystals may act as an in-situ filter aid.

The scope of the work described in chapter 4 was to verify this idea with small batch crystallization and filtration experiments. The crystallization at the eutectic point of the binary system of water and acrylic acid resulted in the formation of two different crystal habits. Acrylic acid crystallizes in a needle-like form, whereas ice crystallizes as spherical-like crystals. The formation of the ice crystals from a eutectic melt improved the initial permeability of a pure acrylic acid crystal bed by a factor of 2. The major impact of the ice

crystals was the improvement of the compressibility behavior. The compressibility coefficients decreased from 0.25 for the acrylic acid crystal bed down to 0.15 with the ice crystals at the eutectic composition. These promising results show that the improvement of filterability of an acrylic acid crystal bed is possible by the in-situ formation of ice crystals. Additionally, the results show that it is possible to increase the yield of an acrylic acid crystallization by overcoming the eutectic limitation, if the generated aqueous product mixture can be used for any applications.

The yield of crystallization processes is mostly limited by the eutectic points as thermodynamic limits and the economically acceptable temperature level. In some cases it is possible to increase the yield and to improve the crystallization performance by the addition of a dedicated third component.

The design of a structured solvent screening method for the rapid identification of possible solvents to increase the yield is described in chapter 5. For a fast validation, an experimental stage-gate process was developed to come up with the required information of each stage at a minimum work load. The stage-gate process based completely on thermal analysis using Differential Scanning Calorimetry. The solvent screening approach and the stage-gate process were successfully adopted to investigate the yield maximization of an acrylic acid crystallization from an aqueous melt by adding a third component. The solvent screening came up with three different solvents, namely acetic acid, propionic acid, and butanoic acid. The complete ternary solid-liquid equilibrium diagrams of the components were measured and finally evaluated. Finally, acetic acid was identified as the favored third component for a eutectic crystallization unit of acrylic acid and water.

For the industrial implementation of the developed eutectic crystallization of acrylic acid and water (ice) an economical benchmark was required to figure out the economical advantages of the new recovery process.

Therefore, the benchmark of the novel eutectic crystallization step was the aim of chapter 6. Simulations of the common and the novel recovery processes were prepared and evaluated regarding the energy demand, the qualitative yield improvement, and the apparatus dimensions.

The early-stage separation of acrylic acid and ice recovers 78 wt% of the acrylic acid without any thermal treatment. This decreases the loss of acrylic acid caused by dimerization and polymerization by 78%. The overall energy consumption of the novel recovery process is reduced to 41%. The amount of wastewater to be incinerated is reduced down to 23%, due to the water removal by the aqueous product itself. This comes along with a reduction of the natural gas required for the wastewater incinerator of 77%. Based on specific design

parameters of the simulations, it was possible to estimate the differences in the main equipment dimensions. The dimensions of the distillation units reduce to around 40%, whereas the dimensions of the melt crystallization units double. The results of the benchmark show that the eutectic crystallization as a novel recovery process is an innovative and promising process considering sustainable requirements like reduced overall specific energy consumption and an improved yield due to the charge material.

Summarizing, the research described in this thesis is an example for an innovative process development using the melt crystallization. Once again, the high selectivity and the energetic advantages of the crystallization step offer the opportunity to improve a common recovery process.

NEDERLANDSE SAMENVATTING

EEN NIEUWE AANPAK VOOR INDUSTRIELE SMELTKRISTALLISATIE VAN ACRYLZUUR

Axel Hengstermann

De kwaliteitsstandaarden voor chemische stoffen worden steeds hoger. Daarbij is het specifieke energieverbruik van chemische producten en productieprocessen van algemeen belang door de contributie van CO₂ uitstoot aan de opwarming van de aarde en uiteindelijk aan de voorspelde klimaatverandering. De chemische industrie is daarom gebrand om nieuwe innovatieve productieprocessen te ontwikkelen om de specifieke energie consumptie te verminderen en de productkwaliteit te verbeteren.

De toepassingen van acrylzuur vereisen een zeer geringe hoeveelheid bijproducten. Deze concentratie kan niet worden bereikt met een normale destillatie eenheid. Daardoor is een stroomafwaarts smelt kristallisatie eenheid voor de ultra-zuivering van acrylzuur een bekend gegeven in de literatuur. Ondanks geïnstalleerde smelt kristallisatie eenheden zijn de bestaande zuiveringsprocessen voor acrylzuur zeer energie intensief.

Het doel van het onderzoek in deze thesis is om na te gaan of het mogelijk is om acrylzuur te zuiveren door middel van oplossings-smelt-kristallisatie vanuit een waterrijke acrylzuur stroom die direct afkomstig is van de synthese eenheid, om zo het specifieke energieverbruik te verminderen. Installatie van een smelt kristallisatie eenheid eerder in het proces zou leiden tot minder thermische spanning voor het acrylzuur en zou het productverlies door polymerisatie van acrylzuur in de destillatie eenheden verminderen.

Voor de ontwikkeling van een nieuwe kristallisatie eenheid zijn de kristalmorfologie en de ontwikkeling daarvan bij verschillende concentraties van bijproducten van groot belang. In hoofdstuk 2 wordt de kristalmorfologie van acrylzuur bestudeerd in relatie tot het water gehalte in de smelt en de toegepaste drijvende kracht, genaamd supercooling β . Het was de bedoeling om de afhankelijkheid van absolute groei snelheden en breedte lengte verhoudingen te meten. De resultaten laten zien dat water in de smelt de formatie van een holle ruimte tot stand brengt op het kristal oppervlak {002} en aanzet tot een naald-vormige kristal tot een maximale lengte-breedte verhouding van 4. Er kon worden vastgesteld dat bij

hogere supercooling en watergehalte de neiging naar naald-vormige kristallen en de lengte van de holle ruimte groter werden.

Naderhand zijn de groeisnelheden van de ontwikkelende oppervlakken gesimuleerd aan de hand van de groeisnelheidsvergelijking voor birth and spread mechanismen. Daarnaast is er een kwalitatief model ontwikkeld om de formatie van een holle ruimte aan de kristal uiteinden te beschrijven. Aan de hand van de gemeten data en het ontwikkelde model kon er een algemene voorspelling worden gemaakt van kristal morfologie onder invloed van water gehalte en supercooling.

De prestatie van een vaste stof/vloeistof scheidingsproces is vaak gelimiteerd door de grootte verdeling en morfologie van de kristallen. Voor de voorspelling van het filtratie gedrag is een robuust en toepasbaar model dat enkel gebaseerd is op de kristallisatie proces parameters noodzakelijk.

Hoofdstuk 3 behandelt het modelleren en het experimentele onderzoek van het filtratie gedrag van acrylzuur kristallen die zijn ontstaan uit waterrijke smelten. Eerst is er een model ontwikkeld om de kompressibiliteit en permeabiliteit van een kristalbed te voorspellen bij verschillende water gehalten en supercoolings van de smelt. Het model is met name gebaseerd op vergelijkingen voor niet-bolvormige deeltjes van Ouchiyaama en het gebruik van snaar lengte verdeling verkregen met een in-line FBRM sonde. Vervolgens zijn experimenten uitgevoerd met een continu-geopereerde geschraapt-oppervlakte kristallisator, uitgevoerd met een in-line FBRM sonde om de snaar-lengte verdeling van de kristallen te meten. De permeabiliteit en kompressibiliteit van de kristal bedden werden vastgesteld door eenvoudige filtratie testen bij verschillende druk verschillen om de invloed van mechanische spanning op het kristalbed vast te stellen. Er kon worden vastgesteld dat de permeabiliteit afneemt van ongeveer 10^{-10} tot 10^{-12} bij een toenemend watergehalte van 5 gw% naar 15 gw% en supercoolings van 0.02 naar 0.1. Daarbij nam de kompressibiliteitscoëfficiënt tegelijkertijd toe van 0.3 tot 0.37. Met aanzienlijke fout toleranties in acht nemend, was het mogelijk om met behulp van het voorgestelde model de experimentele resultaten te herproduceren met de FBRM snaar lengte verdeling als de belangrijkste invoerparameter. Met behulp van het ontwikkelde model is het mogelijk om de prestatie van een industriële acrylzuur filtratie eenheid te voorspellen of om de kristallisatie parameters voor operatie te veranderen.

De filtratie prestaties kunnen vaak worden verbeterd door de toevoeging van filter hulpmiddelen. Het gebruik van filter hulpmiddelen bij smelt kristallisatie processen is echter niet gewenst door de extra vast stof/vloeistof scheiding. Daardoor kwam het idee om acrylzuur te kristalliseren bij het eutectisch punt, waarbij de hardere water kristallen als een in-situ filter hulpmiddel fungeren.

Het werk beschreven in hoofdstuk 4 is bedoeld om dit idee te verifiëren met kleine batch kristallisatie en filtratie experimenten. Kristallisatie bij het eutectisch punt van het binaire systeem acrylzuur-water resulteerde in twee verschillende kristalvormen. Acrylzuur kristalliseert naald-vormig terwijl ijs kristallen als bolvormige kristallen kristalliseren. Het ontstaan van ijskristallen vanuit de eutectische smelt verbeterde de initiële permeabiliteit van een puur acrylzuur kristalbed met een factor 2. De grootste invloed van de ijskristallen was verbetering van het kompressibiliteitsgedrag. De kompressibiliteitscoëfficiënten namen af van 0.25 voor het acrylzuur kristal bed naar 0.15 met de ijs kristallen bij de eutectische samenstelling. Deze veelbelovende resultaten laten zien dat verbetering van de filtreerbaarheid van het acrylzuur kristal bed mogelijk is door het in situ ontstaan van ijs kristallen. Daarbij laten de resultaten zien dat het mogelijk is om de opbrengst van acrylzuur kristallisatie te verhogen door het overwinnen van de eutectische grens, als de waterrijke productmix die ontstaan is gebruikt kan worden voor andere toepassingen.

De opbrengst van kristallisatie processen is met name beperkt door de eutectische punten als thermodynamische beperkingen en de economisch aanvaardbare temperatuur. In sommige gevallen is het mogelijk om de opbrengst te verhogen en de kristallisatie prestaties te verbeteren door toevoeging van een specifieke derde component.

Het ontwerp van een gestructureerde oplosmiddel-screeningsmethode voor snelle identificatie van mogelijke oplosmiddelen om de opbrengst te verhogen wordt beschreven in hoofdstuk 5. Voor snelle validatie werd een experimenteel mijlsteenproces ontwikkeld om met minimale arbeidsinspanning tot de vereiste informatie te komen van elke stap. Het mijlsteen proces is volledig gebaseerd op thermische analyse door gebruik van Differential Scanning Calorimetry. De aanpak van oplosmiddel-screening en het mijlsteenproces werden succesvol gebruikt om de opbrengst maximalisatie te onderzoeken van acrylzuur kristallisatie uit een waterrijke smelt door toevoeging van een derde component. Bij de oplosmiddel-screening kwamen drie verschillende oplosmiddelen naar voren, namelijk azijnzuur, propionique zuur en butter zuur. De complete ternaire vaste stof-vloeistof evenwichts-diagrammen van de componenten zijn gemeten en uiteindelijk geëvalueerd. Uiteindelijk was azijnzuur geïdentificeerd als de geprefereerde derde component voor een eutectische kristallisatie eenheid van acrylzuur en water.

Voor industriële toepassing van de ontwikkelde eutectische kristallisatie van acrylzuur en water (ijs) was een economische standaard vereist om de economische voordelen van het nieuwe winningsproces te bepalen.

Daarom was de standaardisatie van de nieuwe eutectische kristallisatie het doel van hoofdstuk 6. Simulaties van het huidige en het nieuwe winningsproces zijn samen gesteld en

geëvalueerd naar energie consumptie, kwalitatieve opbrengst verbetering en apparaat afmetingen.

De scheiding van acrylzuur en ijs vroeg in het proces wint 78 gw% van het acrylzuur zonder enige thermische behandeling. Dit vermindert het verlies van acrylzuur veroorzaakt door dimerisatie en polymerisatie met 78%. De algehele energie consumptie van het nieuwe winningsproces wordt verminderd tot 41%. De hoeveelheid afvalwater dat moet worden verbrand wordt verminderd tot 23%, door afvoer van water door het waterrijke product zelf.

Dit gaat gepaard met een vermindering van de hoeveelheid aardgas vereist voor de afvalwater verbrander van 77%. Het was mogelijk om de verschillen in de belangrijkste apparaat afmetingen te schatten, gebaseerd op specifieke ontwerp parameters van de simulaties. De afmetingen van de destillatie eenheden nemen af tot ongeveer 40% terwijl de afmetingen van de smelt kristallisatie eenheden verdubbellen. De resultaten van de standaard laten zien dat eutectische kristallisatie als nieuw winningsproces een innovatieve en veelbelovend proces is gezien de duurzame eisen zoals verminderde algehele specifieke energie consumptie en een verbeterde opbrengst door het grondstof.

Samenvattend is het onderzoek beschreven in deze thesis een voorbeeld van een ontwikkeling van een innovatief proces met het gebruik van smelt kristallisatie. Nogmaals, de hoge selectiviteit en de energetische voordelen van de kristallisatie stap bieden een mogelijkheid om het bestaande winningsproces te verbeteren.

GERMAN SUMMARY

EIN NEUER ANSATZ ZUR INDUSTRIELLEN SCHMELZKRISTALLISATION VON ACRYLSÄURE

Axel Hengstermann

Die Qualitätsanforderungen für chemische Produkte sind in der Vergangenheit stetig gestiegen. Die Öffentlichkeit richtet zudem ihren Fokus immer mehr auf den spezifischen Rohstoff- und Energieverbrauch der Herstellungsprozesse. Ausschlaggebend hierfür sind die Verknappung der Fossilienrohstoffressourcen und der Beitrag des emittierten CO₂ an der Erderwärmung und des hiermit verbunden prognostizierten Klimawandels. Die chemische Industrie ist daher bestrebt und angehalten neue und innovative Herstellungsprozesse mit einem geringeren spezifischen Energieverbrauch und gleichzeitig verbesserten Produktqualitäten zu entwickeln.

Spezielle Einsatzgebiete von Acrylsäure erfordern ein sehr geringes NebenkompONENTENNIVEAU. Dieses Konzentrationsniveau ist bei der Acrylsäureaufarbeitung auf herkömmlichem Wege nur durch eine chemische Umwandlung der kritischen NebenkompONENTEN in schwersiedende Komponenten und einer nachgeschalteten Destillationssequenz erreichbar. Aus diesem Grund wird die Feinreinigung von Acrylsäure häufig über eine nachgeschaltete Kristallisation durchgeführt. Dieses Verfahren ist in der Literatur ausreichend beschrieben. Dennoch ist der in der Literatur beschriebene Acrylsäureprozess sehr energieintensiv.

Das Ziel dieser Forschungsarbeit war es daher, die Aufreinigung von Acrylsäure mit Hilfe einer Suspensionskristallisation aus einem wässrigen Acrylsäurestrom, der direkt aus der Synthesesequenz kommt, zu untersuchen. Ziel war es zusätzlich, den notwendigen spezifischen Energiebedarf zu reduzieren und gleichzeitig die thermische Belastung der Acrylsäure zu minimieren und damit einen geringeren Verlust durch Polymerisation in den nachgeschalteten Destillationssequenzen zu erzielen.

Bei der Entwicklung von neuen Suspensionskristallisationsprozessen ist die Kenntnis der auftretenden Kristallmorphologie und deren Entwicklung unter dem Einfluss der NebenkompONENTENKONZENTRATION von großem Interesse. Aus diesem Grund wurde in Kapitel 2 die Morphologie von Acrylsäurekristallen unter dem Einfluss verschiedener

Wassergehalte und Übersättigungsgrade untersucht. Es wurden die absoluten Kristallwachstumsgeschwindigkeiten der unterschiedlichen Kristallflächen und das hieraus resultierenden Seitenlängenverhältnis bestimmt. Es wurde gefunden, dass Wasser in der Schmelze für die Ausbildung eines Hohlraumes auf der Kristallfläche {002} verantwortlich ist. Des Weiteren wurde gefunden, dass Wasser in der Schmelze die Wachstumsgeschwindigkeit der unterschiedlichen Kristallflächen so beeinflusst, dass ein nadelförmiger Habitus mit Seitenlängenverhältnissen von bis zu 4 entsteht. Die Ausbildung nadelförmiger Kristalle wird zudem mit zunehmendem Wassergehalt und zunehmender Übersättigung verstärkt, so dass sich zunehmend nadelförmige Kristalle ausbilden und die Länge des auf der Kristallfläche {002} ausgebildeten Hohlraumes zunimmt.

Im Anschluss an die experimentellen Untersuchungen konnten die Kristallwachstumsgeschwindigkeiten der einzelnen Kristallflächen unter Annahme des „Birth and Spread“-Mechanismus modelliert werden. Für die Ausbildung des Hohlraums auf der Kristallfläche {002} konnte ein qualitatives Modell entwickelt werden. Mit Hilfe der vermessenen Daten und dem aufgestellten Wachstumsmodell kann die Kristallmorphologie als Funktion des Wassergehalts und der Übersättigung vorhergesagt werden.

Die Filtrationseigenschaften einer Suspension hängen signifikant von der Korngrößenverteilung und der Kristallmorphologie ab. Zur Vorhersage der Filtrationseigenschaften industrieller Kristallsuspensionen ist ein robustes Modell wünschenswert, das als Eingangsgrößen lediglich einfach zu vermessende Prozessparameter benötigt. In Kapitel 3 wurde daher eine grundlegende Modellierung einer Fest-Flüssig-Trennungen von industriellen Suspensionen erarbeitet. Anschließend wurden in experimentellen Untersuchungen die Filtrationseigenschaften von Acrylsäurekristallen aus wässrigen Schmelzen vermessen und die notwendigen Modellierungsparameter ermittelt.

Es wurde zunächst ein Modell zur Vorhersage der Kompressibilität und der Permeabilität von Acrylsäurekristallen unter der Variation des Wassergehalts und der Übersättigung entwickelt. Das entwickelte Modell basiert auf bekannten Berechnungsgrundlagen für nicht kugelförmige Partikel von Ouchiya und Tanaka unter der Verwendung einer inline Messung (FBRM) zur Ermittlung der Sehnslängenverteilung. Zur Ermittlung aller relevanten Parameter wurden anschließend kontinuierliche Suspensionskristallisationsversuche mit einem Kratzkristaller durchgeführt. Die Sehnslängenverteilung wurde mit einer inline FBRM-Sonde ermittelt. Anschließend wurde mit einfachen Filtertests die Kompressibilität und Permeabilität in Abhängigkeit vom verschiedenen Differenzdrücken ermittelt. Es wurde gefunden, dass die Permeabilität mit zunehmenden Wassergehalten von 5 Gew.-% auf 15 Gew.-% und zunehmender Übersättigung von 0,02 auf 0,1 deutlich von 10^{-10} m^2 auf 10^{-12} m^2 reduziert wird. Die Kompressibilitätskoeffizienten der Acrylsäurekristalle stiegen dabei von 0,3 auf

0,37 an. Anschließend erfolgte die Modellierung der Permeabilitäten unter Verwendung der vermessenen Sehnenlängenverteilung als Eingangsgröße. Die maximale Abweichung zwischen den ermittelten und modellierten Permeabilitäten betrug 19%.

Unter Berücksichtigung der ermittelten Fehlertoleranzen kann das entwickelte Modell zur Vorhersage der Filtrationseigenschaften einer vorgeschalteten Acrylsäurekristallisation genutzt bzw. die Parameter des Kristallisationsprozesses gezielt gesteuert werden.

Die Verbesserung der Filtrationseigenschaften erfolgt oftmals durch den Einsatz sog. Filterhilfsmittel. Der Einsatz von Filterhilfsmitteln im Bereich der Schmelzkristallisation gestaltet sich eher schwierig und konnte als nicht vorteilhaft identifiziert werden, da eine zusätzliche Filtration zur Abtrennung des Filterhilfsmittels notwendig ist. Für die Filtration von Acrylsäurekristallen wurde daher untersucht, ob die Bildung harter Wasserkristalle am eutektischen Punkt und deren Verwendung als Filterhilfsmittel möglich ist.

Das Ziel von Kapitel 4 war daher, die grundsätzliche Idee der in-situ Bildung von Wasserkristallen als Filterhilfsmittel am eutektischen Punkt mit einfachen Batchkristallisationsversuchen und anschließenden Filtertests zu verifizieren.

Die Kristallisation von Acrylsäure und Wasser am eutektischen Punkt führt zur Bildung zweier unterschiedlicher Kristallmorphologien. Acrylsäure kristallisiert in einer nadelförmigen Struktur aus, wohingegen Eis eine eher kugelförmige Struktur ausbildet. Die anschließenden Filtertest haben gezeigt, dass die Bildung von Eis aus einer eutektischen Mischung die Permeabilität um den Faktor 2 verbessert. Vor allem aber verbessern die gebildeten Eiskristalle die Kompressibilität des Kristallbetts. Die Kompressibilitätskoeffizienten sinken von 0,25 für reine Acrylsäurekristalle auf 0,15 für eine Suspension aus Acrylsäure- und Wasserkristallen, die am eutektischen Punkt gebildet wurden. Die Ergebnisse der Machbarkeitsversuche haben gezeigt, dass die in-situ-Bildung von Eiskristallen die Filtrierbarkeit von Acrylsäurekristallen deutlich verbessern kann. Zudem kann die Ausbeutelimittierung einer reinen Acrylsäurekristallisation durch den eutektischen Punkt durch eine eutektische Kristallisation von Acrylsäure und Wasser umgangen werden. Voraussetzung hierfür ist, dass die wässrige Acrylsäure in der entsprechenden Anwendung eingesetzt werden kann.

Die Ausbeute von Kristallisationsprozessen ist fast immer durch eine thermodynamische Grenze, z.B. dem eutektischen Punkt oder dem ökonomisch vertretbaren Temperaturniveau begrenzt. Es ist jedoch bekannt, dass man z.B. durch die zielgerichtete Zugabe einer Zusatzkomponente, z.B. einem Lösungsmittel, die Ausbeute bei gleicher Temperatur signifikant erhöhen kann.

In Kapitel 5 sollte daher ein Lösungsmittel oder eine Komponente gefunden werden, durch deren Zugabe die Ausbeute einer reinen Acrylsäurekristallisation signifikant erhöht werden kann. Zur Identifikation eines geeigneten Lösungsmittels wurde daher eine strukturierte Stufenmethode zum schnellen Lösungsmittelscreening entwickelt. Zur Reduzierung des Arbeitsaufwands basiert der experimentelle Teil der Methode ausschließlich auf dem Verfahren der dynamischen differentiellen Kalorimetrie (DSC).

Die Screeningmethode wurde anschließend erfolgreich eingesetzt, um entsprechende Lösungsmittel zur Ausbeutesteigerung der Acrylsäurekristallisation aus einer wässrigen Schmelze zu identifizieren. Als mögliche Lösungsmittel konnten Essigsäure, Propionsäure und Buttersäure identifiziert werden. Zur genaueren Evaluierung der drei Lösungsmittel wurden jeweils die ternären Fest-Flüssig-Phasendiagramme mit Acrylsäure und Wasser mittels DSC vermessen. Nach Auswertung der ternären Phasendiagramme konnte Essigsäure als geeignetes Lösungsmittel bzw. Komponente zur Ausbeutesteigerung einer Acrylsäurekristallisation aus einer wässrigen Schmelze identifiziert werden.

Für eine potentielle Implementierung der entwickelten eutektischen Kristallisation aus Kapitel 4 von Acrylsäure und Wasser musste eine Wirtschaftlichkeitsanalyse erstellt werden. Basierend auf der Wirtschaftlichkeitsanalyse wurden dann die aufgezeigten verfahrenstechnischen Vorteile ökonomisch verifiziert.

In Kapitel 6 wurde daher ein aus der Literatur bekanntes Aufarbeitsverfahren als Benchmark mit dem neu entwickelten Verfahren verglichen. Für die Analyse wurde von beiden Aufarbeitsrouten eine entsprechende Aspen-Simulation aufgebaut, so dass ein direkter Vergleich bzgl. des spezifischen Energiebedarfs, der verbesserten Ausbeute und der Apparatedimensionen erstellt werden konnte.

Der Einsatz der eutektischen Kristallisation von Acrylsäure und Wasser aus dem wässrigen Synthesestrom ermöglicht die frühzeitige Abtrennung von 78% der Acrylsäure ohne eine thermische Belastung. Hierdurch kann die Polymerisationsneigung und Dimerisierung von Acrylsäure ebenfalls um 78% reduziert werden. Der spezifische Energieverbrauch des neuen Trennverfahrens kann auf 41% reduziert werden. Gleichzeitig wird durch die eutektische Kristallisation der Abwasseranfall um 77% gesenkt, da Wasser bereits als Teil des Zielproduktes abgetrennt wird. Durch die Reduzierung der Abwasserfracht zu einer Verbrennungsanlage wird gleichzeitig die benötigte Erdgasmenge um 77% reduziert.

Eine Abschätzung der Apparatedimensionen hat gezeigt, dass sich die Durchmesser der Destillationskolonnen auf ca. 40% verkleinern. Die spezifischen Dimensionen der Kristallisationseinheiten hingegen verdoppeln sich wie erwartet.

Die Ergebnisse der Benchmarkanalyse haben gezeigt, dass der Einsatz einer frühzeitigen eutektischen Kristallisation von Acrylsäure und Wasser in Kombination mit einer kleineren

Destillationssequenz einen innovativen und vielversprechenden Trennprozess darstellt. Gleichzeitig können der spezifische Energiebedarf und der spezifische Einsatzstofffaktor nachhaltig verbessert werden.

Die vorgestellte Arbeit ist ein Beispiel für die Entwicklung eines innovativen Prozesses durch den Einsatz der Schmelzkristallisation als Trenntechnologie. Es konnte gezeigt werden, dass die hohe Selektivität und der reduzierte Energiebedarf der Schmelzkristallisation die Möglichkeit aufzeigt, einen bekannten Prozess nachhaltig weiterzuentwickeln.

ACKNOWLEDGEMENTS

Finally, I have reached the end of a long journey called PhD thesis. I prepared this thesis in parallel to a very interesting job as a process engineer at the department of Process Technology of Evonik Industries. The parallelization of an interesting job and the preparation of a PhD thesis has some advantages, but requires also a powerful engagement and discipline to avoid losing the focus of one of both parts. Therefore, I will seize this opportunity to express my gratitude to all those people who have contributed, either directly or indirectly, to preparing my PhD thesis.

Firstly, I would like to thank my promoter Prof. Dr. Peter J. Jansens for his offer to prepare this PhD thesis in cooperation with the Technical University of Delft and Evonik Industries. His scientific input, ideas, and suggestions during the research, but also the critical view and interesting questions on the research topic have helped me to improve the quality of this thesis. I enjoyed the discussion with him, because I felt all the time his enthusiasm about the topic of melt crystallization and his addiction to new and interesting process ideas.

I would also like to thank Dr. Axel Kobus from Evonik Industries. He gave me the opportunity to follow the offer to prepare this PhD thesis and relied on me to be able to parallelize it with my job in his department. Axel Kobus encouraged me the last 5 years; this helped me to finish this work successfully.

Respectfully, I would like to thank and commemorate Michael Rathmann. Michael passed away much too early in 2009. Michael was a great colleague and friend within the last seven years at Evonik Industries. His support in preparing experiments and in solving practical problems was essential for the success of this thesis. Thank you Michael, I hope you rest in peace!

My gratitude goes also to Dr. Franz-Felix Kuppinger from Evonik Industries. It is still a pleasure to me to discuss topics on melt crystallization with Felix. Felix supported and encouraged me the last 5 years by publishing the different parts of the thesis and providing acrylic acid for the experiments.

I am indebted to Dr. Luca Cameretti, a great colleague from Evonik Industries. Luca supported me with the discussion and measurement on solid-liquid phase equilibrium data. The preparation of the thesis would have taken much longer without his support in the English grammar review of the complete thesis.

A large part of this thesis is based on experimental data. These data are used in the different chapters. Therefore, I would like to thank several students who prepared their Master Thesis or their internship on different melt crystallization topics. All students came from different countries. This helped me to improve my English. However, even more it was a pleasure for me to work with four powerful and involved persons and to meet four different cultures. It makes me happy that we still stay in contact! Somath Kadam, Stijn Harms, Nicholas Rigot, and Stefania Pardini, thank you all for the effort and the contribution to this research work!

My gratitude also goes to the other colleagues of Evonik Industries: Ralf Meier, Dr. Andreas Hoff, Udo Knippenberg, Dr. Jörg Leistner, Dr. Kai-Martin Krüger, Dr. Mirko Michel, Olivier Zehnacker, Iris Günther, Stefan Münzner, Martin Haneke, Jürgen Drüner, Stefan Kretschmer, Melanie Wieser, Bernd Dienst, Jörg Schiebelhut, Walter Sterzel, Dr. Jens Haubrock, and Dr. Jürgen Mosler. Thank you very much for being always kind and helpful in all situations.

During the last 5 years, I have met many different people from different disciplines. It was a pleasure for me to discuss different topics with different people. The discussions make me aware that each discipline has a different view on the same problem. Therefore, I would like to thank these people for interesting conversations which helped me a lot. I thank Dr. Hugo Meekes from the Radboud University Nijmegen for his input on crystal face compositions that contributed significantly to the results of chapter 2. I am indebted to Dr. Jochen Schoell from Mettler Toledo for the useful discussions on FBRM measurement technology as a major subject of chapter 3. I thank Dr. Theo de Loos from the Delft University of Technology for the useful review of chapter 5 and his valuable comments. Finally, I am indebted to the members of the promotion committee for approving this thesis: Dr. ir. H. J. M. Kramer, Prof. dr. ir. A. Stankiewicz, Prof. Dr.-Ing. Dr. h.c. Joachim Ulrich, Dr. ir. Dirk Verdoes, Prof. dr. R. F. Mudde, and Prof. dr. ir. B. J. Boersma.

My thanks go also to my parents who supported me during my whole education and especially during my PhD thesis. They always gave me the freedom to make my own decision regarding the way of education.

Finally, I want to thank Claudia, my lovely and wonderful wife. She supported and encouraged me the whole time of the PhD thesis. She gives me everyday strength, happiness, and, most important, love.

Axel

CURRICULUM VITAE

Axel Hengstermann

Born April 21st 1978 in Muenster, Germany

1984 - 1988	Primary School, Münster, Germany
1988 – 1994	Secondary Modern School, Münster, Germany Degree: Specialized High School Maturity
1994 - 1997	Grammar School, Münster, Germany Degree: General qualification for university entrance
1997 – 1998	Civilian Service, Münster, Germany
1998 - 2002	University of Applied Science Münster, Germany Study of Chemical Engineering / Process Technology Degree: Dipl.-Ing. (FH) of Chemical Engineering
2002	Degussa AG Marl / Germany Process Technology & Engineering Diploma Thesis: Design and Start-up of a mobile Pilot Plant for Gas Absorption
2002 until today	Evonik Degussa GmbH Process Technology & Engineering Fluid Processing Department - Process Engineer for Acryl Acid Production - Unit Operation Manager for Crystallization
2006 - 2010	Delft University of Technology – PhD research Process & Energy Department / Separation Technology
2007 until today	University of Applied Science Muenster Assistant Lecturer for Chemical Engineering - Subject Area: Technical Crystallization
Patents	
2006	Separation of two different solid phases from a solution uses crystallizing and flotation with a gas flow, DE102006060117A1.
2003	Washing device, method for purifying a washing product, and use of said washing device, WO2004026429A1.
2007	Process for Preparing Acrylic Acid purified by crystallization from Hydroxypropionic Acid and Apparatus therefore, WO2008023039A1

2007 Method for Producing and Purifying Aqueous Phases,
WO2009130085A1.

Oral Presentations

2006 Hengstermann, A.; Diehl, B.; Rausch, M.; Phoenix aus der
„Pottasche“-Prozessoptimierung als interdisziplinäre
Herausforderung für Verfahreningenieure, ProcessNet-
Fachausschuss Kristallisation, Basel, 2006

2009 Hengstermann A.; Jansens, P.J.; Kadam S.; Einfluss des
Lösungsmittels und der Übersättigung auf die industrielle
Schmelzkristallisation einer organischen Substanz, ProcessNet-
Fachausschuss Kristallisation, Dortmund, 2009

Publications

2009 Hengstermann, A.; Kadam, S.; Jansens, P.J.; Influence of water
content and supercooling on crystal morphology of acrylic acid, J.
of Crystal Growth and Design, 2009, Vol. 9 (4), pp2000–2007.

2010 Hengstermann, A.; Harms, S.; Jansens, P.J.; The Influence of
Water and Supercooling on Permeability and Compressibility of
Crystal Beds formed out of Acrylic Acid Crystals, Chemical
Engineering Technology, 2010, Vol. 33 (3), pp433–443.

PATENT APPLICATION - WO2009130085A1

(12) NACH DEM VERTRAG ÜBER DIE INTERNATIONALE ZUSAMMENARBEIT AUF DEM GEBIET DES PATENTWESENS (PCT) VERÖFFENTLICHTE INTERNATIONALE ANMELDUNG

(19) Weltorganisation für geistiges Eigentum
Internationales Büro



(10) Internationale Veröffentlichungsnummer
WO 2009/130085 A1

(51) Internationale Patentklassifikation
C07C 51/43 (2006.01)

44577 Castrop-Rauxel (DE), JANSSEN, Peter (NL/NL);
Fäulandstrasse 21, NL-6137 KV Simard (NL)

(21) Internationales Aktenzeichen: PCT/EP2009/052831
(22) Internationales Anmeldedatum:
11. März 2009 (11.03.2009)

(25) Erfindungssprache: Deutsch

(26) Veröffentlichungssprache: Deutsch

(30) Angaben zur Priorität:
10 2008 020 688.1
24. April 2008 (24.04.2008) DE

(71) Anmelder für alle Bestimmungsstaaten mit Ausnahme
von US: FVONIK STOCKHAUSEN GMBH (DE/DE);
Bäckerpfad 25, 47805 Krefeld (DE)

(72) Erfinder: und

(75) Erfinder/Anmelder (nur für US): HENGSTERMANN,
Axel (DE/DE); Münsterstrasse 42, 48008 Senden (DE);
KUPPINGER, Frau-Felke (DE/DE); Rudolf-Vinchow-
Strasse 37a, 45768 Marl (DE); LEISTNER, Jörg
(DE/DE); Holbricker Strasse 64, 45721 Haltern am See
(DE); MOSLER, Jürgen (DE/DE); Brüsseler Strasse 20,

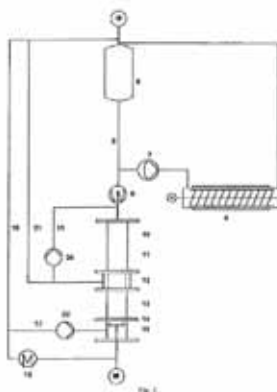
(31) Bestimmungsstaaten (soweit nicht anders angegeben, für
jede verfügbare nationale Schutzrechtsart): AE, AG, AL,
AM, AO, AT, AU, AZ, BA, BB, BG, BH, BR, BW, BY,
BZ, CA, CH, CN, CO, CR, CU, CZ, DE, DK, DM, DO,
DZ, EC, EE, EG, ES, FI, GB, GD, GE, GH, GM, GT,
HN, HR, HU, ID, IL, IN, IS, JP, KE, KG, KM, KN, KP,
KR, KZ, LA, LC, LK, LR, LS, LT, LU, LV, MA, MD,
ME, MG, MK, MN, MW, MX, MY, MZ, NA, NG, NI,
NO, NZ, OM, PG, PH, PL, PT, RO, RS, RU, SC, SD, SE,
SG, SK, SL, SM, ST, SV, SY, TJ, TM, TN, TR, TT, TZ,
UA, UG, US, UZ, VC, VN, ZA, ZM, ZW.

(34) Bestimmungsstaaten (soweit nicht anders angegeben, für
jede verfügbare regionale Schutzrechtsart): AR/PO (BW,
GH, GM, KE, LS, MW, MZ, NA, SD, SL, SZ, TZ, UG,
ZM, ZW), europäisches (AM, AZ, BY, BG, CZ, DE, DK,
EE, ES, FI, FR, GB, GR, HR, HU, IE, IS, IT, LT,
LU, LV, MC, MK, MT, NL, NO, PL, PT, RO, SE, SI,
SK, TR), OAPI (BF, BJ, CF, CG, CI, CM, GA, GN, GQ,
GW, ML, MR, NE, SN, TD, TG).

[Fortsetzung auf der nächsten Seite]

(54) Title: METHOD FOR PRODUCING AND PURIFYING AQUEOUS PHASES

(54) Bezeichnung: VERFAHREN ZUR HERSTELLUNG UND AUFRÄUIGUNG WÄSSRIGER PHASEN

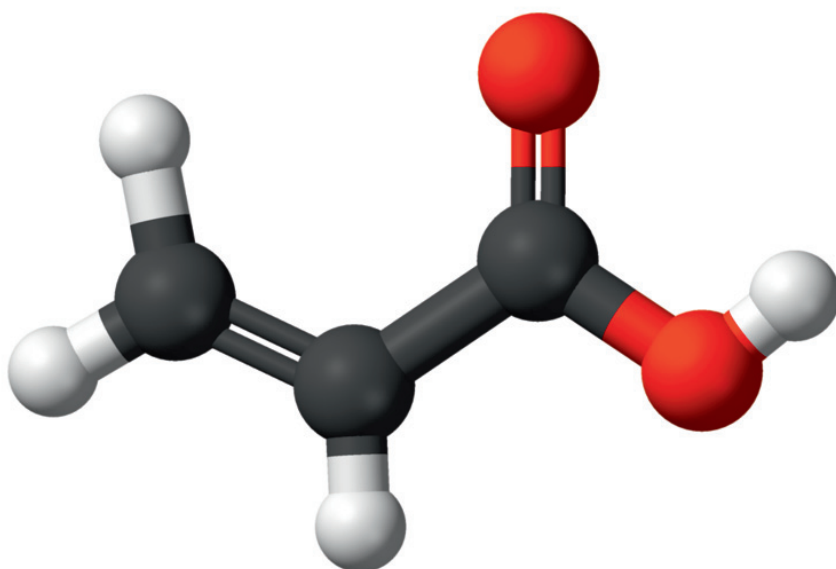


(57) Abstract: The present invention relates to a method for purifying an unpurified phase, containing a target product, preferably (meth)acrylic acid, water, and at least one contaminant differing from the target product and from water, to obtain a purified phase, comprising a process stage comprising the following process steps: a) the target product and water are crystallized from the unpurified phase while forming a suspension containing a mother liquor and crystals, wherein said crystallizing is carried out at a temperature T_1 within the range of $T_1 = 15^\circ\text{C} \leq T_1 \leq T_2 = 3^\circ\text{C}$ ($T_2 =$ eutectic temperature of the unpurified phase); b) the crystals are at least partially separated from the mother liquor; c) at least part of the separated crystals is melted to form a melt, wherein said melting is carried out at a temperature T_3 within the range of $T_3 = T_1 \leq T_3 \leq 20^\circ\text{C}$; and d) at least part of the melt is returned to step b), wherein the part of the melt that is not returned is present as a purified phase. The invention further relates to a method for the production of a purified phase, containing a target product and water, a method for the production of a polymer based on (meth) acrylic acid, polymers that may be obtained by means of said method, chemical products, such as fibers or molded bodies, and the use of polymers.

(57) Zusammenfassung

[Fortsetzung auf der nächsten Seite]

WO 2009/130085 A1



ISBN 978-3-8322-9501-1